THERMODYNAMIC PROPERTIES AND PHASE TRANSITIONS OF SOLID HYDROGEN HALIDES AND THEIR DEUTERIUM ANALOGS

A Thesis

Submitted to

Osaka University

in Partial Fulfilment of the Requirements

for the Degree

of

Doctor of Science

by

AKIRA INABA

[1976]

Doctoral Committee:

Professor Hideaki Chihara, Chairman

Professor Syûzô Seki

Professor Ryôiti Kiriyama

Associate Professor Nobuo Nakamura

ACKNOWLEDGMENTS

The works described in this thesis have been carried out under the direction of Professor Hideaki Chihara. The author would like to express his sincere gratitude to Professor Chihara for his patient guidance and kind encouragement. Thanks are also due to Associate Professor Nobuo Nakamura for his valuable suggestions and discussions. The author would like to express his gratitude to Dr. Tooru Atake for assistance in experiments. The author also wishes to thank Professor Syûzô Seki and Associate Professor Hiroshi Suga and the members of both the Professor Chihara's and Seki's laboratories for their encouragement and fruitful discussions. Finally, the author expresses thanks to his wife Kiyoko and their daughter Kazuko for their encouragement.

CONTENTS

ABSTRACT

In the introductory chapter, a review is given on the earlier works for solid hydrogen halides; with a special emphasis on their structures, molecular motions, molecular interactions, and phase transitions.

Chapter 2 is devoted to measurements of heat capacity and vapor pressure of hydrogen halides. A calibration of the platinum and the germanium resistance thermometers used will also be described.

In chapters 3 to 5, the thermodynamic properties obtained are presented. Discussions are given on the "120 K transition" of single crystal HCl and features of the other phase transitions.

In the last chapter, analyses of thermodynamic properties are made primarily in order to elucidate the mechanism of phase transitions. Both the heat capacity and the entropy of transitions extracted suggested the orientational order-disorder type of mechanism. Our discussions will extend to understanding of the successive phase transitions in terms of molecular interactions.

CHAPTER 1

Introductory Remarks

1-1. Introduction

A hydrogen halide or deuterium halide molecule will be treated as a quasi-sphere, though it is a diatomic molecule, with a protuberance corresponding to the position of the proton or deuteron. In fact, all the solids in phase I are plastic according to definition by Timmerman.[1] On the other hand, the molecular dipole and the quadrupole moment are significant in molecules HCl, HBr, and HI.[2] The former decreases in this order and the latter in a reverse order. When being deuterated, the moment of inertia of each molecule is approximately doubled. In solid, moreover, the existence of hydrogen bonds plays an important role in its properties. Therefore, systematic studies of a series of hydrogen halides and deuterium halides will make clear the interactions in solid, the molecular motion, and the mechanism of transitions.

Phase transitions in solid hydrogen halides and deuterium halides were discovered by calorimetric studies in 1920's and 1947, respectively. Their transition and triple point temperatures are shown in table 1-1. Each temperature values are given from present results as will be described below.

A mile-stone in the history of investigations may

TABLE 1-1. Transition and triple point temperatures in hydrogen halides. (in the unit of K)

HCl	III	98.67				I	159.05	liq.
DCl	III	104.63				I	158.41	liq.
HBr	III	89.53	II	113.60	I' 117.00	I	186.50	liq.
DBr	III	93.67	II	119.96		I	185.64	liq.
HI	III	70.23	II	125.60		I	222.50	liq.
DI	III	77.48	II	128.24		I	221.51	liq.

be set in the year of 1967. At this turning point, neutron diffraction studies were for the first time conducted by Sándor and his coworkers when the positions of deuterons were determined. In 1969, subsequently, ferroelectricity of HCl and HBr in phase III was discovered by Hoshino and his coworkers. These investigations promoted the studies on the phase transition mechanism from a microscopic point of view. A review will be given below on the previous investigations.

1-2. Review of previous works

1-2-1. Diffraction studies

X-ray studies before 1967

The earliest diffraction studies were carried out by Simon et al. and Natta.[3-6] The X-ray determinations of the structure of hydrogen halide crystals were not entirely satisfactory, the different observers did not agree among themselves and moreover some results were not in accord with the corresponding measurements using the polarizing microscope.[7] Thus, Natta found a cubic structure for HBr in phase II whereas the material is optically anisotropic. To sum up the results obtained; (i) phase I has the cubic face centered structure; (ii) for HBr and HI, phase II has probably the tetragonal face centered structure with $c/a > 1$ but the deformation relative to phase I is not large; (iii) phase III has a complicated structure which probably approximates to tetragonal face centered lattice with the axial ratio $c/a > 1$.

X-ray and neutron studies by Sándor and his coworkers

The structural analyses by X-ray diffraction gave no clue to the location of the hydrogen atoms. More reliable analyses should be made by neutron diffraction studies, because they can also determine the positions

of hydrogen (though practically deuteron). The following structures were determined from X-ray and neutron powder diffraction by Sándor and his coworkers.[8-13]

[Phase III]

The low temperature forms in HCl and HBr and their deuterium analogs are isomorphous.

Lattice: Orthorhombic, B-face-centered, with lattice parameters as shown in table 1-2.

Space group: C_{2v}^{12} - $Bb2_1m$.

Number of formula units per unit cell: 4.

Atomic positions: All atoms in x, y, 0, with x = 0, y = 0 for the halogen, and as in table 1-2 for D.

The origin used for this description is not the conventional one given in the International Tables for X-ray Crystallography; instead, it is chosen on a mirror plane, midway between two b-glide planes. In the y direction, where the choice is arbitrary, it has been taken so as to make the y parameter of the halogen atom zero.

The structure is as shown in figure 1-1. All atoms lie at special positions on mirror planes. Taken by themselves the halogen atoms form an all-face-centered array, but the D atoms do not conform to this.

TABLE 1-2. Lattice parameters (in 10^{-10} m) and atomic position parameters of HCl, DCl, and DBr in phase III.

	a	b	c	x_D	y_D	
DCl at 77.4 K	5.053	5.373	5.825	0.081	0.170	neutron
DBr at 84 K	5.44	5.614	6.120	0.075	0.179	study
HCl at 92.4 K	5.082	5.410	5.826			X-ray
DCl at 92.4 K	5.069	5.399	5.829			study

PHASE III

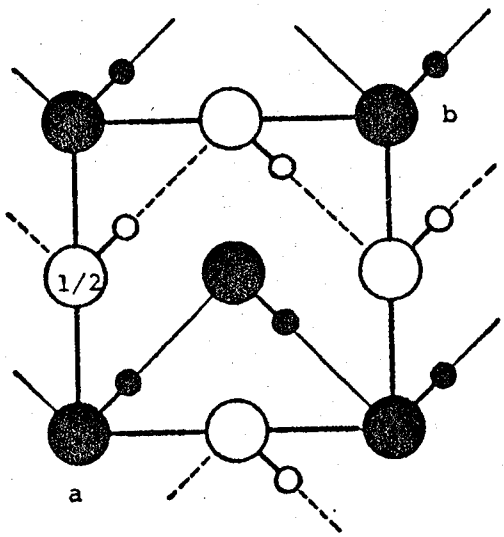

$C_{2v}^{12} - Bb2_1m$

FIGURE 1-1. Arrangement of the molecules in the unit cell of the ordered orthorhombic phase III of HCl, HBr, and their deuterium analogs.

Each D is attached to one halogen, its donor, and points towards another halogen, the acceptor of its Cl-D...Cl or Br-D...Br bond. The halogen atoms are thus bonded in zig-zag chains, with an angle of about 90° between bonds, the chains extending parallel to the y direction, with the y components of the Cl-D or Br-D vectors all pointing in the same sense. The similar array of infinite zig-zag chains of hydrogen bonds are also realized in hydrogen fluoride.[14] The structure can be seen to be polar. Each molecule is a dipole; since their y components are all parallel, the crystal has a net dipole moment or spontaneous polarization. The structure as a whole can be reversed by an electric field, and the material is therefore ferroelectric.

There are three possible ways in which the structure might reverse direction (i.e. switching). (i) Each molecule could change direction by 180°; this means that the D atoms move from positions marked by small open circles in figure 1-2(a) to positions marked by crossed circles. (ii) Each molecule could change direction by 90°, moving its D atoms from the small open circles to the crossed circles of figure 1-2(b). (iii) Each D atom could jump to a new position in its bonds, again moving from the small open circles to

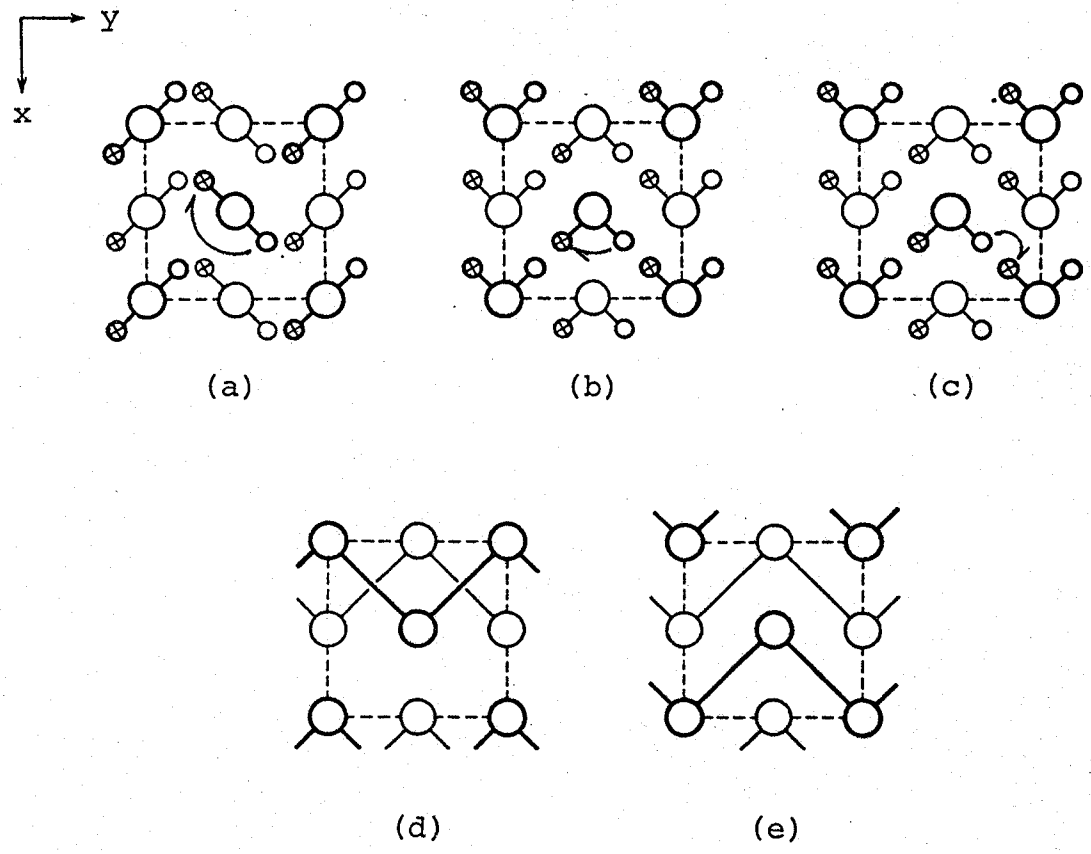

FIGURE 1-2. Structures of hydrogen halides. Large open circles represent halogen atoms, and small circles H or D, actual or average positions. Atoms shown with heavy line are at height 0, and those with thin lines at height 1/2. (a), (b), and (c) Effect of switching the direction of the molecule through 180° flip, 90° flip, and jumping processes, respectively; the small crossed circles represent the new position of H or D. (d) and (e) Relation of the reversed chain at height 0 to the chain in the original direction at height 1/2; corresponding to (a) and , (b) and (c) respectively.

the crossed circles of figure 1-2(c); it is thus indistinguishable from (ii) in its results. In no case do the halogen atoms move, yet in (i) the position of the chain has altered by a distance (a/2 + b/2), as shown in figure 1-2(d), while in (ii) and (iii) it has remained unaltered, as shown in figure 1-2(e). It is not known for certain which mechanism actually occurs in ferroelectric reversal, but all three posibilities are relevant when we consider what happens at the transition.

As for DI, in contrast to DCl and DBr, phase III was found to be ordered monoclinic, space group C_{2h}^{6} - C2/c, with 16 molecules in the unit cell. The molecules form hydrogen bonded squares stacked along the monoclinic c-axis, the directions of the bonds alternating in successive layers. HI in phase III is not ferroelectric.

[Phase II]

The structure of phase II, which is missing in HCl and DCl, are isomorphous for HBr, HI, and their deuterated analogs. It is still orthorhombic, with a unit cell very nearly the same as in phase III, containing 4 molecules, but its space group is now D_{2h}^{18} - Bbcm. The structure is shown in figure 1-2(a),

PHASE II

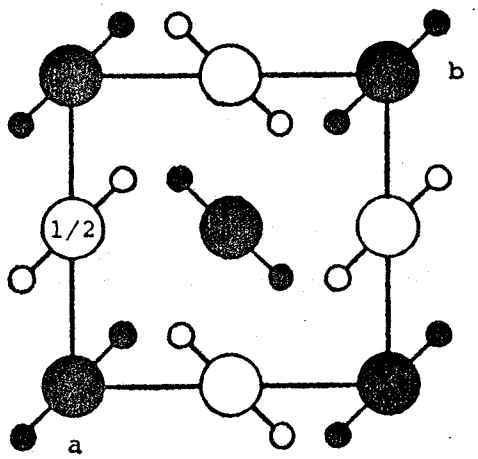

D_{2h}^{18} – Bbcm

FIGURE 1-3. Arrangement of the molecules in phase II of HBr, HI, and their deuterium analogs.

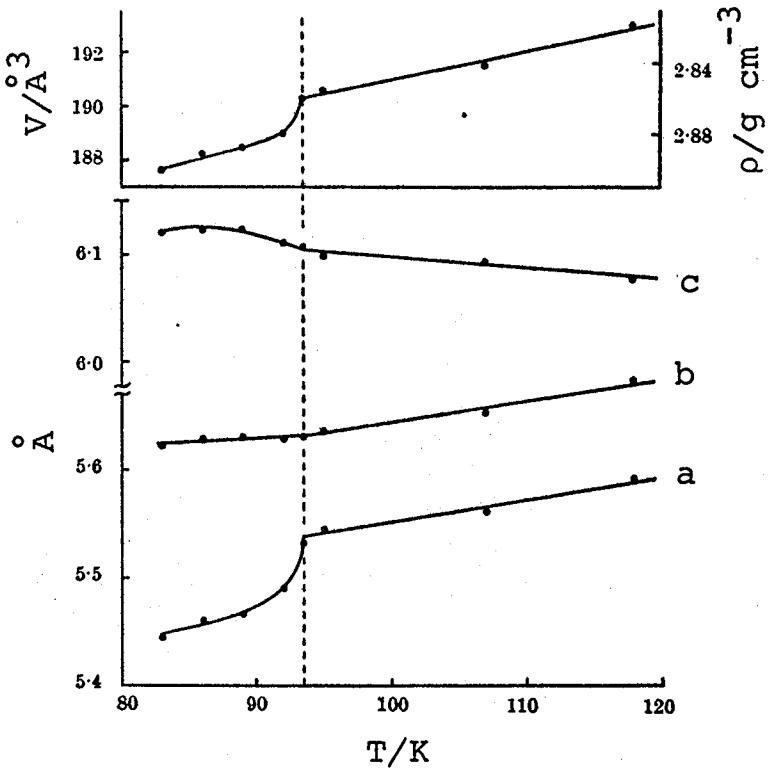

FIGURE 1-4. Temperature dependence of the three edglengths of the orthorhombic unit cell, of the unit cell volume and of the density of deuterium bromide in the III-II transition region.

---

1 Å = 0.1 nm

if we allow small open and crossed circles both to represent statistical half atoms. Each molecule has two equilibrium orientations; one is the same as in the ordered phase, the other opposite to it. The atomic position parameters, and the bond lengths are almost exactly the same as in the low temperature form. The temperature dependence of the three cell parameters over the III-II transition region of DBr was studied by X-ray powder diffraction. The results are shown in figure 1-4 together with the temperature dependence of the unit cell volume and density. They suggest that III-II transition is gradual. In phase III, the thermal expansion along a has the greatest anomalous increase, giving a large positive peak at the transition; that along c decreases, giving a fairly large negative peak, while that along b has a small but fairly sharp increase. Above the transition they all have constant values: $\alpha_a = \alpha_b = 4 \times 10^{-4}\ K^{-1}$, $\alpha_c = -2 \times 10^{-4}\ K^{-1}$.

[Phase I]

The high temperature form, phase I, is the same for all the halides. It is cubic with space group O_h^5 - Fm3m (see figure 1-5). A detailed neutron diffraction study of polycrystalline DCl at 111.5 K

PHASE I

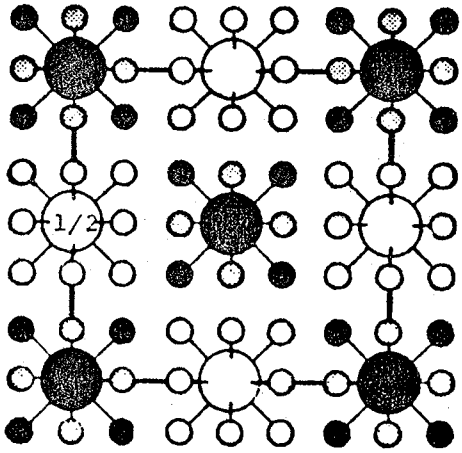

$O_h^5 - Fm3m$

FIGURE 1-5. The structure of phase I of all the halides.

showed conclusively that the molecules were not rotating, but that the average structure had its D atoms distributed equally over twelve sites with position parameters very close to those in phase III. In phase I, the disordered models of 4-, 6-, and 8-fold, and random orientation or free rotation model are all excluded. The cell parameters of HCl and DCl in phase I are shown in table 1-3. It shows that

TABLE 1-3. Lattice parameter (in 10^{-10} m) and atomic position parameters of HCl and DCl.

	a	x_D	y_D	
DCl at 111.5 K	5.47	0.151	0.151	neutron study
HCl at 118.5 K	5.482			X-ray study
DCl at 118.5 K	5.475			

the unit cell of DCl is significantly smaller. This can be interpreted as the difference of the effect of librational molecular motion. The thermal amplitudes are considerably greater. In fact, D-Cl bond length in phase I (1.17 Å), which is calculated from the positional parameters of the atoms, is considerably less than that of phase III (1.25 Å).

The intermediate phase I' of HBr was not investigated by Sándor. Natta claimed that the phase I' of HBr was a face-centered cubic phase. Recent X-ray study by Simon[15] also reported it to be cubic.

Single crystal diffraction studies by Hoshino and his coworkers

[HCl]

In 1969, some evidences for the existence of a new phase I' of HCl between 98 and 120 K were discovered from the single crystal X-ray and neutron diffraction experiments by Hoshino et al.[16-18] The structure of phase I' was explained by a synthetic twin relation of the orthorhombic lattice with the (101) plane as the twin boundary. Possible average structure has the space group D_{2h}^{17} - Bbmm or D_2^4 - $P2_12_12_1$ as shown in figures 1-6(a) and (b), the former being the same as represented in figures 1-2(b) and/or (c).

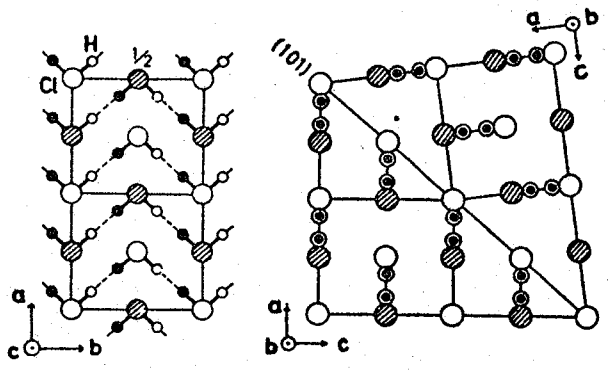

(a) D_{2h}^{17} - Bbmm

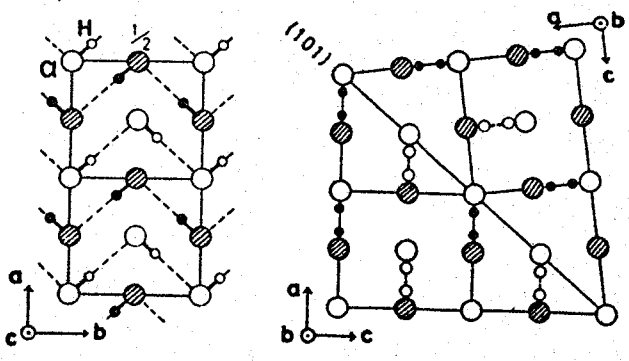

(b) D_2^4 - $P2_12_12_1$

FIGURE 1-6. Two possible average structures for the phase I' of HCl.

However, neither structure can explain the observed intensity of some reflections. As far as the static structure models are concerned, there are no posible structure models to explain the observed data in the phase I'. The dynamical structure models were thus considered.

In the phase I' the molecules may also form linear zig-zag chains as in the ferroelectric phase. As such chains are formed at an instant, however, they are destroyed at the next instant to form the chains stretching in different directions. The average life time of the chain should be much longer than the neutron passage time ($\sim 10^{-13}$ s). Moreover, it was assumed that the change of the direction of the chain corresponds to the movement of the twin boundary by means of the 90° flip of HCl molecules. The mechanism of the movement of the twin boundary is shown in figure 1-7. The difference of the phase I and the phase I' is described by the difference of the length of the hydrogen bonded zig-zag chains and the flipping rate of molecules.

[DCl]

Neutron diffraction measurements of DCl[19-22] using a single crystal revealed that such an anomalous

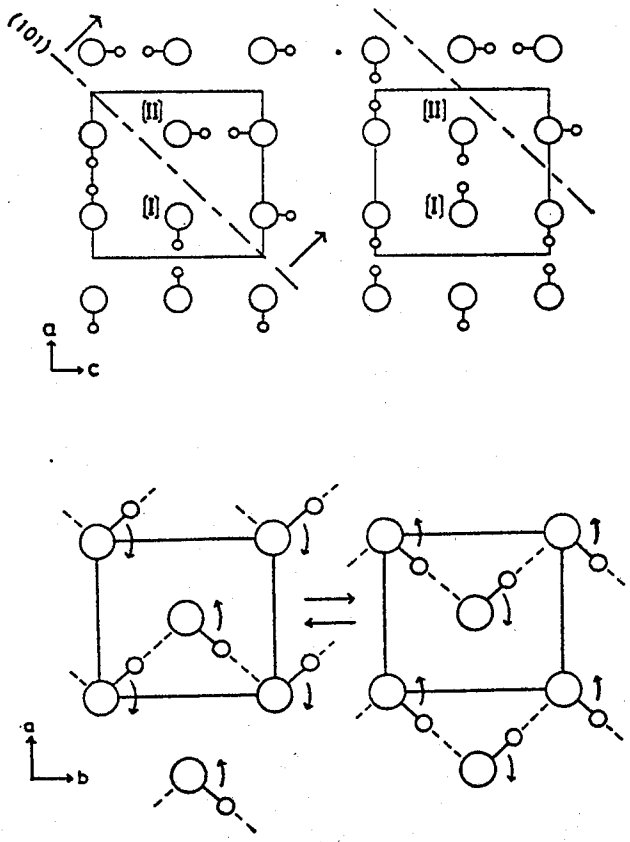

FIGURE 1-7. The mechanism of the movement of the twin boundary by means of the 90° flip.

$1^{\circ} = (\pi/180)$ rad

transition as observed in the higher temperature cubic phase of HCl did not occur. However, disk-like diffuse scattering was recently found in DCl I below 142 K at positions incommensurate with the cubic cell, though it was not always observed and seemed to depend on the sample preparation. Single crystals grown in quartz containers sometimes show anomalous behavior such as the transition observed at 120 K in HCl. These are explained thus to result from the influence of external forces such as stress exerted by the container wall on the crystal. Further, an investigation of the phase transitions in both materials by neutron scattering turned out to be unsuccessful largely due to the experimental difficulties encountered in the growth of single crystals, their cooling down and their passage through the transition without fracture of the crystal.

On the other side, the rotational vibration (i.e. libration) of DCl molecule was investigated by analysing anisotropic temperature factors of deuterium in the powder neutron diffraction measurement by Sándor and Farrow.[12] A similar analysis was developped by Hoshino and his coworkers[19,21] using single crystal diffraction data. Both results are shown in figure 1-8. The mean angular displacements in and out of the (001)

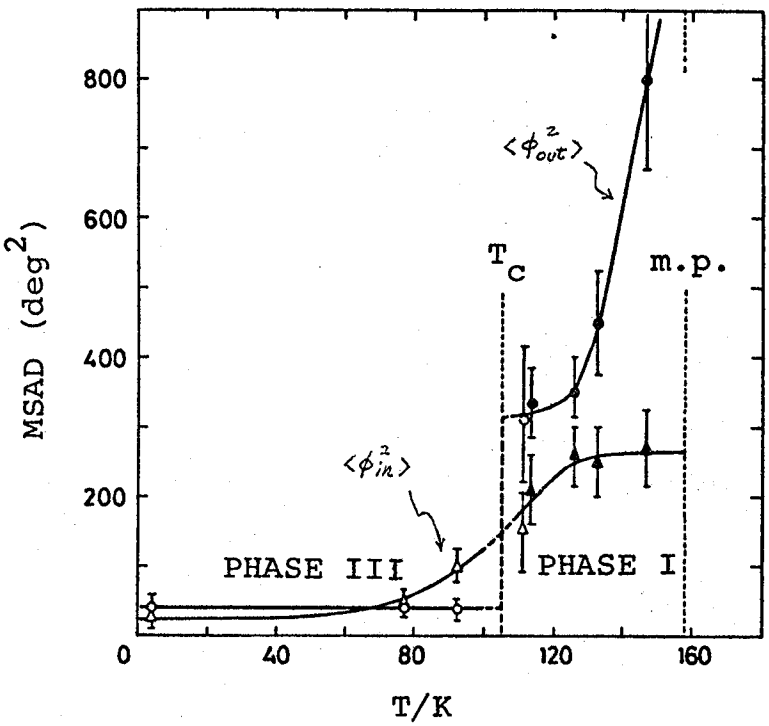

FIGURE 1-8. Temperature variation of mean square angular displacements due to the molecular libration of DCl.

plane are represented in the figure. $<\phi^2_{out}>$ which represents the molecular motion preventing the development of zig-zag chains in the plane (see figure 1-9) increases rapidly above 123 K, whereas $<\phi^2_{in}>$ shows no appreciable change with temperature. The temperature variation of $<\phi^2_{in}>$ and $<\phi^2_{out}>$ corresponds to that of the probability for 90° and 60° flip motion of the

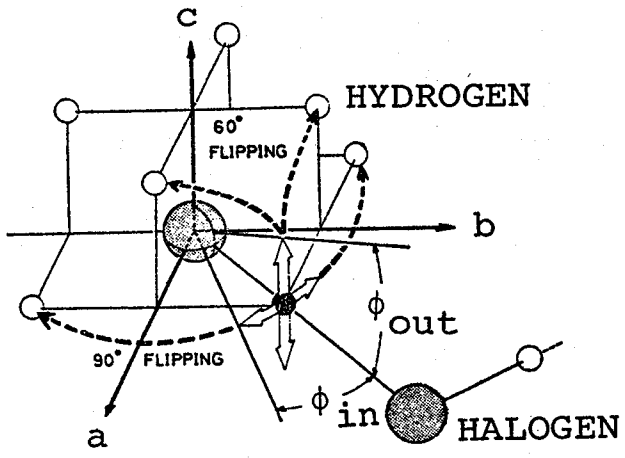

FIGURE 1-9. Twelve-fold disordered structure in the phase I of DCl. In the phase III, the deuterium atom of the central molecule stays at the site 1 and the central molecule is connected with both left and right hand side molecules so that coplanar zig-zag chain formation is made.

molecule, respectively. The molecular motion was also discussed from the NMR and NQR experiments as will be reviewed below.

1-2-2. Infrared and Raman spectral studies

A completely unambiguous determination of the crystal structure by spectral study is out of the question but certain features of the structure can be obtained. In fact, before the neutron diffraction studies of deuterium halides by Sándor et al., many workers investigated[23-26] for the positions of the hydrogen atoms.

In 1955, Hornig and Osberg observed[27] the infrared spectra of HCl, HBr, and HI in phase III and concluded that the HCl and HBr crystals are built of zig-zag hydrogen-bonded chains. Savoie and Anderson remeasured[28] the infrared and Raman spectra of HCl, DCl, HBr, and DBr and suggested the zig-zag chain to be nonplanar, which is in contrast to planar one determined by Sándor et al. Raman study by Ito et al.[29] indicated that the crystal structure of HCl, DCl, HBr, and DBr in phase III is C_{2v}^{9} - $Pn2_1a$ with four molecules in a unit cell, and the nonplanarity of the chain is so small that it is not sensitively reflected to the spectra of lattice vibration region.

The correlation diagram for the proposed crystal structure ($Bb2_1m$) is shown in figure 1-10. It predicts five infrared active lattice modes: three librational modes (A_1, B_1, and B_2) and two optical transitions (A_1 and B_1). Their modes of the two molecules in a primitive unit cell are shown in figure 1-11. Raman study by Ito et al. also indicated two characteristic features in phase III: (1) Rotational lattice vibrations have high frequencies in spite of

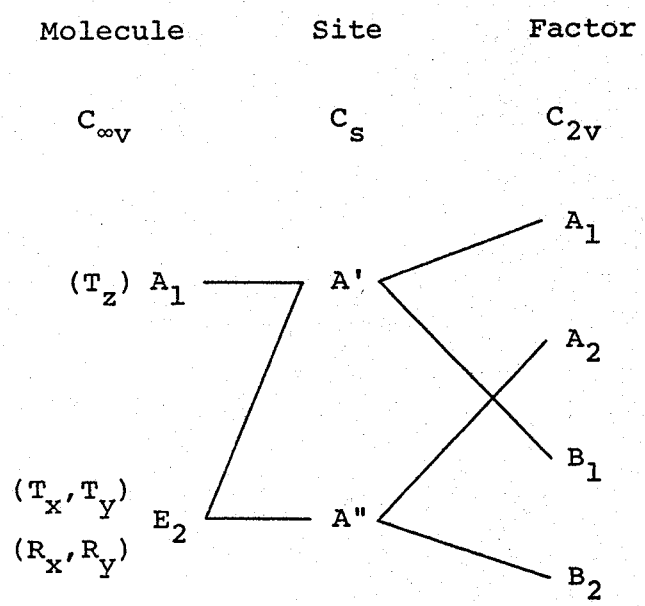

FIGURE 1-10. Correlation diagram for solid phase III.

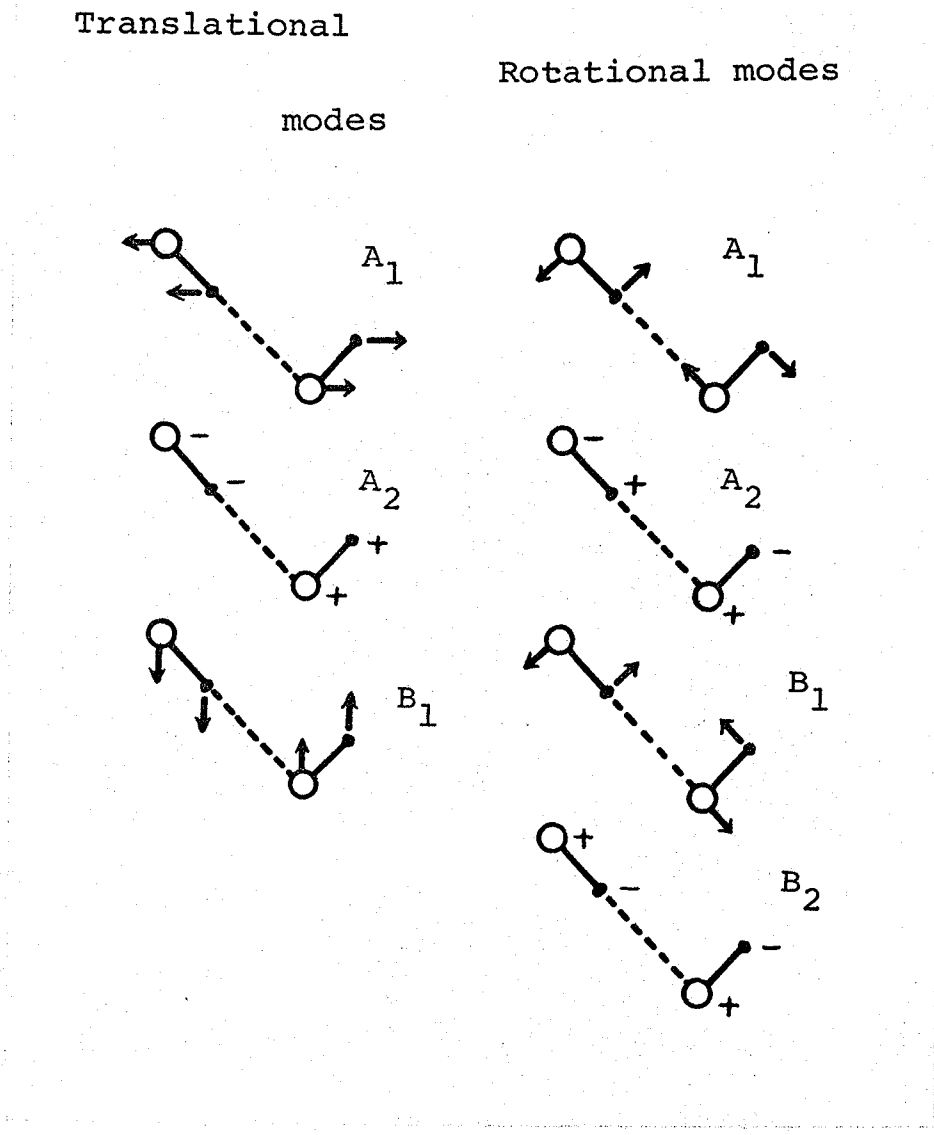

FIGURE 1-11. Translational and rotational lattice vibration of the two molecules in a primitive unit cell of hydrogen halide.

the weakness of the hydrogen bond. (2) The intensity of the intermolecular vibrations is about 10 times stronger than that of libration. These were explained by Hanamura[30] as the effects of charge transfer on Raman scattering. Carlson and Friedrich measured[31] the absolute absorption intensities of the infrared active lattice modes of HCl and HBr. It gave evidence that the molecular dipole moments are less than their gas-phase value as theoretically predicted by Hanamura.

The infrared and Raman spectral bandshapes of internal vibration bands contain information about molecular orientation and translational diffusion. Raman study by Wang et al.[32,33] indicated that HCl molecules undergo rapid reorientation in cubic phase at temperatures higher than 120 K, and satellite peaks develop between 120 and 98.4 K suggesting the evolution of a lower symmetry structure other than the cubic.

There is one thing bothering. Infrared spectral studies by Hiebert and Hornig[34,35] suggested that there are two additional phase transitions at about 25 and 10 K in phase III of HI. However, present calorimetric measurement showed no anomaly at both temperatures as will be mentioned below.

1-2-3. Resonance studies

The ^{35}Cl quadrupole spectra of HCl and DCl in phase III were examined by Marram and Ragle.[36] Activation energies for both compounds were 2.70 $\pm$ 0.05 kcal mol^{-1}† in good agreement with values obtained from dielectric relaxation measurements by Swenson and Cole[37] (2.6 kcal mol^{-1}). The data were discussed in terms of some angular motion of molecule. On the other hand, the proton $T_{1\rho}$ measurements by Genin et al.[38] gave the different activation energy of 1.4 kcal mol^{-1}. The data were interpreted as due to 90° flip motions of the HCl molecules in solid III which, however, are strongly attenuated in that they occur with nonequal site occupation probabilities. The fraction of the time that a molecule spends in the 90° positions was found to be about 0.01 near the III-I transition. Activation energy of 2.7 or 2.6 kcal mol^{-1} was interpreted by O'Reilly[39] to be a 180° flip motion of the molecule which occurs concurrently with the 90° flip processes.

A single librational frequency was determined by Okuma et al.[40] as a function of temperature from ^{35}Cl and ^{37}Cl NQR frequencies for HCl and DCl in phase

---

† 1 kcal mol^{-1} = 4.1840 kJ mol^{-1}.

III, the quasiharmonic treatment being used for calculation. It does not fully account for the temperature dependence probably because of the effect of intermolecular hydrogen bonds. Another interpretation was given by O'Reilly[39] by means of an attenuated 90° flip process of the molecule mentioned above. A mechanism for the ferroelectric phase transition in solid III of HCl is specified which involves the 90° as well as 180° flips of molecules.

In solid I of each hydrogen halide, two types of molecular motion have been detected: (1) a rapid rotational reorientation and (2) translational diffusion of the molecules. From the second moment of the proton and chlorine magnetic resonance, the structure of the high temperature phase was proposed as being a hindered rotational one. An activation energy of 0.7 kcal mol^{-1} for rotation was derived by Okuma et al. The self-diffusion of molecules below the melting point causes narrowing of proton resonance line above 130 K, with an activation energy of 5.6 kcal mol^{-1}.

The activation energies obtained by different techniques and workers are summarized in table 1-4 together with the proposed processes.

TABLE 1-4. Activation energies obtained by NMR and NQR methods.

The values for deuterium compounds are shown in parentheses.

substances	E_a/kcal mol^{-1}	methods	workers	processes
		[Phase III]		
HCl	2.70 ± 0.05 (2.70 ± 0.05)	T_1 of ^{35}Cl	Marram and Ragle (1964)	"some angular motion of molecule"
	1.4	$T_{1\rho}$ of H	Genin et al. (1968)	"rotation"
HBr	(1.2)	line width of ^{79}Br	Kabada et al. (1970) §	"90° defect motion"
		[Phase I]		
HCl	(0.8)	T_1 of ^{35}Cl and D	Powles and Rhodes (1967)	"reorientation"
	(0.7)	line width of ^{35}Cl	Okuma et al. (1968)	"rotation"

TABLE 1-4. Continued.

substances	E_a/kcal mol^{-1}	methods	workers	processes
HCl	0.9	$T_{1\rho}$ of H	Genin et al. (1968)	"rotation"
	(0.85)	T_1 of D		
	4.4	T_1 of H	Krynicki et al. (1966)	"diffusion"
	5.6	line width of H	Okuma et al. (1968)	"diffusion"
	(3.9)	$T_{1\rho}$ of H	Genin et al. (1968)	"diffusion"
HBr	(1.09)	T_1 of D	Genin et al. (1968)	"rotation"
	(6.6)	T_1 of H	Norris et al. (1968) ¶	"diffusion"
	(5.5)	line width of H		
	6.2	$T_{1\rho}$ of H	Genin et al. (1968)	"diffusion"

TABLE 1-4. Continued.

substances	E_a/kcal mol^{-1}	methods	workers	processes
HI	(0.97)	T_1 of D	Genin et al. (1968)	"rotation"
	6.1	$T_{1\rho}$ of H	Genin et al. (1968)	"diffusion"

§ Kabada, P. K.; O'Reilly, D. E. J. Chem. Phys. 1970, 52, 2403.

¶ Norris, M. O.; Strange, J. H.; Powles, J. G.; Rhodes, M.; Marsden, K.; Krynicki, K. J. Phys. C 1968, 1, 422; 445.

1-2-4. Dielectric measurements

Dielectric constant and loss measurements before 1957, which were mainly carried out by Powles[42-44] and Cole and his coworkers,[37,45-49] were summarized by Cole and Havriliak.[47] Static dielectric constants in logarithmic scale of hydrogen and deuterium halides are plotted against temperature in figure 1-12. The activation energies from dielectric experiments are shown in table 1-5.

Ferroelectricity of HCl and HBr in phase III was discovered by Hoshino et al. in 1967.[50] Subsequent measurement of spontaneous poralization from pyroelectric current measurement in HCl by Kobayashi et al.[51] showed that the maximum value of the polarization is 3.64 μC cm^{-2}, which can be compared with 6.4 μC cm^{-2} calculated by using the dipole moment of HCl gas molecule. It was concluded that the dipole moment of HCl in crystal must be reduced to half the value of free molecule. Similar measurement for HI was not carried out by Hoshino et al. because of experimental restrictions. They imagined from the close resemblance of the nature of the thermal and the dielectric properties to those of HBr that HI is also ferroelectric in phase III. However, recent studies of HI by Cichanowski and Cole[49] gave no

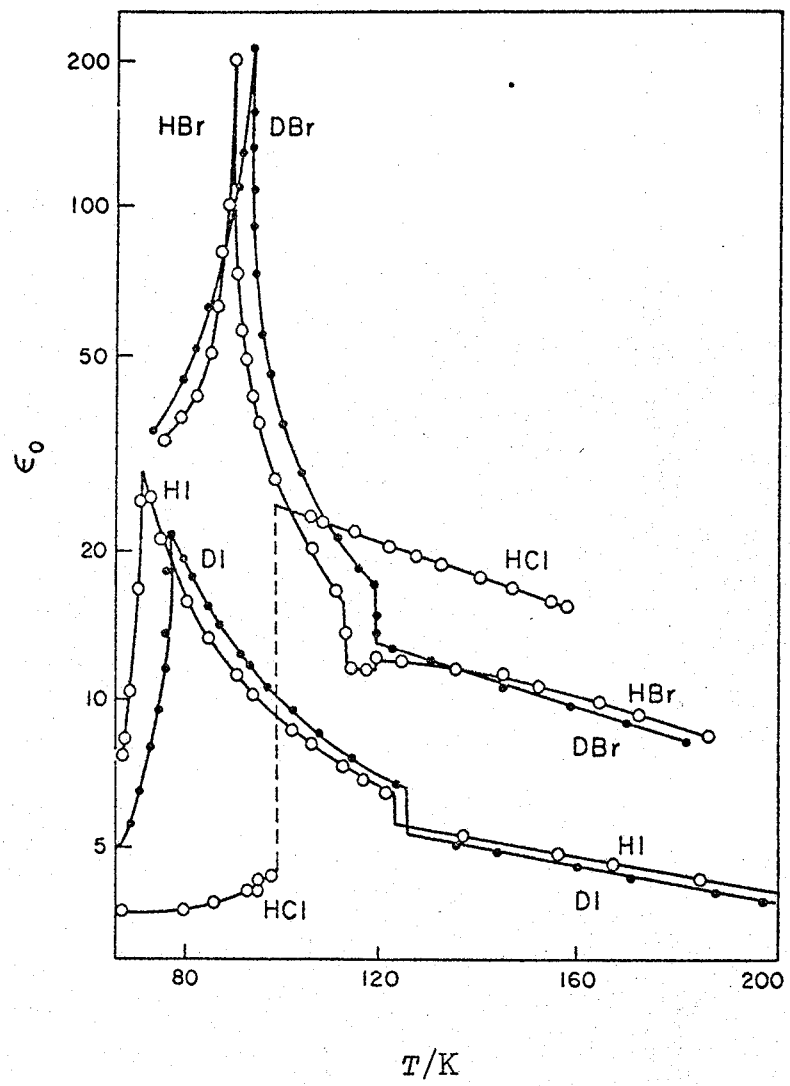

FIGURE 1-12. Temperature dependence of static dielectric constants of hydrogen and deuterium halides.

TABLE 1-5. Activation energies obtained from dielectric relaxation. The values for deuterium compounds are shown in parentheses.

substances	E_a/kcal mol^{-1}
[Phase III]	
HCl	2.6
HBr	2.7 1.6 (1.5) (3.6)
HI	2.2 (2.2)
[Phase II]	
HBr	(1.5)
HI	3.6 (3.1)

indication of ferroelectricity. As far as that goes, solid HI is not isostructural to HCl and HBr in phase III as mentioned above.

1-2-5. Theoretical works on phase transitions

In 1947, Tisza originally suggested[52] that the lower III-II transition is due to the onset of disorder in the dipolar direction while the molecular axes remain parallel. The upper II-I transition is then due to a disordering of the molecular axes. It is further suggested that III-II transition is controlled by dipolar forces and the II-I transition by dispersion forces. Powles developed[53] these idea qualitatively and semiquantitatively. However, it was somewhat hampered both by the paucity of accurate measurements and of the theoretical work available on the intermolecular forces in these materials. Among them, the lack of neutron diffraction study was fatal. In fact, the entropy of transitions was explained from the supposed structures, which are not identical to those of Sándor et al.

In 1954, Krieger and James treated[54] the phase transitions in hydrogen halides in terms of successive rotational or orientational transitions. This model consists of an array of classical rotators with

nextneighbor coupling, the potential energy of coupling being

$$E(\theta_{ij}) = AP_1(\cos\theta_{ij}) + BP_2(\cos\theta_{ij}) \qquad (1)$$

where θ_{ij} is the angle between the molecular axes of symmetry. The model shows a single second-order transition, a single first-order transition, two first-order transitions, or a second-order transition followed by a first-order transition as temperature rises. The modification of this model was developed by Kobayashi et al.[55] in terms of a two-dimensional rotational transition model with two sublattices of A and B. The potential energy is assumed to have the form

$$V = J \sum_{\substack{(AA)\\(BB)}} \cos(\phi_i - \phi_j) + \frac{3}{4} K \sum_{(AB)} \cos 2(\phi_i - \phi_j) \qquad (2)$$

where J and K represent the dipolar and quadrupolar (or van der Waals) interactions, respectively.

In 1970, Hanamura indicated[56] that many properties of molecules in molecular crystals of hydrogen halides can be shown theoretically to deviate from those of free molecules. The model proposed is that of zig-zag chain formation by a charge-transfer process of the π electron to the σ^* antibonding state of the neighboring

molecule. The strong Raman scattering due to intermolecular vibrations as observed by Ito et al. can be explained. The succeeding paper[57] showed how essential the hydrogen bonding effects are in phase transitions and how successive phase transitions and ferroelectricity are induced by the intermolecular interactions, i.e. dipole interactions, quadrupolar interactions, and hydrogen bonding forces.

A thermodynamical explanation for the entropies of the lower transitions of HCl, HBr, DCl, and DBr were attempted by Aston[58] assuming that the change in librational frequencies at the transitions. This assumption, however, is not realistic as shown in the Raman study by Ito et al.[29] Another analysis will be required.

1-3. Purpose of the present investigation

As reviewed above, ever since the structures of hydrogen halides were determined by neutron diffraction studies, the phase transitions were described as those of orientational order-disorder type in connection with the molecular interactions. Nevertheless, previous thermodynamical considerations are not sufficient tc elucidate the mechanism of the phase transitions. One of the reasons may be found in the lack of the data with high accuracy and precision. Since the earlier measurement of heat capacity, what is worse still, did not extend below 15 K, the heat capacity associated with transition could not be satisfactorily elucidated. A quantitative estimate of the disorder present in the crystal should be made from the anomalous part of heat capacity and entropy. The analysis of thermodynamic results therefore needs reexamination particularly now that the conflicting conclusions have been reached from neutron diffraction experiments for the existence of "120 K transition" in HCl. One of the aims of this investigation is, therefore, to improve the heat capacity data in terms of precision and of the shape of anomalies in the transition regions over the previous works. Through the thermodynamical

analyses of the data obtained, our ultimate object is to try to understand the mechanism of phase transitions in hydrogen halides.

REFERENCES to CHAPTER 1

1. Timmerman, J. J. Phys. Chem. Solids 1961, 18, 1.
2. Stogryn, D. E.; Stogryn, A. P. Mol. Phys. 1966, 11, 371.
3. Simon, F.; Simon, C. Z. Phys. 1924, 21, 168.
4. Natta, G. Nature 1931, 127, 168; 235.
5. Ruhemann, B.; Simon, F. Z. Phys. Chem. B 1931, 15, 389; 1932, 15, 398.
6. Natta, G. Gazz. Chim. Ital. 1933, 63, 425.
7. Kruis, A.; Kaishew, R. Z. Phys. Chem. B 1938, 41, 427.
8. Sándor, E.; Farrow, R. F. C. Nature 1967, 213, 171.
9. Sándor, E.; Farrow, R. F. C. Nature 1967, 215, 1265.
10. Sándor, E.; Johnson, M. W. Nature 1968, 217, 541.
11. Sándor, E.; Johnson, M. W. Nature 1969, 223, 730.
12. Sándor, E.; Farrow, R. F. C. Disc. Faraday Soc. 1969, 48, 78.
13. Sándor, E.; Clarke, J. H. Acta Cryst. A 1972, 28, S188.
14. Atoji, M.; Lipscomb, W. N. Acta Cryst. 1956, 7, 173.
15. Simon, A. Z. Naturforsch. 1970, 25b,1489.
16. Shimaoka, K.; Niimura, N.; Motegi, H.; Hoshino, S. J. Phys. Soc. Japan 1969, 27, 1078.
17. Hoshino, S.; Shimaoka, K.; Niimura, N.; Motegi, H.; Maruyama, N. J. Phys. Soc. Japan 1970, 28 Suppl., 189.

18. Niimura, N.; Shimaoka, K.; Motegi, H.; Hoshino, S. J. Phys. Soc. Japan 1972, 32, 1019.
19. Niimura, N.; Fujii, Y.; Motegi, H.; Hoshino, S. Acta Cryst. A 1972, 28, S192.
20. Fujii, Y.; Hoshino, S.; Motegi, H. Tech. Report, ISSP, A, 1972, 538.
21. Niimura, N.; Fujii, Y.; Motegi, H.; Hoshino, S. J. Phys. Soc. Japan 1973, 35, 842.
22. Press, W.; Cox, D. E.; Axe, J. D.; Shirane, G.; Harada, J.; Fujii, Y.; Hoshino, S. Tech. Report, BNL, 1975.
23. Callihan, D.; Salant, E. O. J. Chem. Phys. 1934, 2, 317.
24. Hettner, G. Ann. Phys. 1938, 32, 141.
25. Lee, E.; Sutherland, G. B. B. M.; Wu, C. K. Proc. Roy. Soc. (London) A 1940, 176, 493.
26. Friedrich, H. B.; Person, W. B. J. Chem. Phys. 1963, 39, 811.
27. Hornig, D. F.; Osberg, W. E. J. Chem. Phys. 1955, 23, 662.
28. Savoie, R.; Anderson, A. J. Chem. Phys. 1966, 44, 548.
29. Ito, M.; Suzuki, M.; Yokoyama, T. J. Chem. Phys. 1969, 50, 2949.
30. Hanamura, E. J. Chem. Phys. 1969, 52, 797.

31. Carlson, R. E.; Friedrich, H. B. J. Chem. Phys. 1971, 54, 2794.

32. Wang, C. H.; Fleury, P. A. J. Chem. Phys. 1970, 53, 2243.

33. Wang, C. H.; Wright, R. B. Mol. Phys. 1974, 27, 345.

34. Hiebert, G. L.; Hornig, O. F. J. Chem. Phys. 1957, 26, 1762.

35. Hiebert, G. L.; Hornig, O. F. J. Chem. Phys. 1957, 27, 1216.

36. Marram, E. P.; Ragle, J. L. J. Chem. Phys. 1964, 41, 3546.

37. Swenson, R. W.; Cole, R. H. J. Chem. Phys. 1954, 22, 284.

38. Genin, D. J.; O'Reilly, D. E.; Peterson, E. M.; Tsang, T. J. Chem. Phys. 1968, 48, 4525.

39. O'Reilly, D. E. J. Chem. Phys. 1970, 52, 2396.

40. Okuma, H.; Nakamura, N.; Chihara, H. J. Phys. Soc. Japan 1968, 24, 452.

41. Powles, J. G.; Rhodes, M. Phys. Lett. 1967, 24A, 523.

42. Powles, J. G. Nature 1950, 165, 686.

43. Powles, J. G. Compt. rend. 1950, 230, 836.

44. Powles, J. G. J. Phys. Radium 1952, 13, 121.

45. Brown, N. L.; Cole, R. H. J. Chem. Phys. 1953, 21, 1920.

46. Havriliak, S.; Cole, R. H. J. Chem. Phys. 1955, 23, 2455.

47. Cole, R. H.; Havriliak, S. Jr. Disc. Faraday Soc. 1957, 23, 31.

48. Groenewegen, P. P.; Cole, R. H. J. Chem. Phys. 1967, 46, 1069.

49. Cichanowski, S. W.; Cole, R. H. J. Chem. Phys. 1973, 59, 2420.

50. Hoshino, S.; Shimaoka, K.; Niimura, N. Phys. Rev. Lett. 1967, 19, 1286.

51. Kobayashi, T.; Ida, M.; Kawada, S. J. Phys. Soc. Japan 1969, 27, 1365.

52. Tisza, L. Phys. Rev. 1947, 72, 161.

53. Powles, J. G. Trans. Faraday Soc. 1952, 48, 430.

54. Krieger, T. J.; James, H. M. J. Chem. Phys. 1954, 22, 796.

55. Kobayashi, K. K.; Hanamura, E.; Shishido, F. Phys. Lett. 1969, 28A, 718.

56. Hanamura, E. J. Chem. Phys. 1970, 52, 797.

57. Hanamura, E. J. Phys. Soc. Japan 1970, 28 Suppl., 192.

58. Aston, J. G. J. Chem. Thermodynamics 1969, 1, 241.

CHAPTER 2

Experimental

2-1. Materials

HCl and DCl

HCl in steel bomb with a claimed purity of 99.0 mol per cent was purchased from Matheson Co., Inc. After being dried in liquid state over phosphorus pentoxide, it was distilled three times in vacuo. Solid HCl with redish pink color was not observed, which had been described by Giauque and Wiebe.[1] The final purity was 99.98_0 mol per cent as determined by the fractional melting method during the calorimetry in the last series of the measurements. Probable impurities are H_2, Cl_2, and $POCl_3$, the last one being one of the products of the reaction of gaseous HCl with P_2O_5. The presence of H_2 should affect the heat capacity of HCl at about 14 K as seen in the results of Clusius,[2] who estimated the amounts of H_2 from excess heat capacity. However, present results showed no such indication (see below). Total amounts of specimen used for the calorimetric measurements were determined to be $(0.2025_8 \pm 0.0002)$ mol by P-V-T measurements using a calibrated volume of the external gas-handling system. Non-ideality of HCl gas was corrected for by the Berthelot equation with the critical pressure of 8.26 MPa and the critical temperature of 324.7 K.[3] The uncertainty in sample amounts arising from that of the critical constants is

not more than 0.01 per cent.

DCl gas was prepared by the reaction:

$$SiCl_4 + 2D_2O \longrightarrow SiO_2 + 4DCl \qquad (2\text{-}1)$$

Commercial $SiCl_4$ and D_2O (CEA) with an isotopic purity of 99.84 per cent were separately outgassed and $SiCl_4$ was transferred upon D_2O. The reaction proceeded slowly in 24 hr. The DCl thus prepared was stored in the gaseous state and subsequent purification procedures were the same as those for HCl. The purity was 99.97_6 mol per cent. Amounts of specimen used were ($0.2106_6 \pm 0.0002$) mol, the critical constants employed being 8.26 MPa and 323.5 K.[4]

HBr and DBr

HBr (Matheson Co., Inc., claimed purity 99.8 mol per cent) was dried in liquid state over phosphorus pentoxide and distilled three times in vacuo. The final purity was 99.98_7 mol per cent as determined by the fractional melting method. Total amounts of specimen used for the calorimetric measurements were determined by P-V-T measurements to be ($0.1933_3 \pm 0.0002$) and ($0.2046_6 \pm 0.0002$) mol for Samples I and II, respectively. Non-ideality of HBr gas was corrected for by the Berthelot equation with the critical pressure

of 8.56 MPa[5] and the critical temperature of 363.1 K.[6] The correction amounted to 0.8 per cent of the total amounts.

DBr gas for Sample I was purchased from Stohler Isotope Chemicals. Its stated isotopic purity was 99 per cent. DBr for Sample II was prepared in the dark by the reaction:

$$PBr_3 + 3D_2O \longrightarrow D_3PO_3 + 3DBr \qquad (2\text{-}2)$$

D_2O (CEA) used had a stated isotopic purity of 99.84 per cent. For both samples, purification procedures were the same as those for HBr and the purity was 99.92_7 mol per cent. Amounts of specimen used were $(0.0965_3 \pm 0.0002)$ and $(0.2053_5 \pm 0.0002)$ mol for Samples I and II respectively, the constants employed being 8.56 MPa and 362.0 K.[4] The gases contaminated stopcock grease (silicone) of the external gas-handling system.

HI and DI

HI (Matheson Co., Inc., claimed purity 98.0 mol per cent) was dried in the liquid state over phosphorus pentoxide and distilled three times in vacuo. The final purity was 99.97_5 mol per cent as determined by the fractional (intermittent) melting method.

Total amounts of specimen used for the calorimetric study were determined by P-V-T measurements to be $(0.1890_4 \pm 0.0002)$ mol. Non-ideality of HI gas was corrected for by the Berthelot equation with the critical pressure of 8.40 MPa and the critical temperature of 424.1 K.[6]

DI gas was prepared in the dark by the reaction:

$$P + 5I + 4D_2O \longrightarrow D_3PO_4 + 5DI \qquad (2\text{-}3)$$

D_2O (CEA) used had a stated isotopic purity of 99.84 per cent. Purification procedures were the same as those for HI and the purity was 99.99_4 mol per cent. Amounts of specimen used were $(0.2190_8 \pm 0.0002)$ mol, the critical constants employed being 8.40 MPa and 421.8 K.[4] The gases considerably contaminated stopcock grease (silicone) of the external gas-handling system.

2-2. Calorimeter

The cryostat and adiabatic calorimeter (gold) designed for condensed substances have been described previously.[7] A measuring circuitry including the automatic adiabatic control system was the same as reported earlier,[7] except for the use of automatic data acquisition system for temperature measurements below 5 K. Both before and after the whole series of measurements of HX and DX, the heat capacity of the empty vessel was measured below 300 K. The two independent measurements gave consistent results, indicating that no permanent reaction such as corrosion of the calorimeter had taken place.

2-3. Temperature scales

The calorimeter is equipped with two thermometers, a platinum resistance thermometer (Model 8164, Leeds & Northrup Co.) to use above 14 K and a germanium resistance thermometer (CR-1000, CryoCal Inc.) to use below 14 K. We shall now describe their calibrations.

Platinum thermometer

This thermometer was originally calibrated in 1966 by the U. S. National Bureau of Standards based on the IPTS-48 and NBS-55 temperature scales. The scale was then converted to the IPTS-68.[8] In order to check for the aging effect during the eight years, recalibration was carried out in 1974[9] against the triple, boiling, and sublimation points n-H_2, Ne, N_2, O_2, and CO_2 and also their vapor pressure scales. However, fixed points of n-H_2 and CO_2 could not be realized because of ortho-para conversion phenomenon and insufficient heat treatment, respectively.
The results shown in figure 2-1 suggest that the platinum scale showed increases of 2∿3 mK in 8 year's time between 14 and 90 K. However, it was ascertained that the slope of the scale did not change appreciably to such an extent as to affect the heat capacity values.

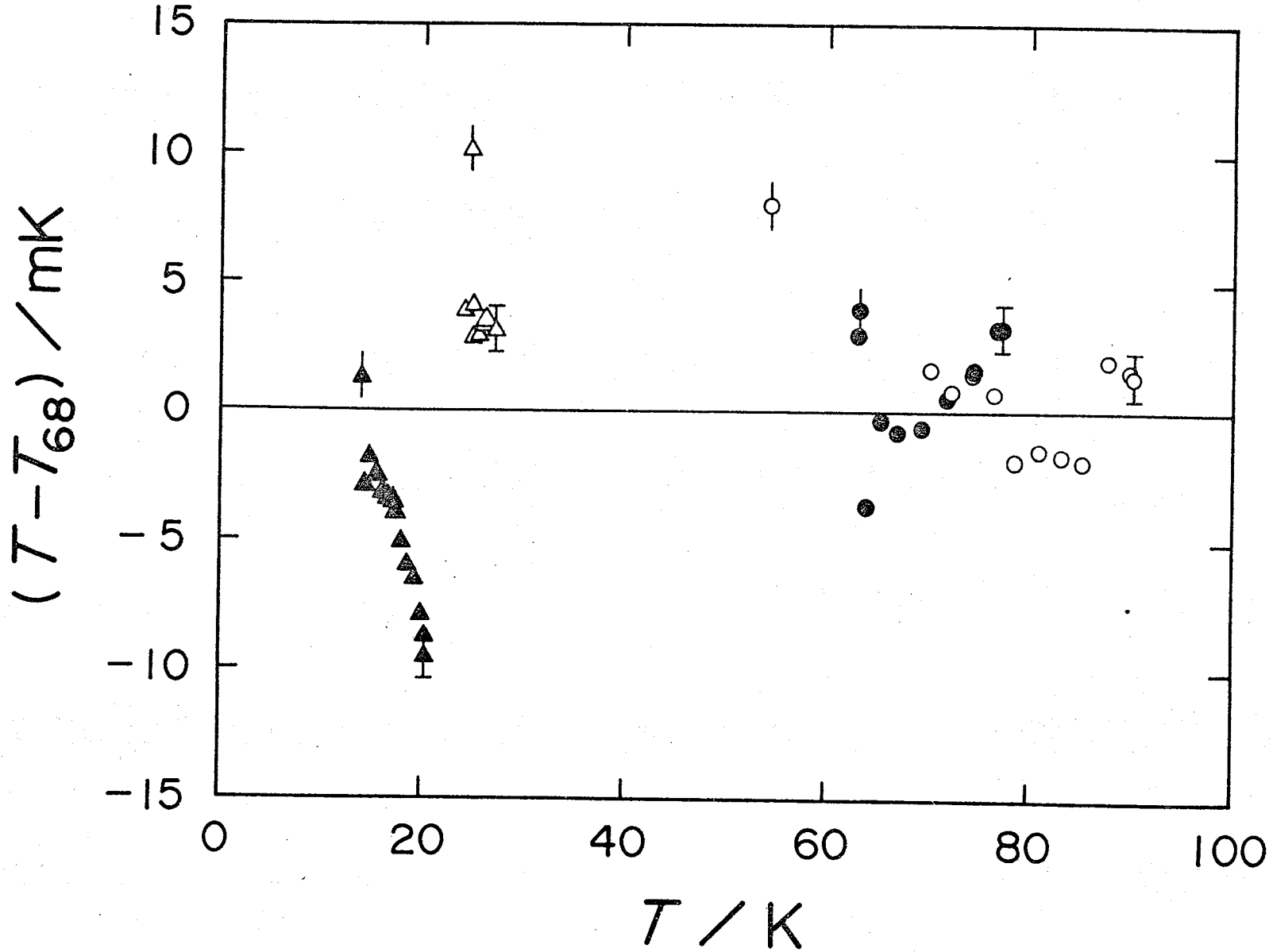

FIGURE 2-1. Calibration of the platinum thermometer based on IPTS-68 against triple (|) and boiling (I) points and vapor pressure thermometers. ▲, n-H_2; △, Ne; ●, N_2; ○, O_2.

Germanium thermometer

The germanium scale was fixed by the 1958 ^{4}He vapor pressure scale below 4.2 K and the ^{4}He gas thermometric temperature scale between 4.2 and 15 K.[9]

The following function was used for fitting the calibration points by the method of least squares.

$$\log_{10} R = \sum_{i=1}^{10} A_i \cdot T^{(i-4)} \qquad (2\text{-}4)$$

The scale could be determined to within $\pm$5 mK as shown in figure 2-2. However, T_{58} scale was found to be lower by about 0.2 per cent at 4.2 K than thermodynamic temperature scale. This discontinuity is in agreement with the one reported at the 10th meeting of the Comité Consultatif de Thermométrie (CCT) held in Paris in May 1974.[10] The resulting error in heat capacity did not exceed 0.5 per cent, which is much smaller than 5 per cent in this temperature region as will be seen below.

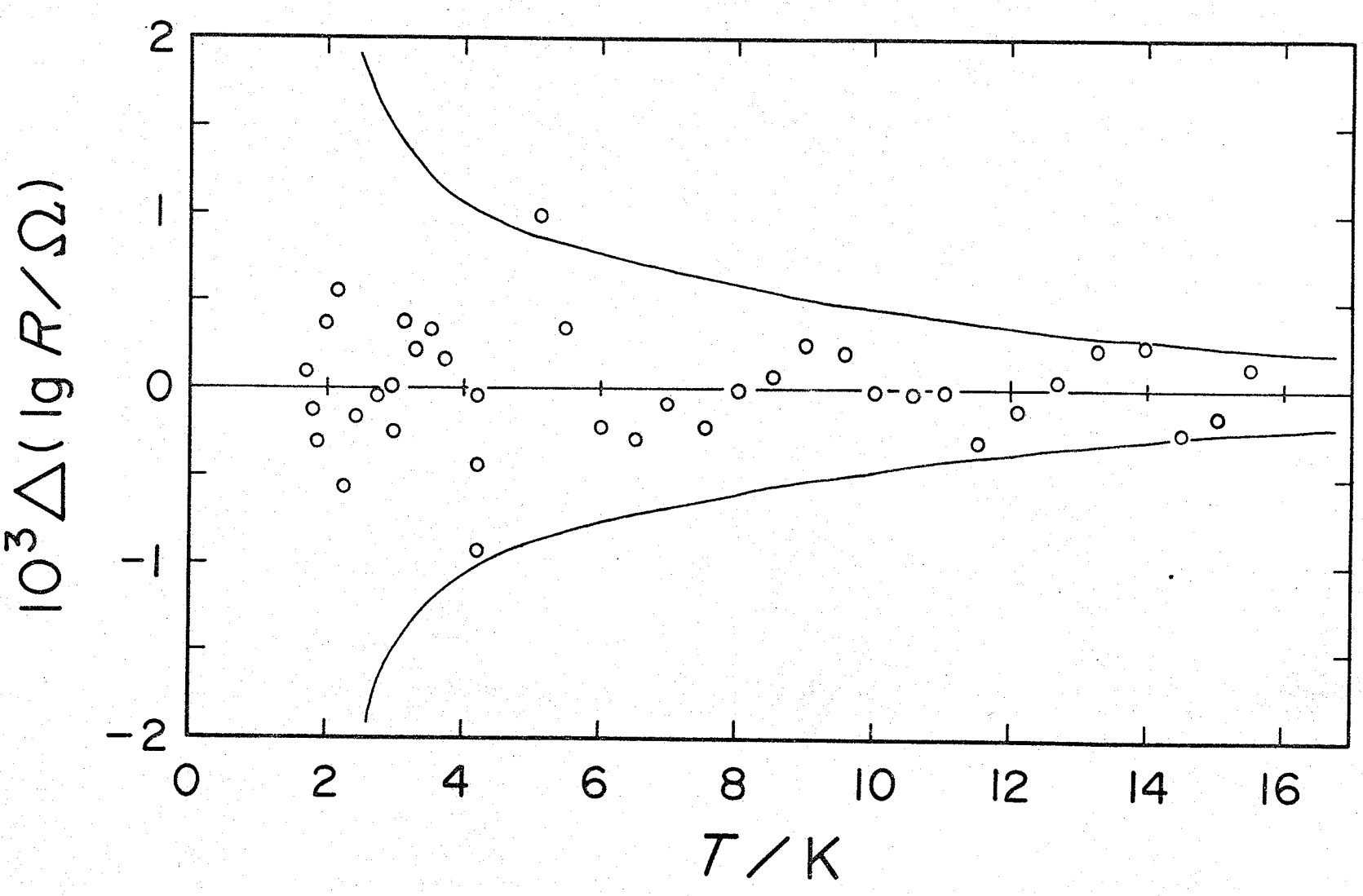

FIGURE 2-2. Calibration of the germanium thermometer based on T_{58} and ^{4}He gas thermometer scales. The deviations from the scale obtained by the method of least squares are plotted. Two curves show the deviation of $\pm$ 5 mK.

2-4. Heat capacity measurements

The heat capacities of HCl and DCl were measured between 2 and 164 K. The temperature increments were about 0.3 K at the lowest temperatures and about 1 K at 10 K. These were increased to about 2.5 K at higher temperatures, except in the vicinity of transtitions of HCl and DCl and near 120 K in HCl. Where vapor pressure was significant, the temperature of the filling tube was so adjusted that the calorimeter was the coldest in order to prevent distillation of the specimen out of the calorimeter. Thus, the top of the adiabatic shield was made slightly warmer (up to 0.3 K) than the calorimeter vessel. The resulting temperature drift due to heat leakage was taken into account in calculating the heat capacity. This correction did not usually exceed about 0.2 per cent of total heat capacity. No helium gas was introduced into the calorimeter vessel for heat exchange. Equilibration times after heating were a few seconds at the lowest temperatures, 3 min at 20 K, and 10 min at 80 K. About 80 K, except for the transition regions, the sample vapor helped to improve the equilibration time. The calorimeter vessel contributed about 60 per cent of the total heat capacity at all temperatures covered.

The heat capacities of HBr and DBr were measured

between 2 and 190 K. The temperature increments were about 0.2 K at the lowest temperatures and about 1 K at 10 K. These were increased to about 2.5 K at higher temperatures, except in the vicinity of transitions. Above 140 K, where vapor pressures were significant, the filling tube and also the top of the adiabatic shield were made slightly warmer than the calorimeter vessel in order to prevent distillation. No helium gas was introduced into the vessel for heat exchange. The calorimeter vessel contributed not more than about 60 per cent of the total heat capacity for HBr and DBr (Sample II) at all temperatures covered. For DBr (Sample I), the contribution increased up to about 75 per cent.

The heat capacities of HI and DI were measured between 2 and 225 K. The temperature increments were about 0.3 K at the lowest temperatures and about 1 K at 10 K. These were increased to about 2.5 K at higher temperatures, except in the vicinity of transitions. Above 150 K where vapor pressures were significant, the filling tube and also the top of the adiabatic shield were made slightly warmer than the calorimeter vessel in order to prevent distillation. No helium gas was introduced into the vessel for heat exchange. The calorimeter vessel contributed about 20 per cent

to the total heat capacity at the lowest temperatures. It increased up to 60 per cent above 50 K except in the vicinity of transitions.

2-5. Vapor pressure measurements

The vapor pressures of the solid in phase I and the liquid were measured in conjunction with the heat capacity measurements. A quartz Bourdon gage (Texas Instruments Inc., Model 144-01) was used for pressure measurements. The gage was calibrated against a mercury manometer: The ratio of pressure value to gage reading was a smooth function of the pressure to within 0.1 per cent up to 105 kPa. The mean density of mercury at the temperature in a barometric column supported by the pressure being measured is given by reference 8. The gravitational acceleration at our laboratory was taken to be 9.79695 m s^{-2}, which had been corrected for latitude and altitude from the value of 9.7970375 m s^{-2} at Osaka International Airport. The precision of pressure measurements is ± 1 Pa but the accuracy is probably somewhat less than this because of undetectable drift of null point.

2-6. Dilatometry

After measurements of heat capacity and vapor pressure for Sample II of HBr were concluded, an attempt was made to determine the thermal expansion of solid HBr by using helium gas as the dilatometric sensor between 65 and 120 K. The volumes of the specimen and the empty vessel were about 6 and 44 cm^3, respectively. The latter volume was separately measured as a function of temperature after driving the specimen out of the vessel. The equilibrium temperature and helium pressure were measured at about 5 K intervals. To obtain the maximum sensitivity, helium gas pressure was adjusted to about 100 kPa, some helium gas being withdrawn each time it tends to exceed the working range of the Bourdon gage. Expansion of the helium gas and of the vessel was subtracted from the measured pressure increment to compute the change of the specimen. Since the precision of pressure measurement was 10 parts per million at 100 kPa, the smallest detectable expansivity α is given by

$$\alpha \cdot \Delta T \cdot (v/V) = 10 \text{ parts per million}, \qquad (2\text{-}5)$$

where ΔT is the temperature increment, v the volume of specimen, and V the volume of helium gas. In the present experiment, detectable limit of α is estimated

to be 1.3×10^{-5} K^{-1}. Since the expansivity of an average molecular crystal is of the order of 10^{-4} K^{-1}, determination of the expansivity to two significant figures was anticipated by this experimental technique. In fact, the volume changes at three transitions of HBr were observed. Quantitatively, however, expansivities obtained were systematically amaller than those estimated from densities by the X-ray diffraction method. The data obtained, therefore, will not be presented. Supposed origins of error are adsorption or desorption of the helium gas, undetectable drift of null point of the Bourdon gage, and inaccuracy of virial coefficients of helium.

REFERENCES to CHAPTER 2

1. Giauque, W. F.; Wiebe, R. J. Am. Chem. Soc. 1928, 50, 101.
2. Clusius, K. Z. Phys. Chem. B 1929, 3, 41.
3. Gambill, W. R. Chem. Eng. 1959, 66, 157.
4. Kopper, H. Z. Phys. Chem. A 1936, 175, 469.
5. Drozdowski, E.; Pietrzak, J. Bull. Acad. Crac. A 1913, 239.
6. Woolsey, G. J. Am. Chem. Soc. 1937, 59, 1577.
7. Atake, T.; Chihara, H. Bull. Chem. Soc. Japan 1974, 47, 2126.
8. The International Temperature Scale of 1968. Metrologia 1969, 5, 35.
9. Chihara, H.; Inaba, A. Teion Kogaku 1975, 10, 84.
10. Mitsui, K. Keiryo Kanri 1975, 24, 36.

CHAPTER 3

Thermodynamic Properties of HCl and DCl

3-1. Heat capacity

The experimental results without curvature corrections are listed in chronological order in appendices 3A and B for HCl and DCl, respectively. Smoothed values of the heat capacity of the solids are given in table 3-1. Strictly speaking, what was measured was the heat capacity under the saturated vapor pressure, which is commonly denoted by C_s. However, the difference between C_s and C_p is negligibly small because the pressures are low in the measured temperature range. Above 130 K, corrections for the vaporization of HCl or DCl, which occurred during the heat capacity measurements, were significant (about 0.1 per cent at 130 K). Quantities relevant for these corrections were evaluated as follows. The vapor volume in the calorimeter vessel was calculated by using 1.46_9 and 1.4_3 g cm^{-3} for the density of HCl[1] at 107 K and at the triple point, respectively, and the liquid density by Kanda.[2] Density of solid and liquid DCl was assumed to be larger by 3 per cent than that of HCl on the basis of the X-ray diffraction data at 118.5 K[3] and the molecular weight. The heat capacity of the gases calculated from the spectroscopic data[4] is close to (7/2)R in the temperature range where the values were required. The total corrections amounted

TABLE 3-1. The heat capacity of solid HCl and DCl at rounded values of temperatures.

$\frac{T}{K}$	$\frac{C_p}{JK^{-1}mol^{-1}}$	
	HCl	DCl
2	0.0052	0.0053
3	0.0179	0.0180
4	0.043	0.044
5	0.088	0.090
6	0.161	0.167
8	0.429	0.439
10	0.920	0.944
12	1.647	1.678
15	3.101	3.133
20	5.980	6.014
25	8.870	8.956
30	11.54	11.72
35	13.89	14.24
40	15.94	16.54
45	17.77	18.65
50	19.43	20.63
55	20.98	22.51
60	22.46	24.31

TABLE 3-1. Continued.

T/K	C_p / $JK^{-1}mol^{-1}$	
	HCl	DCl
65	23.88	26.03
70	25.27	27.68
75	26.69	29.30
80	28.16	30.93
85	29.75	32.62
90	31.59	34.45
95	34.20	36.49
100	39.99	38.86
110	41.45	44.74
120	42.93	46.11
130	44.43	47.50
140	46.04	48.94
150	48.00	50.80
153	48.84	52.00

to at most about 3 per cent of the total input energy.

The results for HCl and DCl are shown in figures 3-1 and 3-2, respectively. Both solid HCl and DCl have one isothermal phase transition. A discussion of other "transition" at 120 K in solid HCl will be given below.

The measured heat capacities of solid HCl and DCl are compared with earlier results in figures 3-3 and 3-4, respectively. The results are plotted as differences from a smooth curve corresponding to the values given in table 3-1. The deviation of the present results from the smooth curve, which indicates the precision, is ± 5 per cent at the lowest temperatures, which decreases to less than ± 0.5 per cent at 10 K, ± 0.1 per cent above 20 K, and ± 0.2 per cent at higher temperatures. Giauque and Wiebe's results for HCl[5] are systematically lower than the present results by about 1 per cent below 80 K, but the differences are within the combined limits of error. Results of Clusius[6] are similar to those of Eucken and Karwat.[7] Both results, however, were fairly scattered and different from ours. Four results agree well at about 20 and 90 K, which approximately correspont to the temperatures of liquid hydrogen and liquid air. Below 15 K, the results to be compared with ours are only those of Clusius. Their results are in

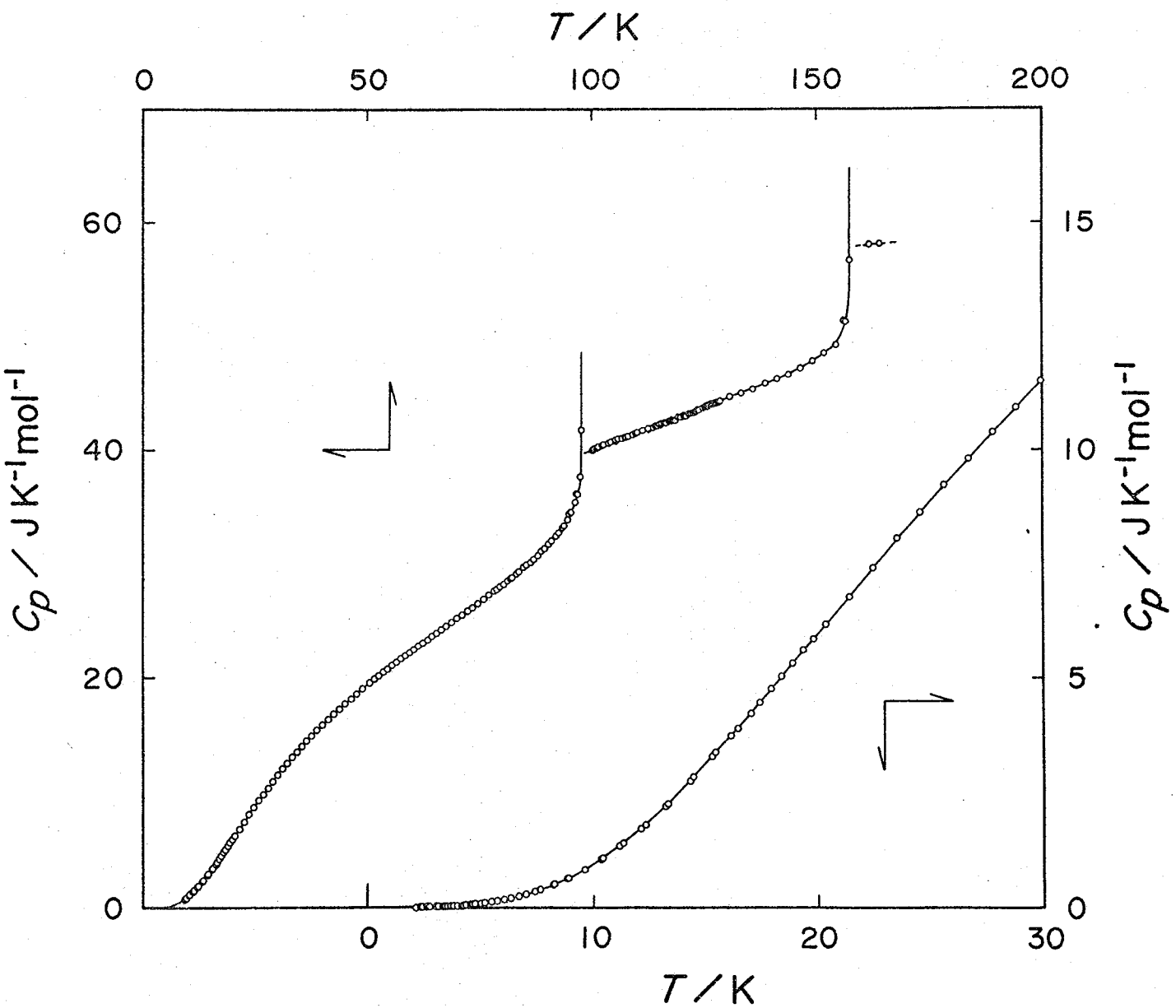

FIGURE 3-1. Heat capacity of HCl.

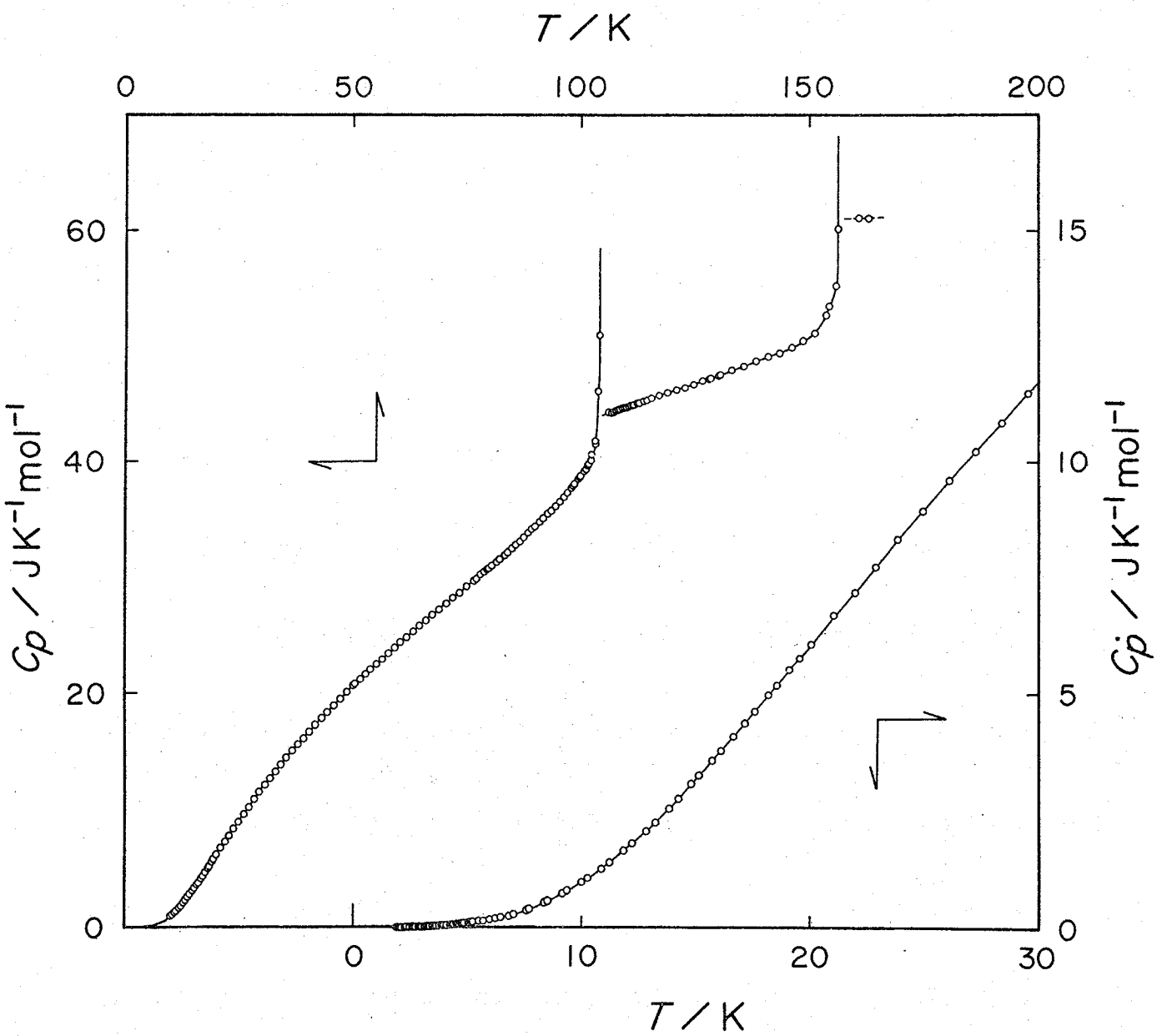

FIGURE 3-2. Heat capacity of DCl.

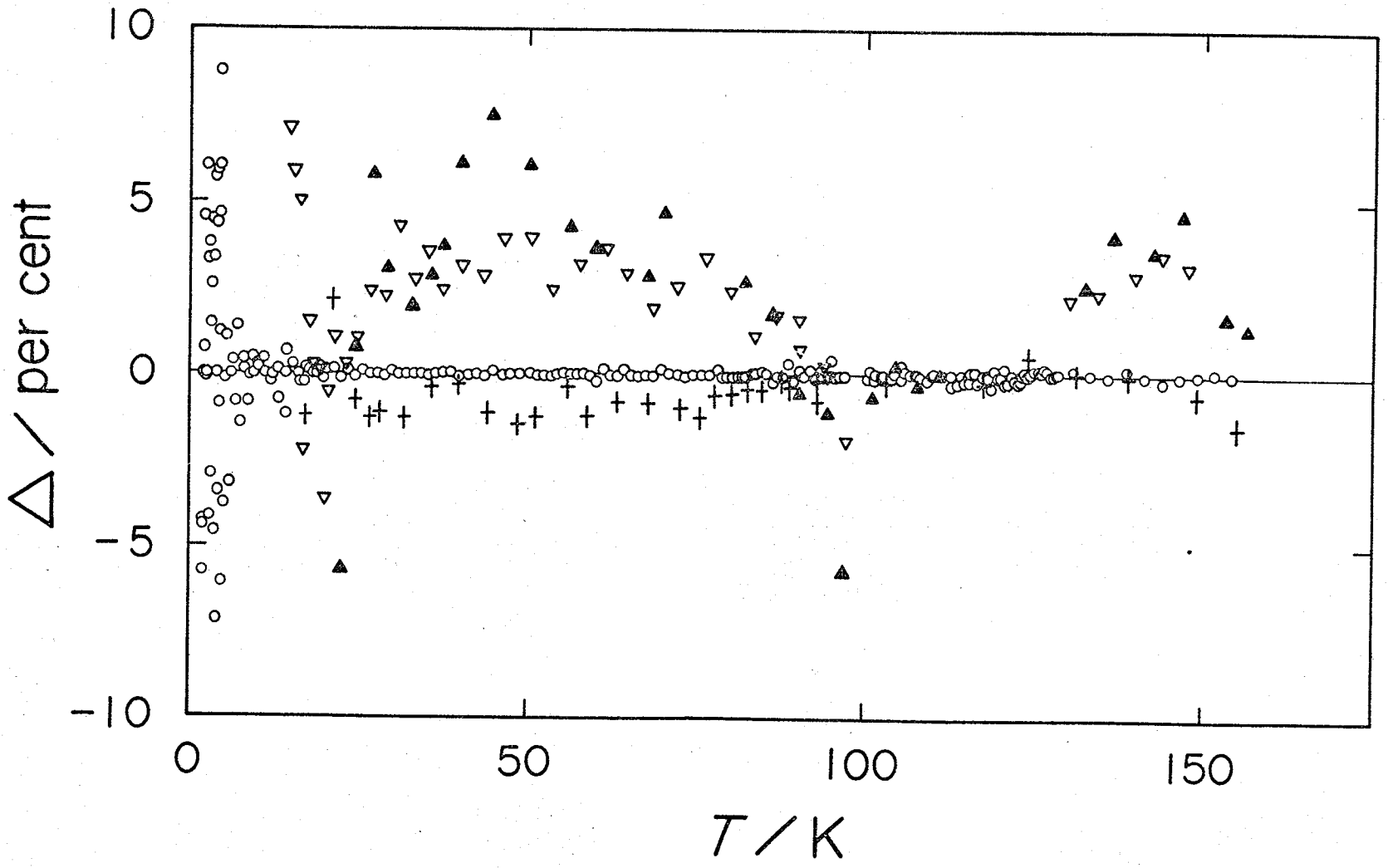

FIGURE 3-3. A comparison of heat capacity results for solid HCl. o, present results; ∇, Clusius;[6] +, Giauque and Wiebe;[5] ▲, Eucken and Karwat.[7] Δ/per cent = [C_p(obs.)-C_p(smooth)] x 100 / [C_p(smooth)], where C_p(smooth) is given in table 3-1.

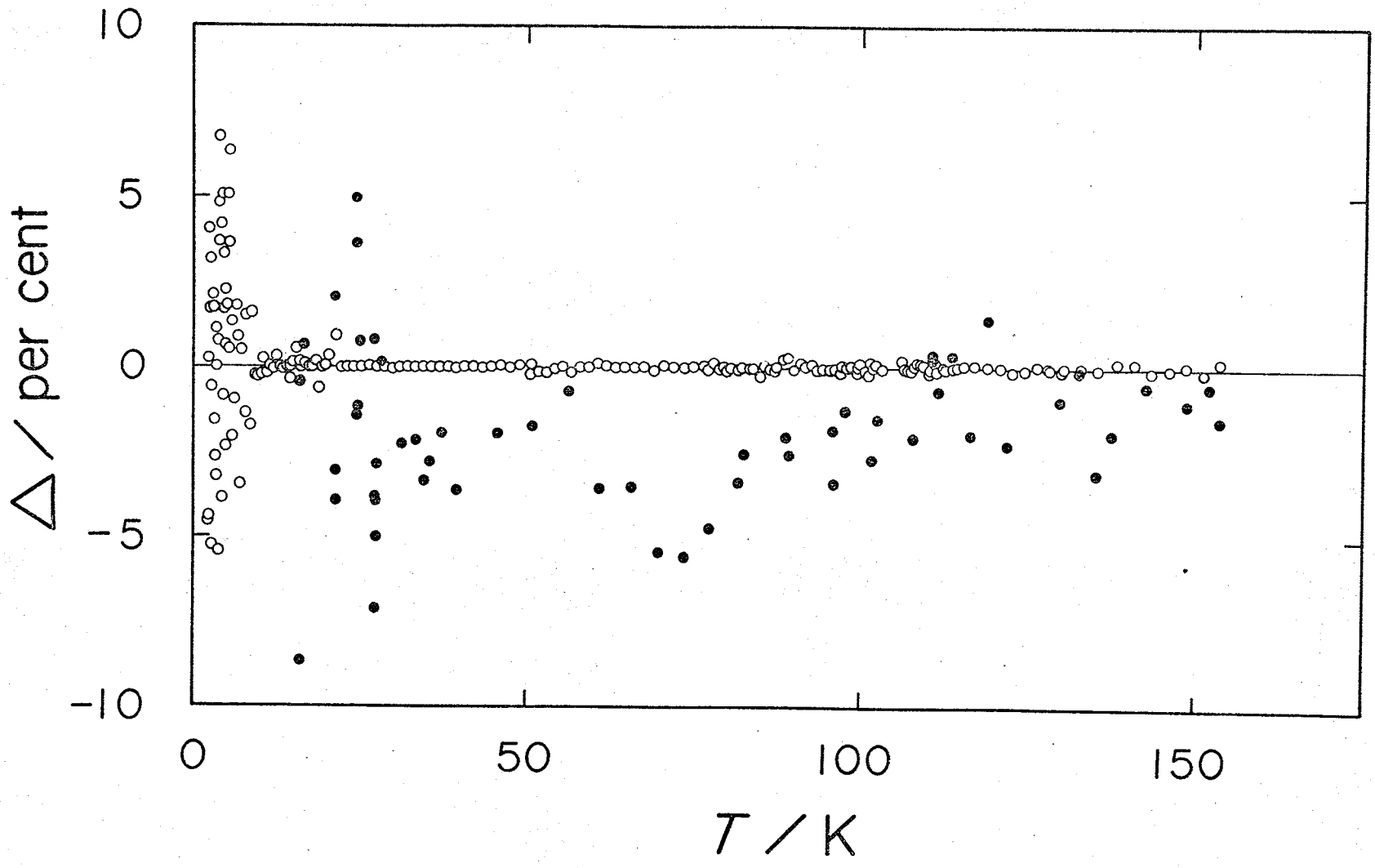

FIGURE 3-4. A comparison of heat capacity results for solid DCl. o, present results; ●, Clusius and Wolf.[8]
Δ/per cent = [C_p(obs.)-C_p(smooth)] x 100 / [C_p(smooth)], where C_p(smooth) is given in table 3-1.

excess of our smoothed heat capacities by more than 20 per cent, which can't be plotted in figure 3-3. It was explained to come from 0.25 mol per cent of H_2 as an impurity.[6]

Heat capacities of DCl have been measured above 15 K by Clusius and Wolf.[8] A comparison of their results with present results shows agreement in absolute value only at about 20 K. At other temperatures, however, they are systematically lower than ours.†

A more sensitive comparison in the lower temperature region can be made by use of equivalent Debye temperature Θ_D, whose temperature dependence for $3N_A$ degrees of freedom is shown in figures 3-5 and 3-6 for HCl and DCl, respectively. The Debye temperature curves for HCl and DCl are almost superimposable below about 25 K although the former is consistently higher by a factor of 1.008. Above 25 K the DCl curve declines more rapidly.

---

† It is probably significant to note that Clusius gave, compared with ours, larger values in the case of HCl and smaller values in the case of DCl.

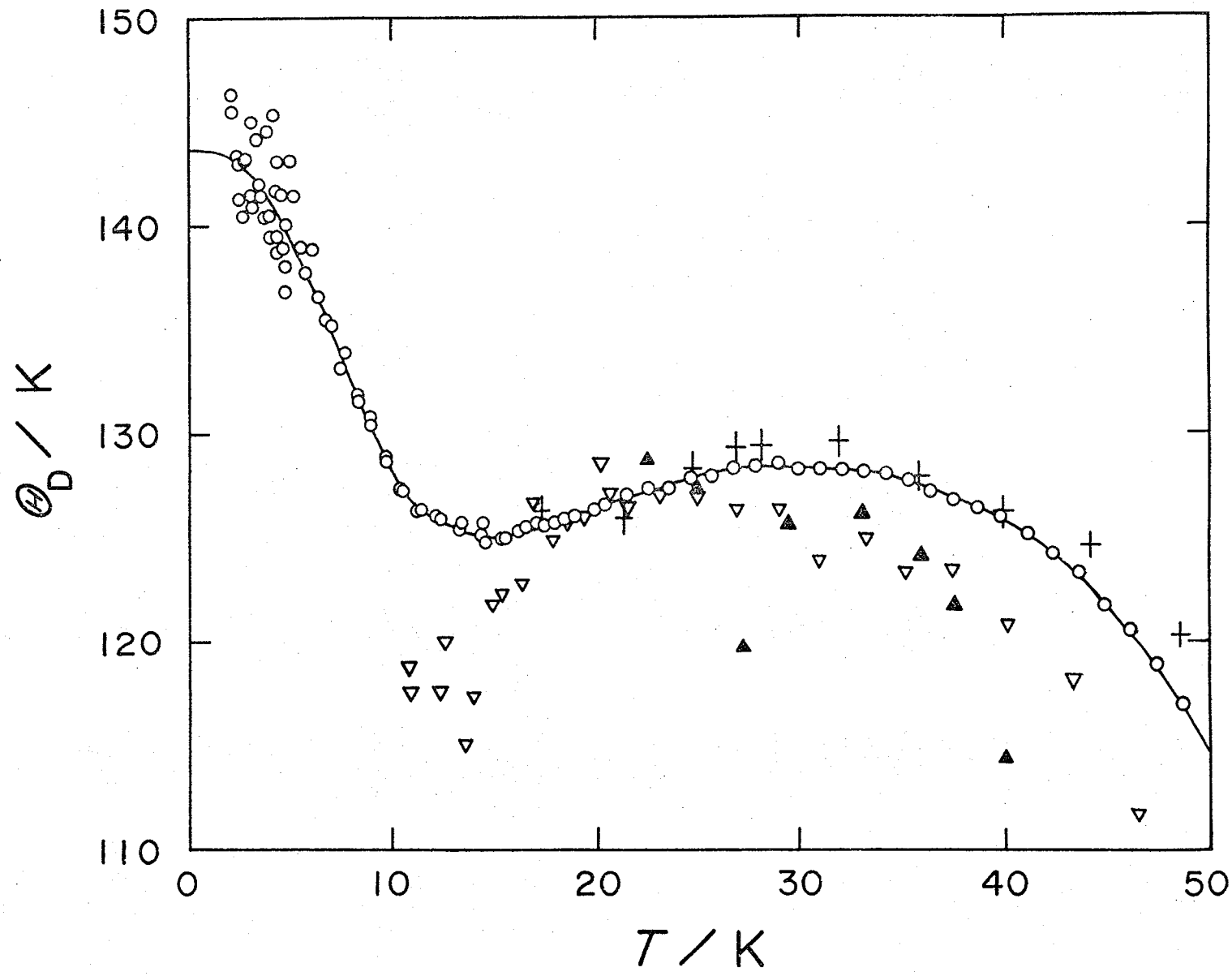

FIGURE 3-5. The Debye characteristic temperature of HCl derived from the measured heat capacities, assuming 3N degrees of freedom. o, present results; ∇, Clusius;[6] +, Giauque and Wiebe;[5] ▲, Eucken and Karwat.[7]

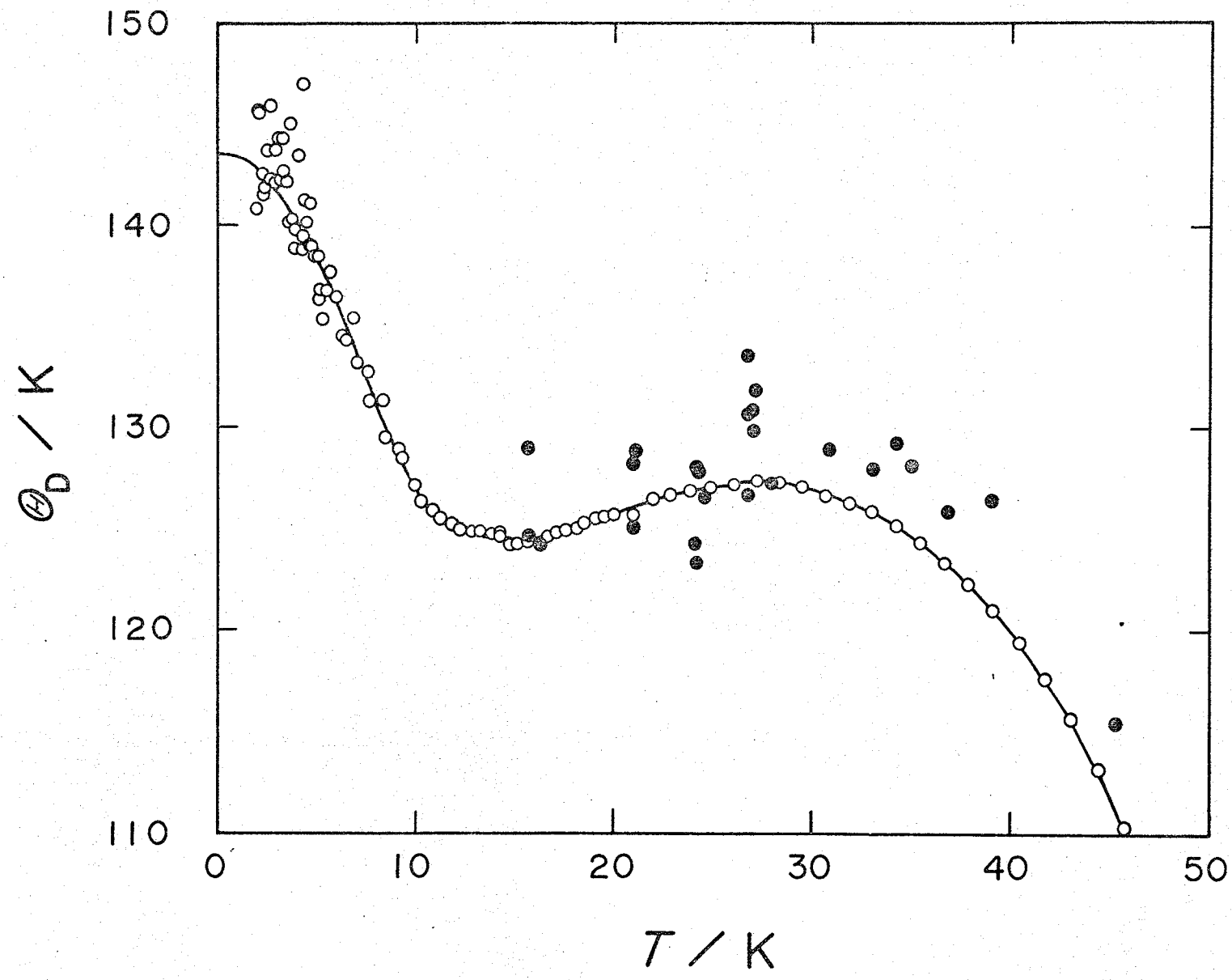

FIGURE 3-6. The Debye characteristic temperature of DCl derived from the measured heat capacities, assuming 3N degrees of freedom. o, present results; ●, Clusius and Wolf.[8]

3-2. Vapor pressure

Measured vapor pressures of the solid HCl and DCl are tabulated in the second column of tables 3-2 and 3-3, respectively. The results were fitted to the Antoine equation as follows by the method of least squares;

$$\text{HCl} \quad \log_{10}(P/\text{Pa}) = -911.31(K/T)+9.1875+0.004313(T/K) \qquad (3\text{-}1)$$

$$\text{DCl} \quad \log_{10}(P/\text{Pa}) = -1079.74(K/T)+11.5304-0.003896(T/K) \qquad (3\text{-}2)$$

Deviations from equations 3-1 and 3-2 are included in tables 3-2 and 3-3, respectively. Fitting of the results was also made to equations of the form

$$\log_{10}(P/\text{Pa}) = -A(K/T)+B \qquad (3\text{-}3)$$

The resulting coefficients A and B are given in table 3-4, where they are compared with values reported by others. A comparison with earlier results of solid HCl is shown plotted in figure 3-7 as differences from equation 3-1. The difference probably arises not only from the vapor pressure value but also from the temperature scale used. Therefore, a comparison of triple point pressure should be also referred to. In fact, Giauque and Wiebe's pressures[5] are systematically higher than ours below the triple point,

TABLE 3-2. Vapor pressures of HCl.

T / K	P / kPa	P-P(eq. 3-1) / kPa
	Solid	
131.983	0.713	0.002
134.459	0.976	-0.001
137.181	1.366	-0.002
139.873	1.881	-0.005
142.540	2.562	-0.002
145.177	3.442	0.003
147.787	4.564	0.008
150.366	5.969	0.006
152.914	7.724	0.007
155.392	9.862	0.019
155.432	9.877	-0.005
156.618	11.080	0.005
157.402	11.908	-0.024
157.794	12.364	-0.018
	Liquid	
160.600	15.744	
161.040	16.283	
162.913	18.909	
165.205	22.543	

TABLE 3-3. Vapor pressures of DCl.

T / K	P / kPa	P-P(eq. 3-2) / kPa
	Solid	
134.086	0.892	-0.011
136.802	1.285	0.012
139.485	1.786	0.023
142.125	2.395	-0.002
144.738	3.195	-0.016
147.314	4.212	-0.025
149.856	5.492	-0.022
152.355	7.081	0.003
153.052	7.584	0.008
154.876	8.981	-0.044
155.214	9.361	0.043
156.782	10.764	-0.020
157.029	11.089	0.057
	Liquid	
159.542	13.832	
159.808	14.058	
161.797	16.631	
164.039	19.855	

TABLE 3-4. Coefficients A and B for the vapor pressure equation:

$$\log_{10}(P/Pa) = -A(K/T)+B$$

	A	B
HCl		
Present work	1002.24	10.4424
Giauque and Wiebe (1928)[a]	1011.46	10.5068
Karwat (1924)[b]	1026.95	10.6023
DCl		
Present work	996.94	10.3929

[a] From reference 5.

[b] From reference 9.

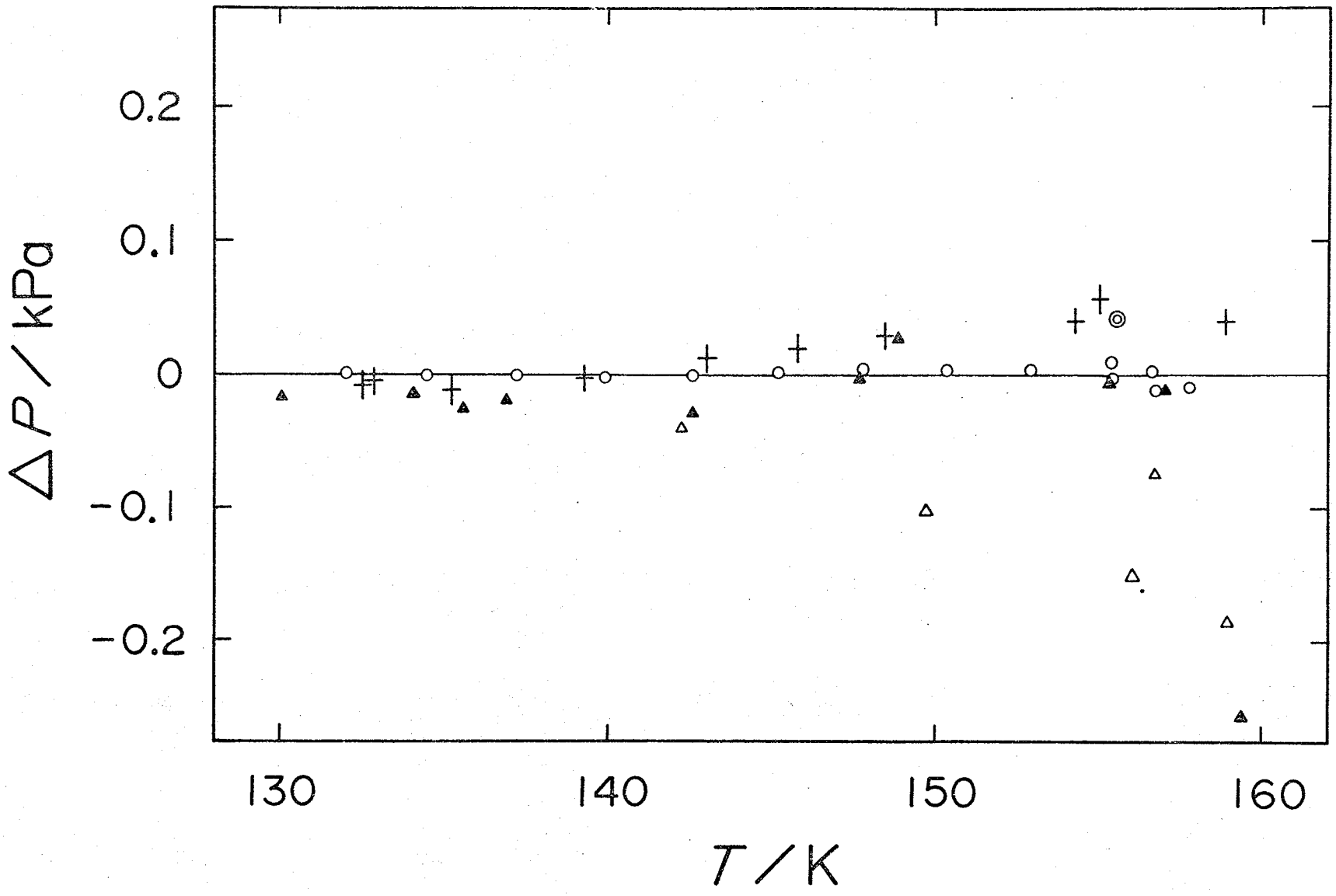

FIGURE 3-7. A comparison of vapor pressure results for solid HCl. o, present results; +, Giauque and Wiebe;[5] ▲, Karwat;[9] ◎, Henglein;[11] Δ, Henning and Stock.[12] ΔP = P(obs.)-P(smooth), where P(smooth) is given by equation 3-1.

whereas their pressure at the triple point is lower (see table 3-6). As a whole, present results for solid HCl are in agreement with those of Giauque and Wiebe and Karwat.[9]

As for solid DCl, the other measurement reported near the triple point is only one by lewis et al.,[10] which is about 150 Pa larger than ours. Isotope effect of vapor pressure of the solids may be represented by the following equation led from the type of equation 3-3.

$$\log_{10}(P_{HCl}/P_{DCl}) = -5.30(K/T)+0.0495 \qquad (3\text{-}4)$$

Lewis et al. gave fairly different equation:

$$\log_{10}(P_{HCl}/P_{DCl}) = -57.7(K/T)+0.387 \qquad (3\text{-}5)$$

Their results on solid DCl consist of only four measured points above 152 K and equation 3-5 shows that $P_{HCl} = P_{DCl}$ at 149 K, whereas our experimental results indicate that $P_{HCl} > P_{DCl}$ above 130 K.

3-3. Enthalpy of fusion and transition

The heats of fusion and transition were measured in the usual way of starting the heat input at a temperature somewhat below the melting or the transition temperature and terminating the input when the temperature had risen somewhat above. A correction for the $\int C_p dT$ was applied. The results for fusion are given in table 3-5. Other measurements are also included for the sake of comparison. In the series XIV both for HCl and for DCl, the fusion was done in stages and measurements of the equilibrium temperatures and pressures were determined likewise. The results are given in table 3-6. The triple points of pure HCl and DCl, given as (159.052 $\pm$ 0.005) and (158.410 $\pm$ 0.005) K, respectively, were estimated from a plot of the equilibrium temperature against the reciprocal of the fraction melted. From this plot, amounts of a liquid-soluble solid-insoluble impurity were also estimated. The triple point pressure of DCl calculated from the smoothed vapor pressure is not in good agreement with the measured vapor pressures. In either event, however, Clusius and Wolf's result is lower than ours. The results for isothermal phase transitions are given in table 3-7. The enthalpy of DCl obtained by Clusius and Wolf is about 3 per cent smaller than ours. Entropies of the

TABLE 3-5. The enthalpy of fusion of HCl and DCl.

Series no.	T_1 / K	T_2 / K	$H(T_2)-H(T_1)$ / $Jmol^{-1}$	ΔH_f / $Jmol^{-1}$
		HCl		
XIII	157.402 - 161.040		2181.0	1970.9
XIV[a]	157.794 - 160.620		2133.6	1970.0
			Average	1970.5
			Giauque and Wiebe (1928)[b]	1991.6
			Eucken and Karwat (1924)[c]	2110.8
		DCl		
XIII	156.782 - 159.808		2128.1	1944.6
XIV[a]	157.029 - 159.542		2097.6	1945.3
			Average	1945.0
			Clusius and Wolf (1947)[d]	1979.9

TABLE 3-5. Continued.

[a] In this series, the fusion was done in stages.

[b] From reference 5.

[c] From reference 7.

[d] From reference 8.

TABLE 3-6. The triple point of HCl and DCl.

Fraction melted	T / K	P / kPa
	HCl	
0.344	158.988	13.82
0.619	159.019	13.87
0.757	159.022	13.89
0.895	159.028	13.90
(1.000)	159.030±0.002	13.899[a]
T_f (pure HCl)	159.052±0.005	
Rossini et al. (1952)[b]	158.94	
Milosavljević (1949)[c]	159.34	13.791
Clusius (1941)[d]	158.9	13.812±0.001
Giauque and Wiebe (1928)[e]	158.91±0.05	13.83
Eucken and Karwat (1924)[f]	159.	
Karwat (1924)[g]	159.34	13.79

TABLE 3-6. Continued.

Fraction melted	T / K	P / kPa
	DCl	
0.330	158.325	12.50
0.598	158.365	12.60
0.813	158.377	12.59
0.948	158.380	12.59
(1.000)	158.383±0.002	12.478[a]
T_f (pure DCl)	158.410±0.005	
Clusius and Wolf (1947)[h]	158.44	12.17
Lewis et al. (1934)[i]	158.2	

a The value obtained from smoothed vapor pressure equation.

b From reference 13.

c From reference 14.

d From reference 6.

e From reference 5.

f From reference 7.

g From reference 9.

h From reference 8.

i From reference 10.

TABLE 3-7. The enthalpy of transition of HCl and DCl.

Series no.	T_1 / K	T_2 / K	$H(T_2)-H(T_1)$ / $Jmol^{-1}$	$H(100)-H(97)$ / $Jmol^{-1}$
		HCl		
II[a]	97.313 -	100.233	1295.5	1297.4
III[a]	97.062 -	100.584	1317.2	1296.2
IV	97.310 -	100.330	1298.7	1297.1
V	97.089 -	101.353	1347.3	1296.4
			Average	1296.8±0.6

	T_{tr} / K	ΔH_{tr} / $Jmol^{-1}$
Present work	98.67±0.01	1186.
Giauque and Wiebe (1928)[b]	98.36±0.05	1190.
Eucken and Karwat (1924)[c]	98.75	1229.
Rossini et al. (1952)[d]	98.38	
Clusius (1929)[e]	98.9	

TABLE 3-7. Continued.

Series no.	T_1 / K	T_2 / K	$H(T_2)-H(T_1)$ / $Jmol^{-1}$	$H(106)-H(103)$ / $Jmol^{-1}$
		DCl		
II	103.809	106.475	1500.4	1514.0
III[a]	103.153	105.784	1500.0	1514.3
IV[a]	102.574	106.378	1547.5	1513.5
V	103.530	105.920	1489.5	1514.6
			Average	1514.0±0.6

	T_{tr} / K	ΔH_{tr} / $Jmol^{-1}$
Present work	104.63±0.01	1386.
Clusius and Wolf (1947)[f]	105.03	1339.

[a] In this series, the transition was done in stages.

[b] From reference 5.

[c] From reference 7.

[d] From reference 13.

[e] From reference 6.

[f] From reference 8.

latent heat part of transitions were determined to be (12.02 $\pm$ 0.01) and (13.25 $\pm$ 0.01) J K^{-1} mol^{-1} for HCl and DCl, respectively.

3-4. 120 K transition in HCl

The heat capacity measurements of HCl near 120 K consist of three series. In the series I and III, the temperature increments were about 1 K, so as not to overlook any small heat anomaly. These were increased to about 2.5 K in the series XIII.

In an attempt to determine the heat capacity of single crystal HCl, the data (series I) shown by filled circles in figure 3-10 were obtained after the following heat treatment; the sample was solidified at 159 K in 100 min, maintained at 157 K for 4 hr, and cooled down to 113 K at a rate of -0.03 K min^{-1}, where the measurements of heat capacities were commenced upwards. The open circles (series III and XIII) in figure 3-8 are considered to correspond to the heat capacity of polycrystalline sample because the sample was once cooled down below 98 K. The heat capacity curve is smooth and continuous throughout the temperature range between 98 K and the triple point and there is no anomaly at or near 120 K. The supposedly single crystal also gives essentially the same heat capacity as the polycrystalline specimen. Both showed good agreement with the results by Giauque and Wiebe within the combined limits of error. If we overlooked a small heat anomaly at 120 K, its corresponding entropy would amount to

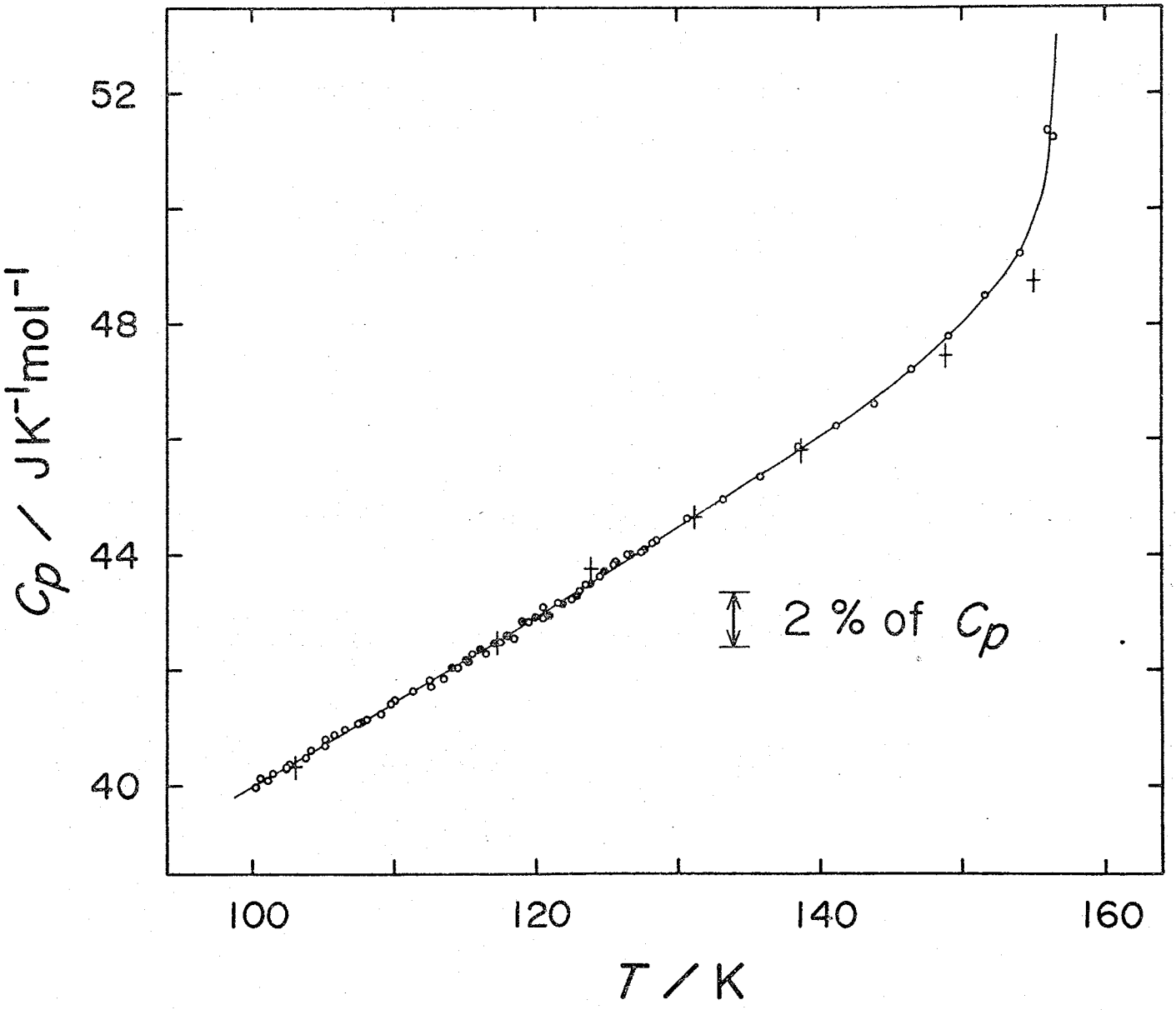

FIGURE 3- 8 . Heat capacity of solid HCl in the paraelectric phase. o, single crystal, present results; o, polycrystalline sample, present results; +, Giauque and Wiebe.[5]

$\sim 10^{-3}$ J K^{-1} mol^{-1} at most. To amplify whatever anomaly there may be at 120 K, a plot of differential heat capacity is shown in figure 3- 9. One may thus safely conclude that the "transition" at 120 K, if any, can't be seen by the heat capacity measurements.

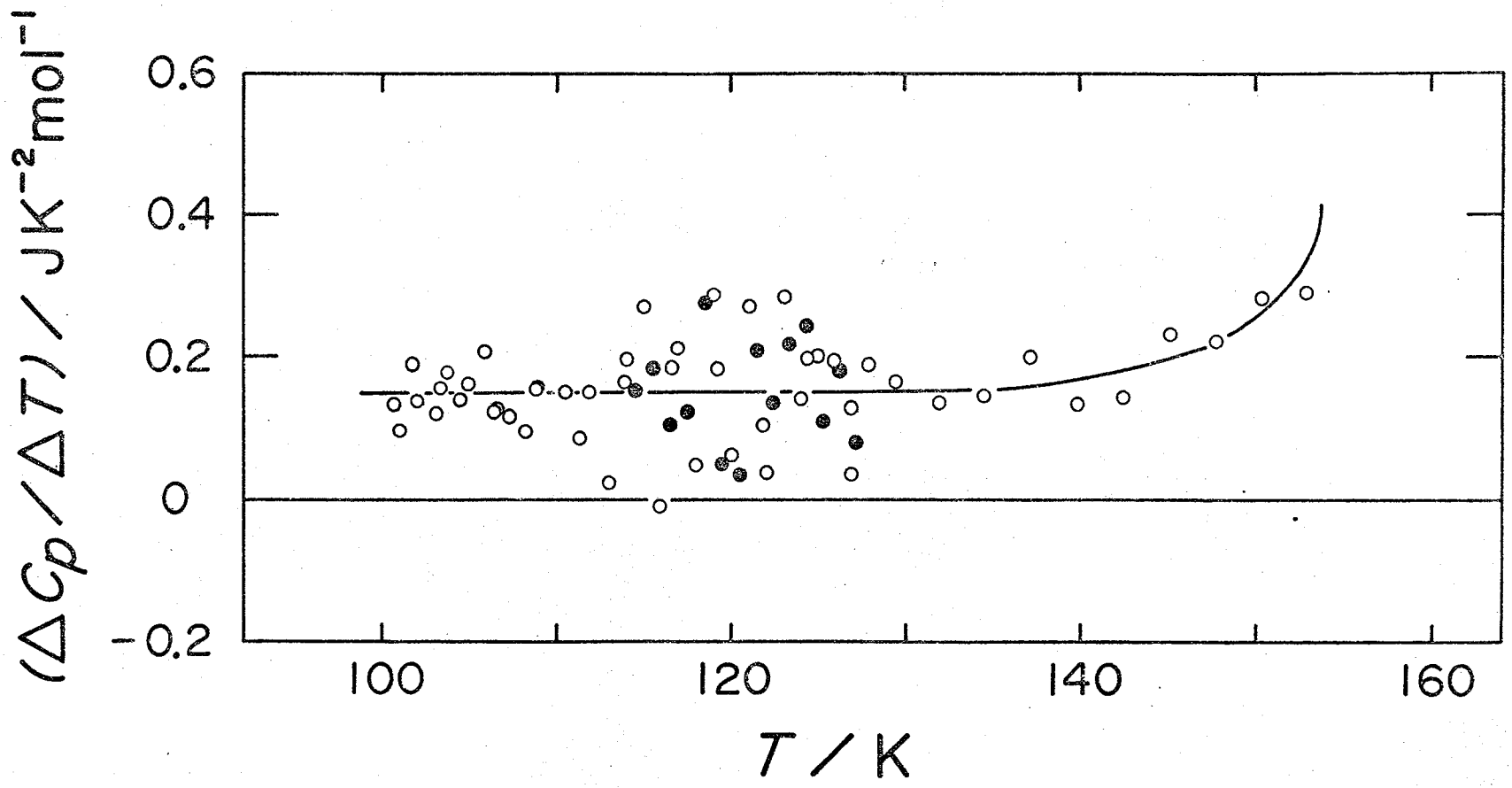

FIGURE 3- 9. The differential heat capacity. ●, single crystal; ○, polycrystalline sample.

3-5. Thermodynamic functions

The thermodynamic functions of HCl and DCl were calculated from the smoothed heat capacity values and other data described above. The contribution of the heat capacities below the lowest temperature was estimated by a smooth extraporation, which was negligibly small. The results are given in tables 3-8 and 3-9 for HCl and DCl, respectively. The entropy of liquid HCl at triple point was calculated to be 76.79 J K^{-1} mol^{-1}, which is in good agreement with 76.57 J K^{-1} mol^{-1} obtained by Giauque and Wiebe.(5) The entropy of liquid DCl at the triple point, however, was 81.02 J K^{-1} mol^{-1} in contrast with 79.36 J K^{-1} mol^{-1} by Clusius and Wolf.(8) This discrepancy arises from the difference in the results of the heat capacity and transition enthalpy measurements as shown above.

TABLE 3-8. Thermodynamic functions of HCl.

T / K	$S^{\circ}(T)-S^{\circ}(0)$ / $JK^{-1}mol^{-1}$	$\{H^{\circ}(T)-H^{\circ}(0)\}/T$ / $JK^{-1}mol^{-1}$	$-\{G^{\circ}(T)-H^{\circ}(0)\}/T$ / $JK^{-1}mol^{-1}$
		Solid	
10	0.274	0.212	0.062
20	2.296	1.712	0.584
30	5.793	4.079	1.714
40	9.745	6.520	3.225
50	13.69	8.764	4.925
60	17.50	10.80	6.705
70	21.18	12.67	8.512
80	24.74	14.42	10.32
90	28.24	16.12	12.12
100	43.88	29.82	14.06
110	47.76	30.81	16.95
120	51.43	31.76	19.67
130	54.93	32.68	22.25
140	58.28	33.58	24.70
150	61.52	34.47	27.05
159.0	64.40	35.36	29.04
		Liquid	
159.0	76.79	47.75	29.04

TABLE 3-9. Thermodynamic functions of DCl.

T / K	$S^{\circ}(T)-S^{\circ}(0)$ / $JK^{-1}mol^{-1}$	$\{H^{\circ}(T)-H^{\circ}(0)\}/T$ / $JK^{-1}mol^{-1}$	$-\{G^{\circ}(T)-H^{\circ}(0)\}/T$ / $JK^{-1}mol^{-1}$
		Solid	
10	0.281	0.217	0.064
20	2.329	1.735	0.594
30	5.866	4.129	1.737
40	9.919	6.648	3.271
50	14.06	9.046	5.014
60	18.15	11.29	6.863
70	22.15	13.39	8.763
80	26.06	15.38	10.68
90	29.90	17.29	12.61
100	33.75	19.22	14.53
110	51.05	33.95	17.10
120	55.00	34.90	20.10
130	58.74	35.81	22.93
140	62.31	36.70	25.61
150	65.75	37.58	28.17
158.4	68.74	38.49	30.25
		Liquid	
158.4	81.02	50.77	30.25

REFERENCES to CHAPTER 3

1. Simon, F.; v. Simson, C. Z. Phys. 1924, 21, 168.
2. Kanda, E. Bull. Chem. Soc. Japan 1937, 12, 473.
3. Sándor, E.; Farrow, R. F. C. Nature 1967, 213, 171.
4. Plyler, E. K.; Tidwell, E. D. Z. Electrochem. 1960, 64, 717.
5. Giauque, W. F.; Wiebe, R. J. Am. Chem. Soc. 1928, 50, 101.
6. Clusius, K. Z. Phys. Chem. B 1929, 3, 41.
7. Eucken, A.; Karwat, E. Z. Phys. Chem. 1924, 112, 467.
8. Clusius, K.; Wolf, G. Z. Naturforsch. 1947, 2a, 495.
9. Karwat, E. Z. Phys. Chem. 1924, 112, 486.
10. Lewis, G. N.; MacDonald, R. T.; Schutz, P. W. J. Am. Chem. Soc. 1934, 56, 495.
11. Henglein, F. A. Z. Phys. 1923, 18, 64.
12. Henning, F.; Stock, A. Z. Phys. 1921, 4, 226.
13. Rossini, F. D.; Wagman, D. D.; Evans, W. H.; Levine, S.; Jaffe, I. NBS Circ. 1952, 500, 549.
14. Milosavljević, D. M. Glasnik Hem. Drostva Beograd 1949, 14, 13.

Appendix 3A. Measured heat capacities of HCl.

T / K	C_p / $JK^{-1}mol^{-1}$	T / K	C_p / $JK^{-1}mol^{-1}$
		52.358	20.15
Series I		53.318	20.44
114.067	42.05	54.282	20.76
115.065	42.20	55.250	21.07
116.059	42.38	56.223	21.35
117.049	42.48	57.201	21.64
118.035	42.60	58.177	21.94
119.016	42.87	59.150	22.20
119.993	42.92	60.129	22.44
120.968	42.95	61.118	22.82
121.938	43.15	62.116	23.05
122.905	43.28	63.127	23.34
123.868	43.49	64.149	23.68
124.829	43.72	65.185	23.92
125.786	43.83	66.273	24.22
126.739	44.00	67.415	24.54
127.688	44.07	68.572	24.86
		69.734	25.23
Series II		70.904	25.53
51.390	19.85	72.080	25.86

Appendix 3A. Continued.

T/K	C_p/$JK^{-1}mol^{-1}$	T/K	C_p/$JK^{-1}mol^{-1}$
73.264	26.17	101.426	40.21
74.457	26.53	102.608	40.38
75.651	26.88	104.113	40.61
76.847	27.23	105.770	40.88
78.044	27.62	107.413	41.09
79.441	27.98	109.042	41.24
81.035	28.45		
82.074	28.77	Series III	
83.652	29.31	78.717	27.77
85.260	29.86	80.230	28.20
86.892	30.39	81.720	28.66
88.535	31.12	83.078	29.12
90.164	31.69	84.619	29.65
91.780	32.38	86.237	30.11
93.384	33.16	87.828	30.72
94.973	34.35	89.395	31.28
96.539	36.12	90.948	31.96
97.677	41.70	92.529	32.64
Transition		93.739	33.28
100.575	40.13	94.549	33.80

Appendix 3A. Continued.

T / K	C_p / $JK^{-1}mol^{-1}$	T / K	C_p / $JK^{-1}mol^{-1}$
95.363	34.48	116.476	42.28
96.172	35.29	117.490	42.50
96.818	36.04	118.517	42.55
97.302	37.58	119.538	42.84
97.771	41.97	120.555	42.90
98.173	75.16	121.568	43.17
Transition		122.569	43.21
100.213	39.97	123.552	43.49
101.131	40.09	124.524	43.62
102.380	40.33	125.493	43.82
103.774	40.49	126.456	44.00
105.162	40.68	127.432	44.04
106.539	40.97	128.519	44.24
108.077	41.14		
109.775	41.41	Series IV	
111.293	41.64	Transition,	
112.505	41.82	Continuous Heating	
113.528	41.84		
114.500	42.03		
115.482	42.29		

Appendix 3A. Continued.

T/K	C_p/$JK^{-1}mol^{-1}$	T/K	C_p/$JK^{-1}mol^{-1}$
		3.531	0.0303
Series V		3.946	0.0430
Transition,		4.364	0.0605
Continuous Heating		4.765	0.0821
Series VI		Series VIII	
2.067	0.00548	2.128	0.00607
2.351	0.00858	2.440	0.0100
2.658	0.0132	2.737	0.0136
3.014	0.0188	3.043	0.0180
3.412	0.0270	3.355	0.0245
3.825	0.0360	3.668	0.0347
4.231	0.0518	3.991	0.0456
4.613	0.0712	4.343	0.0586
		4.732	0.0784
Series VII			
2.120	0.00601	Series IX	
2.428	0.00952	4.178	0.0461
2.760	0.0139	4.564	0.0653
3.129	0.0213	4.997	0.0827

Appendix 3A. Continued.

T/K	C_p/$JK^{-1}mol^{-1}$	T/K	C_p/$JK^{-1}mol^{-1}$
5.491	0.1199	13.220	2.194
6.066	0.1621	14.339	2.751
6.700	0.2352		
7.429	0.3377	Series XI	
8.280	0.4845	8.884	0.6082
		9.630	0.8137
Series X		10.446	1.0693
4.365	0.0552	11.359	1.3956
4.749	0.0757	12.342	1.7902
5.188	0.0959	13.355	2.241
5.734	0.1403	14.396	2.744
6.344	0.1948	15.311	3.278
7.010	0.2710	16.168	3.731
7.665	0.3648	17.046	4.211
8.265	0.4787	17.961	4.763
8.910	0.6194	18.902	5.316
9.623	0.8070	19.831	5.864
10.367	1.0433		
11.184	1.3359	Series XII	
12.140	1.7008	14.482	2.846

Appendix 3A. Continued.

T/K	$C_p/JK^{-1}mol^{-1}$	T/K	$C_p/JK^{-1}mol^{-1}$
15.478	3.368	36.380	14.501
16.466	3.883	37.489	14.964
17.423	4.453	38.615	15.412
18.398	5.015	39.864	15.875
19.378	5.619	41.134	16.363
20.382	6.183	42.354	16.815
21.428	6.787	43.609	17.257
22.492	7.410	44.849	17.729
23.543	8.054	46.107	18.142
24.592	8.628	47.411	18.583
25.650	9.235	48.755	19.023
26.728	9.805	50.343	19.542
27.808	10.388		
28.872	10.942	Series XIII	
29.926	11.520	102.363	40.30
30.975	12.037	105.168	40.80
32.038	12.547	107.625	41.10
33.117	13.044	110.054	41.48
34.198	13.525	112.608	41.70
35.285	14.009	115.283	42.14

Appendix 3A. Continued.

T / K	C_p / $JK^{-1}mol^{-1}$	T / K	C_p / $JK^{-1}mol^{-1}$
117.925	42.63		
120.537	43.10	Series XIV	
123.124	43.37	156.005	51.35
125.687	43.87	157.206	56.67
128.224	44.20	Fusion	
130.738	44.61	161.756	58.06
133.221	44.95	164.059	58.15
135.820	45.32		
138.527	45.86		
141.206	46.22		
143.858	46.60		
146.482	47.20		
149.077	47.77		
151.640	48.49		
154.173	49.22		
156.417	51.25		
Fusion,			
Continuous Heating			

Appendix 3B. Measured heat capacities of DCl.

T / K	C_p / $JK^{-1}mol^{-1}$	T / K	C_p / $JK^{-1}mol^{-1}$
		74.807	29.25
Series I		76.311	29.76
50.421	20.81	77.839	30.25
51.560	21.20	79.393	30.73
52.707	21.63		
53.883	22.09	Series II	
55.111	22.56	76.981	29.92
56.393	22.99	78.629	30.47
57.719	23.50	80.336	31.03
59.048	23.97	82.052	31.61
60.365	24.47	83.779	32.19
61.697	24.92	85.489	32.82
63.074	25.37	87.223	33.42
64.486	25.86	88.994	34.19
65.910	26.33	90.750	34.79
67.347	26.80	92.507	35.48
68.821	27.26	94.267	36.16
70.321	27.79	96.032	36.92
71.819	28.27	97.797	37.80
73.314	28.75	99.550	38.62

Appendix 3B. Continued.

T/K	C_p/JK^{-1}mol^{-1}	T/K	C_p/JK^{-1}mol^{-1}
101.279	39.65	101.570	39.74
102.973	41.78	102.627	40.60
Transition,		103.651	46.10
Continuous Heating		Transition	
		106.284	44.22
Series III		107.283	44.38
79.737	30.79	108.278	44.58
81.433	31.38	109.268	44.68
83.115	31.95	110.256	44.74
84.797	32.45	111.240	44.86
86.493	33.12	112.514	45.06
88.160	33.86	114.266	45.34
89.849	34.37		
91.591	35.09	Series IV	
93.348	35.76	97.758	37.74
95.120	36.52	99.600	38.70
96.894	37.28	100.991	39.33
98.331	38.03	102.048	40.13
99.422	38.50	103.090	41.53
100.502	39.09	103.985	50.99

Appendix 3B. Continued.

T / K	C_p / $JK^{-1}mol^{-1}$	T / K	C_p / $JK^{-1}mol^{-1}$
Transition			
105.982	44.31	Series V	
106.873	44.27	Transition,	
107.861	44.48	Continuous Heating	
108.844	44.64		
109.824	44.64	Series VI	
110.898	44.94	1.985	0.00516
112.160	45.03	2.254	0.00786
113.610	45.20	2.569	0.0111
115.244	45.49	2.886	0.0163
116.940	45.73	3.189	0.0219
118.851	45.97	3.484	0.0286
120.746	46.21	3.787	0.0382
122.629	46.38	4.076	0.0446
124.500	46.68	4.391	0.0584
126.359	47.01	4.764	0.0783
128.205	47.21	5.180	0.1055
130.037	47.42		
		Series VII	
		2.051	0.00542

Appendix 3B. Continued.

T/K	C_p/JK^{-1}mol^{-1}	T/K	C_p/JK^{-1}mol^{-1}
2.322	0.00840		
2.655	0.0117	Series IX	
2.968	0.0171	4.514	0.0649
3.280	0.0228	4.886	0.0853
3.584	0.0325	5.269	0.1147
3.895	0.0429	5.720	0.1393
4.240	0.0554	6.242	0.1942
4.649	0.0727	6.858	0.2526
5.134	0.1038	7.611	0.3662
Series VIII		Series X	
2.096	0.00580	4.340	0.0500
2.382	0.00920	4.696	0.0716
2.695	0.0132	5.100	0.0971
3.019	0.0178	5.520	0.1277
3.331	0.0247	5.996	0.1650
3.635	0.0306	6.489	0.2191
3.949	0.0438	7.036	0.2865
4.303	0.0571	7.713	0.3945
		8.521	0.5541

Appendix 3B. Continued.

T/K	C_p/$JK^{-1}mol^{-1}$	T/K	C_p/$JK^{-1}mol^{-1}$
9.393	0.7575	19.565	5.763
10.287	1.0431		
11.236	1.3771	Series XII	
12.232	1.7818	14.261	2.737
13.244	2.226	15.165	3.247
14.273	2.732	16.121	3.764
		17.166	4.357
Series XI		18.193	4.968
8.393	0.5069	19.129	5.508
9.191	0.7025	20.062	6.069
10.003	0.9423	21.040	6.694
10.885	1.2448	21.995	7.198
11.849	1.6161	22.899	7.733
12.857	2.049	23.872	8.309
13.861	2.529	24.961	8.934
14.806	3.053	26.101	9.585
15.743	3.556	27.256	10.207
16.672	4.079	28.408	10.846
17.601	4.608	29.565	11.473
18.565	5.168	30.734	12.109

Appendix 3B. Continued.

T/K	C_p/$JK^{-1}mol^{-1}$	T/K	C_p/$JK^{-1}mol^{-1}$
31.891	12.705	135.444	48.23
33.043	13.274	138.143	48.73
34.230	13.863	140.805	49.13
35.452	14.459	143.431	49.38
36.677	15.042	146.026	49.87
37.913	15.607	148.585	50.47
39.162	16.164	151.106	51.04
40.429	16.731	153.615	52.68
41.720	17.288	155.829	55.21
43.042	17.837	Fusion,	
44.397	18.406	Continuous Heating	
45.789	18.975		
47.223	19.535	Series XIV	
48.654	20.12	154.133	53.54
50.145	20.64	156.121	60.21
		Fusion	
Series XIII		160.670	61.11
127.813	47.18	162.918	61.05
130.337	47.54		
132.842	47.91		

CHAPTER 4

Thermodynamic Properties of HBr and DBr

4-1. Heat capacity

The measured heat capacity values are presented as C_p in appendices 4A and B for HBr and DBr, respectively. Curvature corrections were not applied, but may be computed from the values since each series is results of continuous measurements. The smoothed values at rounded temperatures are given in table 4-1.

Above 140 K, corrections arising from vaporization of HBr or DBr were significant. Relevant quantities for such corrections were evaluated as follows. The density of solid HBr in phase I was obtained from the X-ray data[1] at 120, 130, and 140 K, and the liquid density from Strunk and Wingate.[2] Densities of DBr were assumed to be identical to those of HBr. The heat capacity in the gaseous phase is (7/2)R in the temperature range required.

The results for HBr and DBr are plotted in figures 4-1 and 4-2, respectively. Solid HBr has three transitions with a tail extending down to lower temperatures. In contrast, solid DBr has two gradual transitions. Such an isotope effect is not seen in other hydrogen halides.

The measured heat capacities of solid HBr and DBr are compared with earlier results in figures 4-3 and 4-4, respectively. The results are plotted as

TABLE 4-1. The heat capacity of solid HBr and DBr at rounded values of temperatures.

$\frac{T}{K}$	$\frac{C_p}{JK^{-1}mol^{-1}}$.	
	HBr	DBr
2	0.0151	0.0156
3	0.055	0.055
4	0.141	0.138
5	0.296	0.292
6	0.537	0.533
8	1.374	1.337
10	2.634	2.634
12	4.262	4.198
15	6.846	6.792
20	10.90	10.90
25	14.20	14.34
30	16.75	17.12
35	18.79	19.46
40	20.47	21.56
45	22.00	23.43
50	23.46	25.28
55	24.98	27.14
60	26.71	29.21

TABLE 4-1. Continued.

T / K	C_p / $JK^{-1}mol^{-1}$	
	HBr	DBr
65	28.68	31.38
70	31.10	33.81
75	34.33	36.80
80	39.28	40.94
85	49.80	47.25
90	———	62.55
95	41.57	46.72
100	43.67	47.84
110	50.50	53.56
120	45.09	———
130	45.24	49.16
140	45.81	49.77
150	46.65	50.56
160	47.69	51.58
170	48.94	53.12
180	50.62	57.67

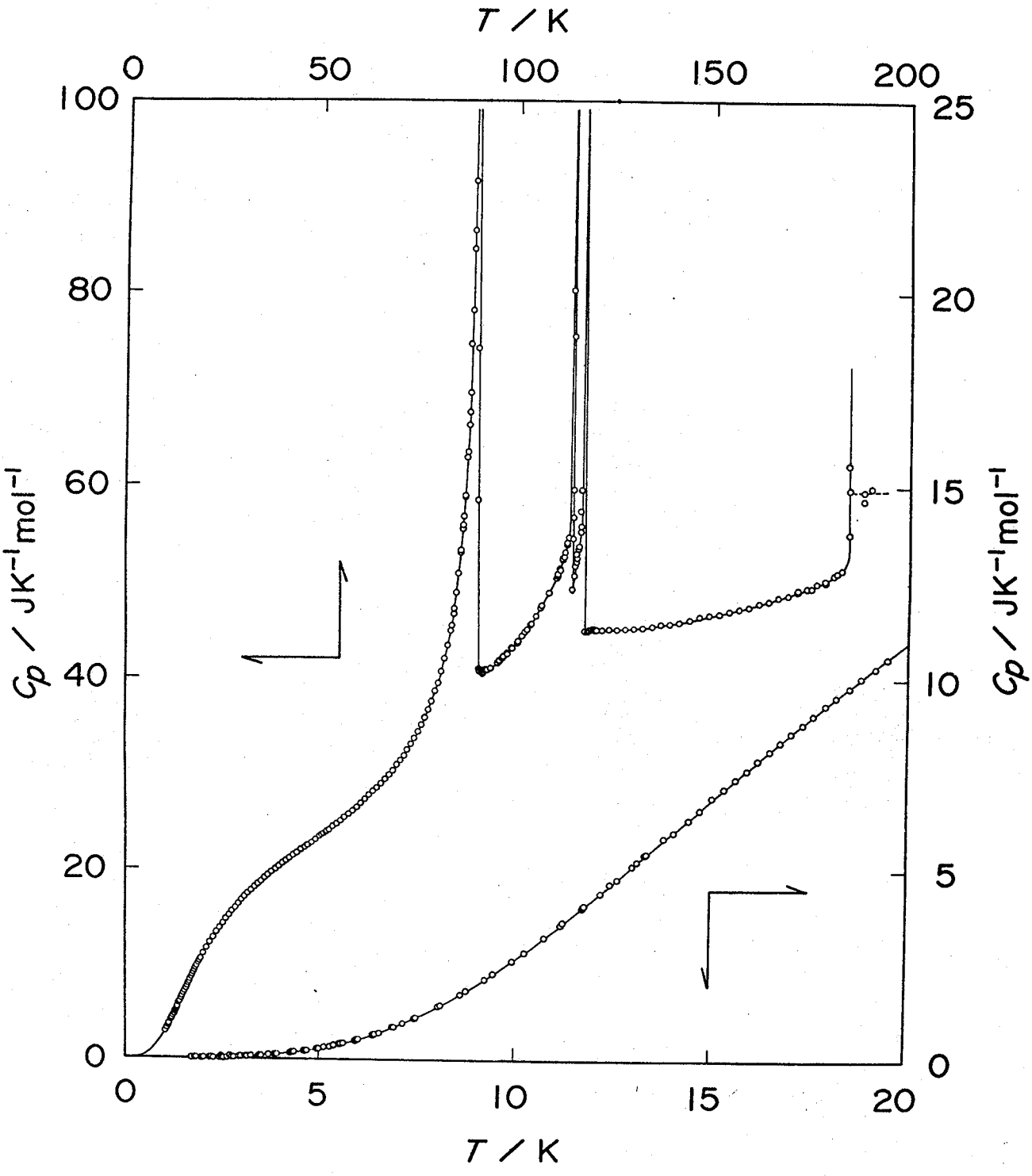

FIGURE 4-1. Heat capacity of HBr.

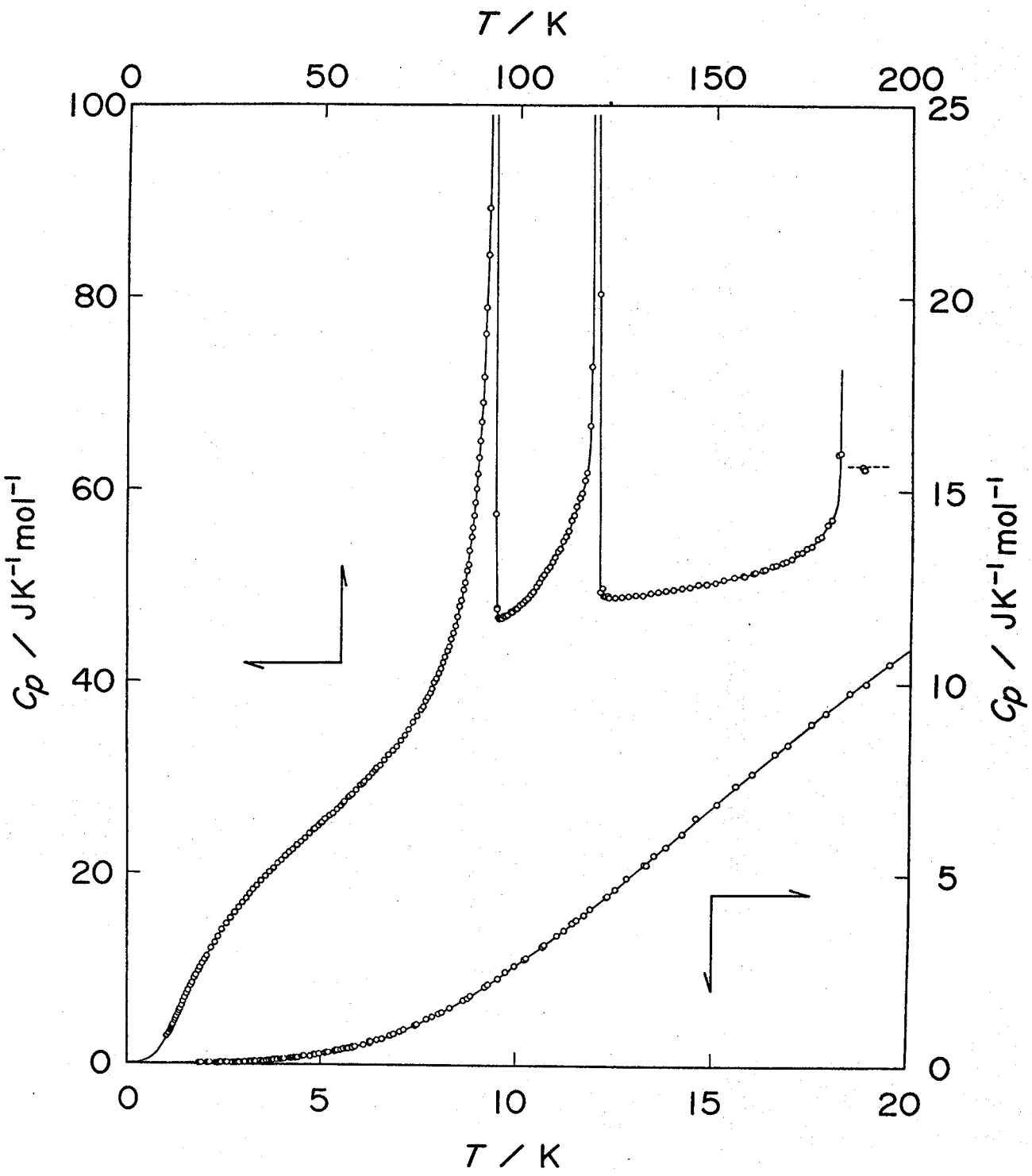

FIGURE 4-2. Heat capacity of DBr.

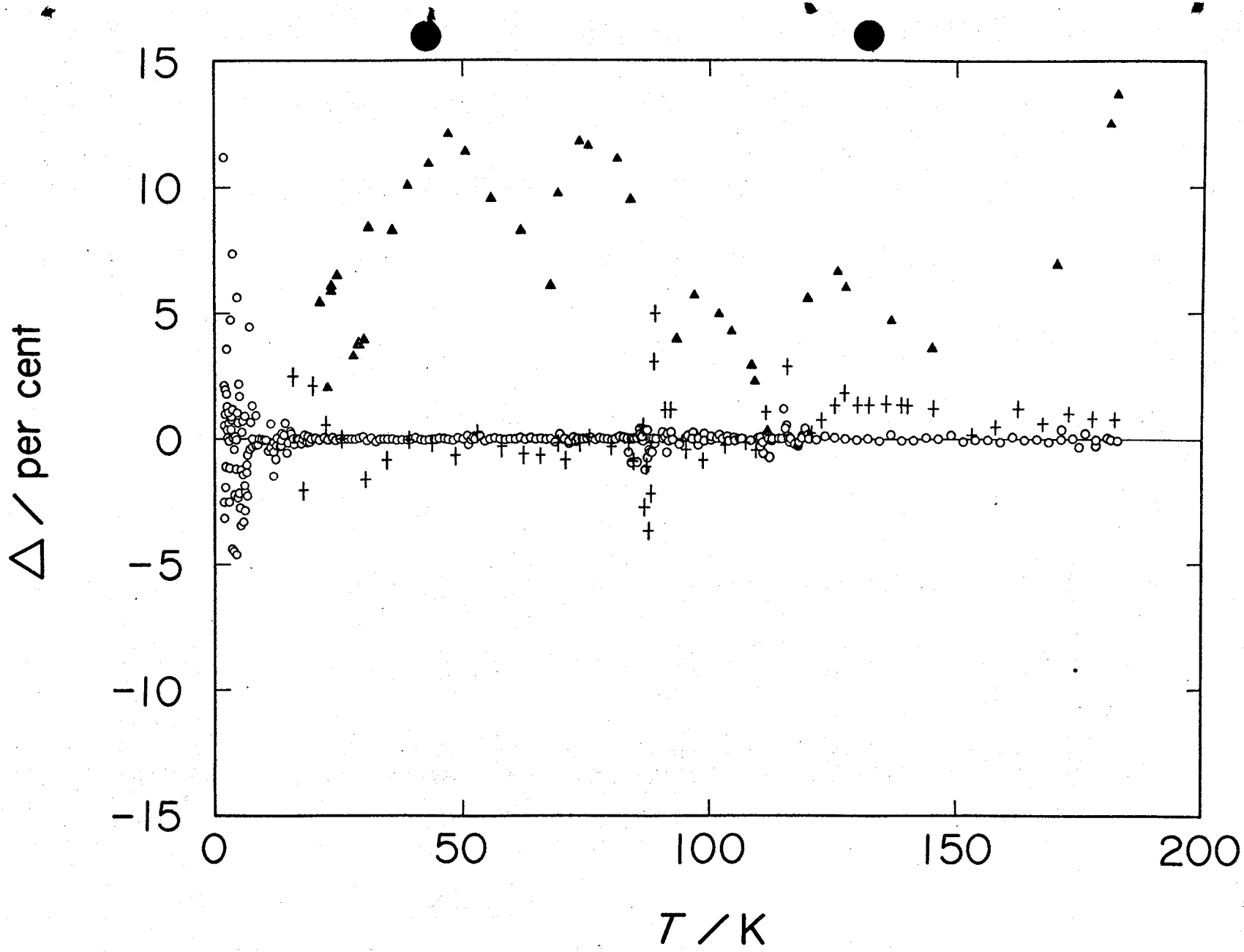

FIGURE 4-3. A comparison of heat capacity results for solid HBr. o, present results; +, Giauque and Wiebe;[3] ▲, Eucken and Karwat.[4] Δ/per cent = [C_p(obs.)-C_p(smooth)] x 100 / [C_p(smooth)], where C_p(smooth) is given in table 4-1.

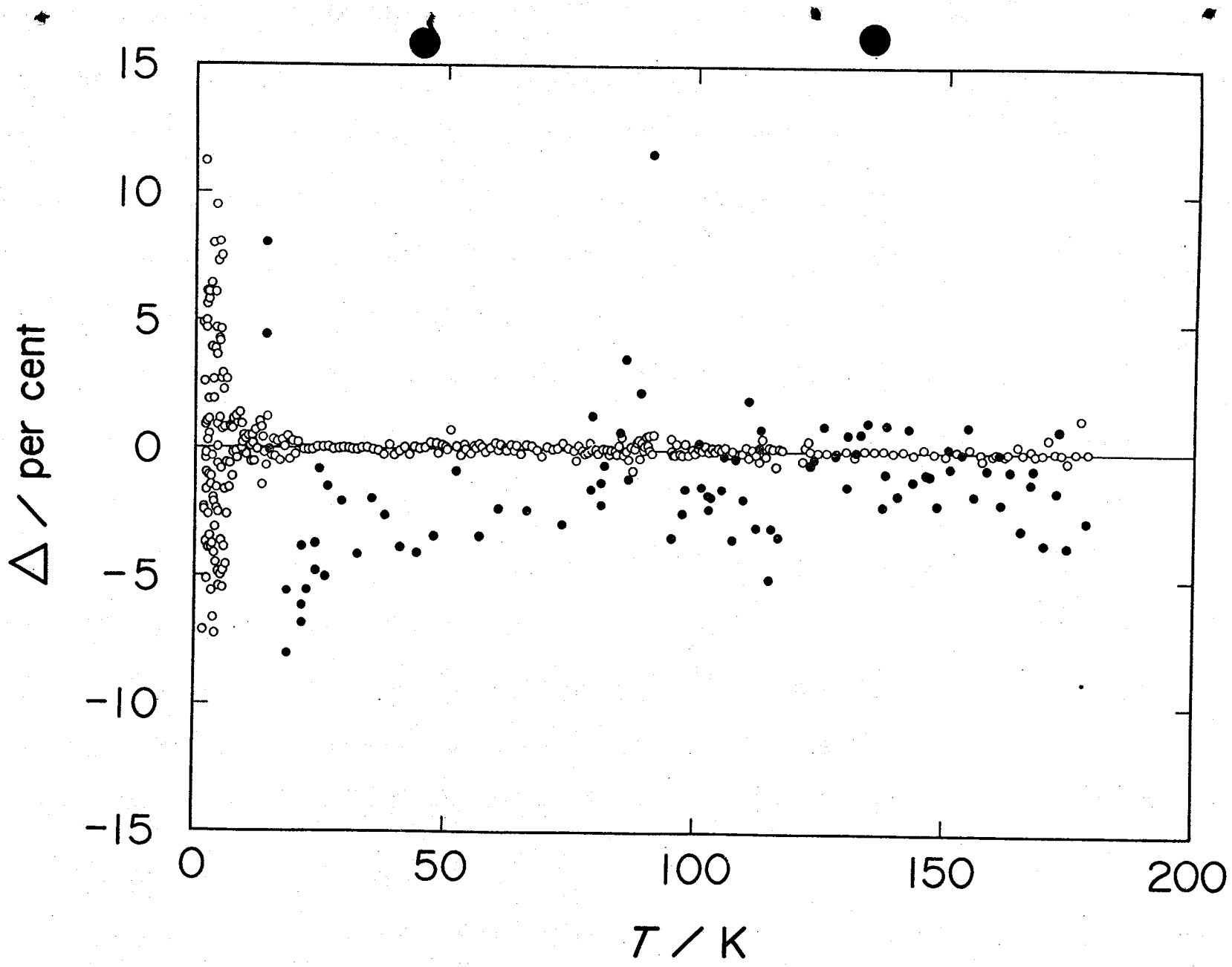

FIGURE 4-4. A comparison of heat capacity results for solid DBr. o, present results; ●, Clusius and Wolf.[5]
Δ/per cent = [C_p(obs.)-C_p(smooth)] x 100 / [C_p(smooth)], where C_p(smooth) is given in table 4-1.

differences from a smooth curve corresponding to the values given in table 4-1. The scatter of our measured points of solid HBr is ±5 per cent at the lowest temperatures, ±0.5 per cent at 10 K, ±0.1 per cent above 20 K, and ±0.2 per cent at higher temperatures. Near the transitions, it increased up to ±1 per cent because of small temperature increments. Since the amounts of DBr in Sample I are small, the scatter is somewhat larger than that of HBr. For both HBr and DBr, two samples gave identical results within the extent of scatter except for two points at about 2.5 K in the Series X of HBr Sample I, which showed larger values by some tens of per cent than the smooth heat capacity. They obviously come from poor manual control of adiabatic condition at the lowest temperature.

Giauque and Wiebe's results for HBr are in agreement with the present results within the combined limits of error. Eucken and Karwat's and Clusius and Wolf's results indicated the similar systematic deviations as reported for HCl and DCl, respectively.

A more sensitive comparison in the lower temperature region is made by use of equivalent Debye temperature Θ_D, whose temperature dependence for 3N degrees of freedom is shown in figures 4-5 and 4-6 for HBr and DBr, respectively.

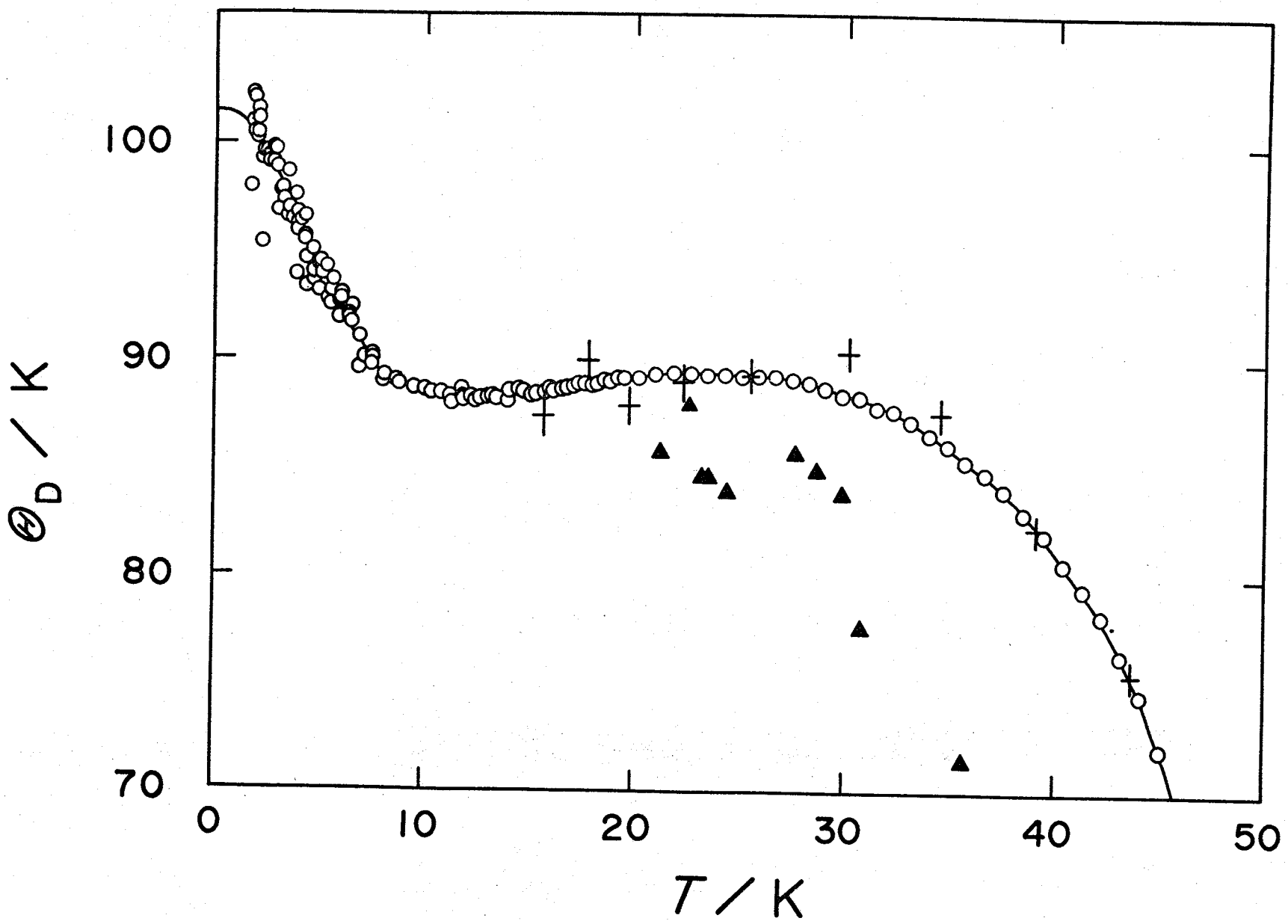

FIGURE 4-5. The Debye characteristic temperature of HBr derived from the measured heat capacities, assuming 3N degrees of freedom. o, present results; +, Giauque and Wiebe;[3] ▲, Eucken and Karwat.[4]

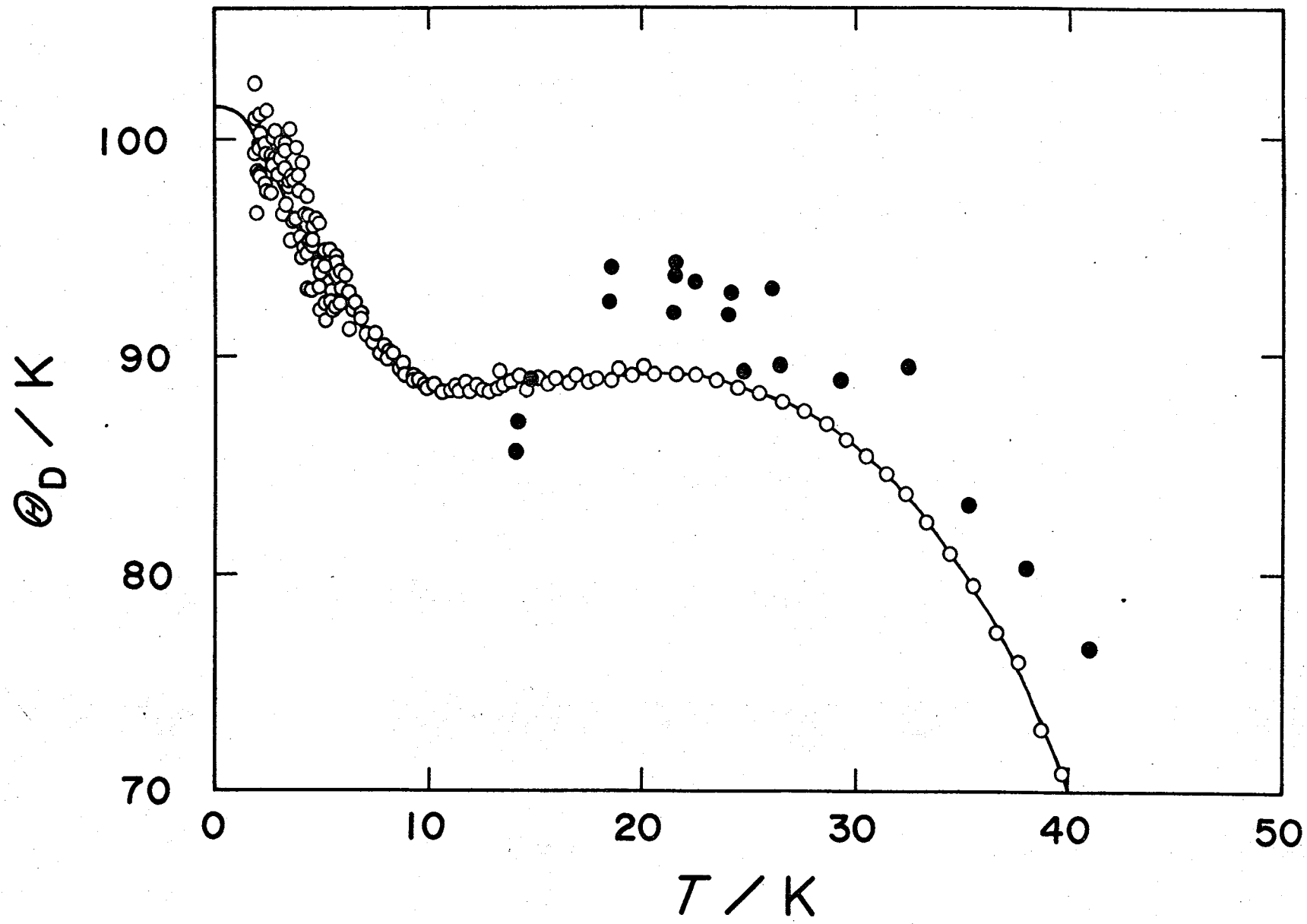

FIGURE 4-6. The Debye characteristic temperature of DBr derived from the measured heat capacities, assuming 3N degrees of freedom. o, present results; ●, Clusius and Wolf.[5]

The Debye temperature curves for HBr and DBr are almost superimposable below about 20 K although the former is slightly lower near 8 and 12 K. Above 22 K the DBr curve declines more rapidly.

4-2. Vapor pressure

Measured vapor pressures of the solid and liquid HBr (Sample I) and DBr (Sample II) are listed in tables 4-2 and 4-3, respectively. The results were fitted to the following equations by the method of least squares;

$$\text{HBr} \quad \log_{10}(P/\text{Pa}) = -520.14(K/T)+3.9279+0.018146(T/K) \quad (4\text{-}1)$$

$$\text{DBr} \quad \log_{10}(P/\text{Pa}) = -786.73(K/T)+6.8945+0.009893(T/K) \quad (4\text{-}2)$$

Deviations from equations 4-1 and 4-2 are included in tables 4-2 and 4-3, respectively. A comparison with the results reported others is given in table 4-4. The differences are appreciable: for example, at 177 K, McIntosh and Steele's results[6] show a pressure higher than ours by 9 kPa, Henglein's results[7] a pressure lower by 70 Pa. The results of Bates et al., which consist of only 3 points for both solids, indicate no isotope effect in contrast to present results.

The equations 4-1 and 4-2 indicate that a plot of log P against T^{-1} has such a slope that increases at higher temperatures. One of possibilities that might give such an effect would be decomposition of hydrogen bromide to release some hydrogen in the vapor phase. However, there were no indications of decomposition

TABLE 4-2. Vapor pressures of HBr.

T / K	P / kPa	P-P(eq. 4-1) / kPa
	Solid	
150.506	1.619	0.023
153.018	2.019	-0.001
155.512	2.521	-0.021
158.017	3.154	-0.034
160.507	3.943	-0.036
162.976	4.915	-0.025
165.423	6.104	0.004
165.432	6.122	0.017
167.865	7.558	0.052
170.304	9.250	0.045
172.721	11.300	0.064
175.143	13.761	0.077
177.518	16.513	-0.046
179.866	20.002	0.054
179.869	20.012	0.059
181.907	23.352	-0.057
183.919	27.304	-0.059
184.262	28.140	0.043
185.595	30.975	-0.151
185.605	31.079	-0.071

TABLE 4-2. Continued.

T / K	P / kPa	P-P(eq. 4-1) / kPa
	Liquid	
187.360	34.500	
187.449	34.906	
189.271	38.865	
189.363	39.342	
189.375	39.380	
191.241	44.244	

TABLE 4-3. Vapor pressures of DBr.

T/K	P/kPa	P-P(eq. 4-2)/kPa
	Solid	
156.027	2.494	0.007
158.498	3.153	-0.001
160.949	3.959	-0.010
163.383	4.946	-0.015
165.844	6.178	-0.007
168.326	7.695	0.007
170.828	9.556	0.027
173.347	11.798	0.025
175.879	14.518	0.021
178.437	17.741	-0.071
181.037	21.914	0.049
183.300	26.012	-0.037
	Liquid	
186.881	33.439	

TABLE 4-4. Coefficients A and B for the vapor pressure equation:

$$\log_{10}(P/Pa) = -A(K/T)+B$$

	A	B
HBr		
Present work	1035.12	10.0556
Bates et al. (1935)[a]	1103	10.434
Henglein (1923)[b]	1138.6	10.631
McIntosh and Steele (1906)[c]	807	8.92
DBr		
Present work	1069.80	10.2457
Bates et al. (1935)[a]	1103	10.431

[a] From reference 8.

[b] From reference 7.

[c] From reference 6.

in the temperature drift of heat capacity determinations nor in the purity determination at the triple point which was conducted after all the vapor pressure measurements had been concluded.

4-3. Enthalpy of fusion

The results for fusion experiments are given in table 4-5. A correction for the $\int C_p dT$ was applied to compute the enthalpy of fusion ΔH_f from cumulative enthalpy $H(T_2)-H(T_1)$. Measurements by other workers are also included for the sake of comparison. The mean values of the enthalpy of fusion of HBr and DBr obtained were (2398.7 $\pm$ 1.0) and (2369 $\pm$ 4) J mol^{-1}, respectively. The rather large uncertainty in DBr comes from smallness of amount of specimen used as Sample I.

The triple points of pure HBr and DBr, given as (186.500 $\pm$ 0.004) and (185.64 $\pm$ 0.01) K respectively, were estimated from a plot of the equilibrium temperature against the reciprocal of the fraction melted (see table 4-6). Although the melting was broader in DBr because of larger amount of impurities, this plot was approximately linear.

TABLE 4-5. The enthalpy of fusion of HBr and DBr.

Sample	Series no.	T_1 / K	T_2 / K	$H(T_2)-H(T_1)$ / $Jmol^{-1}$	ΔH_f / $Jmol^{-1}$
			HBr		
I	XXIII	185.595	187.360	2502.1	2398.9
I	XXIV[a]	185.605	187.449	2505.4	2397.7
II	IV[a]	186.099	188.478	2538.4	2399.4
				Average	2398.7 ± 1.0
			Giauque and Wiebe (1928)[b]		2406
			Eucken and Karwat (1924)[c]		2594
			DBr		
I	XIII[a]	182.593	186.762	2616.0	2369
I	XIV	182.790	186.585	2590.4	2365
II	IX[a]	183.300	186.881	2579.9	2372
				Average	2369 ± 4
			Clusius and Wolf (1947)[d]		2403

TABLE 4-5. Continued.

[a] In this series, the fusion was done in stages.

[b] From reference 3.

[c] From reference 4.

[d] From reference 5.

TABLE 4-6. The triple point of HBr and DBr.

Sample	Fraction melted	T / K	P / kPa
		HBr	
I	0.134	186.416	32.79
	0.319	186.453	32.88
	0.504	186.467	32.98
	0.688	186.476	33.03
	0.874	186.482	33.10
	(1.000)	186.484 ± 0.002	33.31[a]
II	0.245	186.440	
	0.464	186.462	
	0.684	186.477	
	0.902	186.483	
	(1.000)	186.484 ± 0.002	
T_f (pure HBr)		186.500 ± 0.004	
Giauque and Wiebe (1928)[b]		186.24 ± 0.05	
Eucken and Karwat (1924)[c]		187.0	
Clusius and Wolf (1947)[d]			33.1

TABLE 4-6. Continued.

Sample	Fraction melted	T / K	P / kPa
		DBr	
I	0.251	185.269	
	0.376	185.414	
	0.495	185.450	
	0.609	185.491	
	0.735	185.505	
	0.891	185.528	
	(1.000)	185.548 ± 0.005	
II	0.300	185.343	30.16
	0.561	185.474	30.73
	0.819	185.527	30.96
	(1.000)	185.548 ± 0.005	30.91[a]
T_f (pure DBr)		185.64 ± 0.01	
Clusius and Wolf (1947)[d]		185.62	30.9

[a] The value obtained from smoothed vapor pressure equation.

[b] From reference 3.

[c] From reference 4.

[d] From reference 5.

4-4. Transitions in solids

Details of thermal behavior of a phase transition may be manifested by the enthalpy change through the transition region. Figure 4-7 refers to the transition between phase III and II and figure 4-8 to that between phase II and I including phase I' of HBr.

The different series of results were normalized on the high temperature side of transitions. The transition temperatures were then determined from the point at which the rate of change of enthalpy with temperature is a maximum.

In the lower transition of HBr or DBr, the time to reach equilibrium after heating was off became an hour or more. At each such point, the rate of change of temperature with time was followed for 40 min, the results fitted to a first-order rate law, and the equilibrium temperature (T_∞) obtained by extraporation. The temperatures plotted were determined in this way. In HBr, the time required to come within 0.001 K of T_∞ was about 40 min. Transitions were found to be continuous.

The upper two transitions of HBr obviously differ from each other in equilibration time. On the low temperature side of the transition at 113.60 K it requires a very long time; In fact, the time required

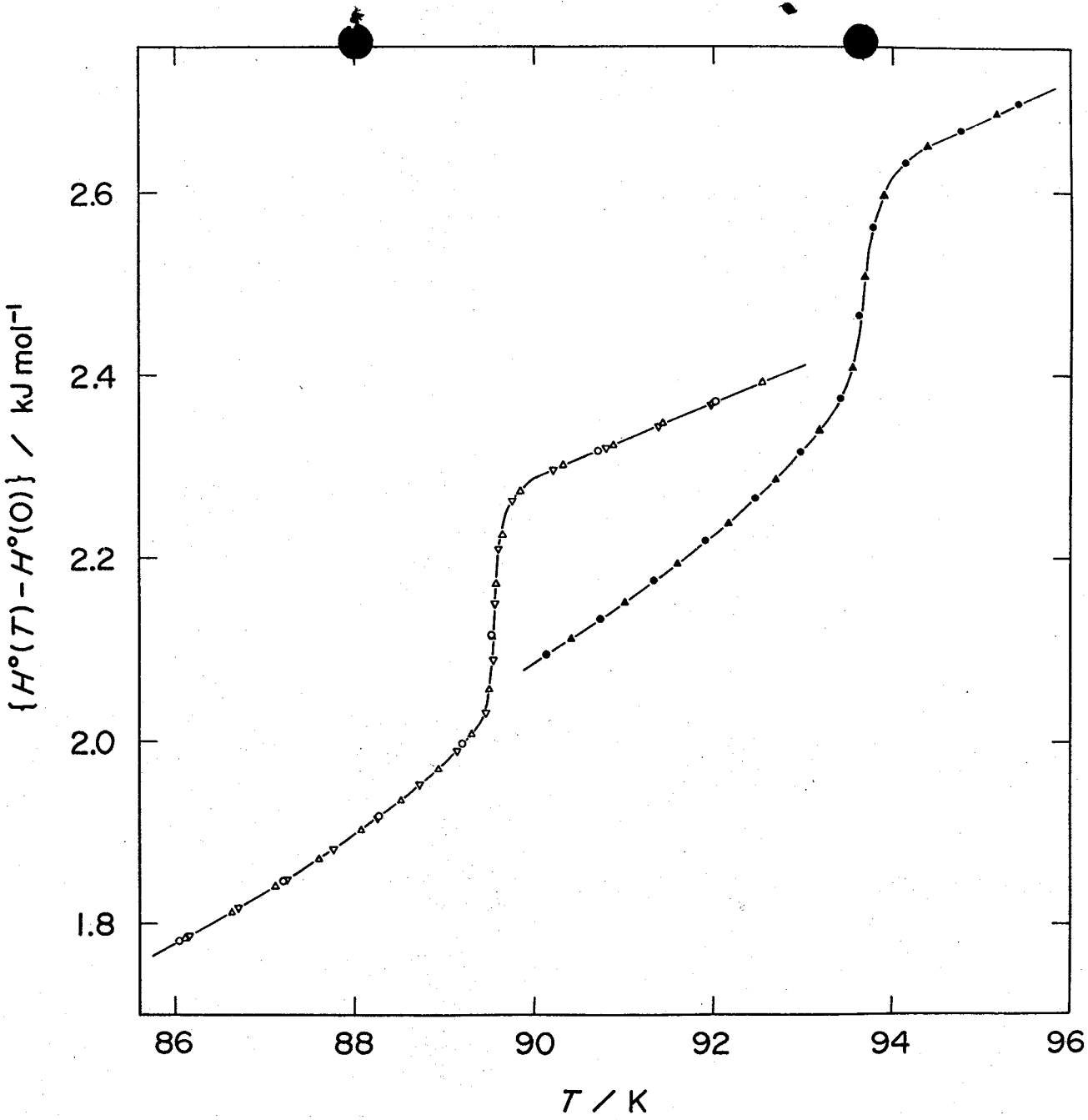

FIGURE 4-7. Enthalpy change in the region phase III → phase II of HBr and DBr. The different series of measurements are normalized on the high temperature side of transitions. HBr Sample I: [o, (I); Δ, (XIII)]. HBr Sample II: ∇, (II). DBr Sample I: [●, (VI); ▲, (VII)].

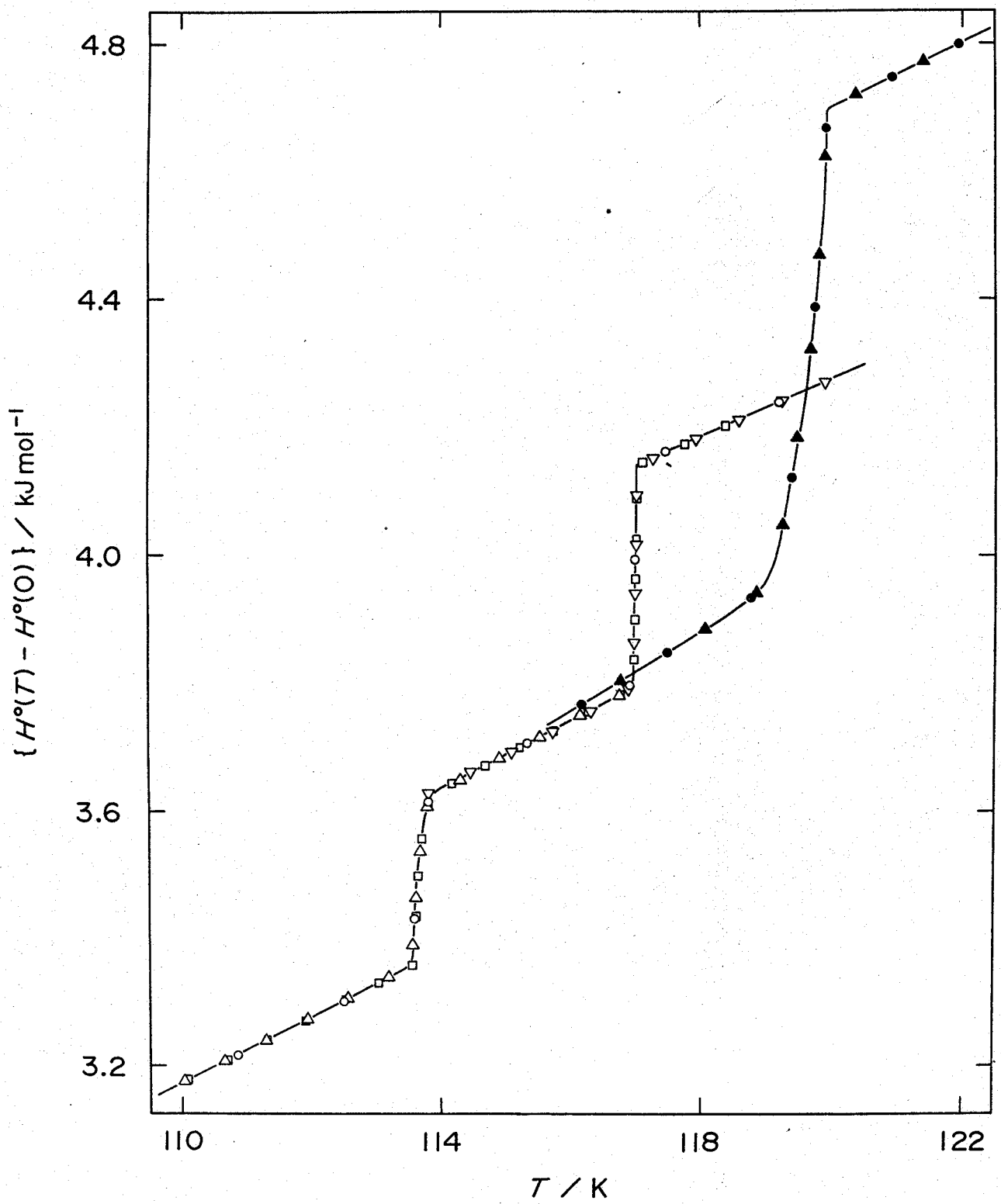

FIGURE 4-8. Enthalpy change in the region phase II → phase I of HBr and DBr. The different series of measurements are normalized on the high temperature side of transitions. HBr Sample I: [o, (XIV); Δ, (XV), ∇, (XVI)]. HBr Sample II: □, (III). DBr Sample I: [●, (VIII), ▲, (IX)].

until $T-T_{\infty}$ becomes 0.001 K was estimated to be about 5 hr from the observation during an hour in contrast to 20 min in the transition at 117.00 K. The upper transition of DBr is a discontinuous one with a tail to lower temperature side. The calorimetric studies of the transitions are, however, complicated by the occurrence of hysteresis[9] because the geometry of calorimeter vessel and the method of heating inevitably cause non-uniform heating of the specimen. Therefore, there is some ambiguity in the order or type of transition to be specified by the experimental results.

The enthalpy changes of the transitions measured are shown in tables 4-7 and 4-8 for III-II and II-I transitions, respectively. In the transition at 117.00 K of HBr, ΔH_{tr} could be unambiguously estimated because of its sharpness. It is 4.5 per cent smaller than the value of Giauque and Wiebe.[3]

TABLE 4-7. The enthalpy of transitions between phase III and II of HBr and DBr including the "normal" part of heat capacity.

Sample	Series no.	T_1 / K	T_2 / K	$H(T_2)-H(T_1)$ / $Jmol^{-1}$	$H(90.5)-H(88.5)$ / $Jmol^{-1}$
			HBr		
I	I[a]	88.266 - 90.702		399.0	373.2
I	XIII[a]	88.506 - 90.308		365.2	373.5
II	I	88.955 - 90.089		316.9	372.1
II	II[a]	88.714 - 90.791		367.3	372.0
				Average	372.7 ± 0.8

	T_{tr} / K
Present work	89.53 ± 0.01
Giauque and Wiebe (1928)[b]	89.2
Eucken and Karwat (1924)[c]	90

TABLE 4-7. Continued.

Sample	Series no.	T_1 / K	T_2 / K	$H(T_2)-H(T_1)$ / $Jmol^{-1}$	$H(94.5)-H(92.5)$ / $Jmol^{-1}$
		DBr			
I	VI[a]	92.450 - 94.760		402.7	385.7
I	VII[a]	92.678 - 94.387		363.5	384.9
I	VIII	91.823 - 94.265		429.7	384.2
I	IX	90.821 - 94.405		511.0	385.4
				Average	385.1 ± 0.9

	T_{tr} / K
Present work	93.67 ± 0.01
Clusius and Wolf (1947)[d]	93.5

[a] In this series, the transition was done in stages.

[b] From reference 3.

[c] From reference 4.

[d] From reference 5.

TABLE 4-8. The enthalpy of transitions between phase II and I of HBr and DBr including the "normal" part of heat capacity.

Sample	Series no.	T_1 / K	T_2 / K	$H(T_2)-H(T_1)$ / $Jmol^{-1}$	$H(118)-H(113)$ / $Jmol^{-1}$
		HBr (II-I)			
I	XXI	113.143 - 118.165		855.1	855.4

Sample	Series no.	T_1 / K	T_2 / K	$H(T_2)-H(T_1)$ / $Jmol^{-1}$	$H(115.5)-H(113)$ / $Jmol^{-1}$
		HBr (II-I')			
I	XIV[a]	112.508 - 115.344		404.9	385.9
I	XV[a]	113.185 - 115.517		376.0	385.1
I	XVII	113.152 - 115.289		366.7	386.1
I	XX	112.967 - 115.366		380.1	385.4
II	III[a]	113.041 - 115.725		395.7	386.0
				Average	385.7 ± 0.4

	T_{tr} / K
Present work	113.60 ± 0.01
Giauque and Wiebe (1928)[b]	113.4

TABLE 4-8. Continued.

Sample	Series no.	T_1 / K	T_2 / K	$H(T_2)-H(T_1)$ / $Jmol^{-1}$	$H(118)-H(115.5)$ / $Jmol^{-1}$
		HBr (I'-I)			
I	XIV[a]	115.344 - 117.466		453.7	469.6
I	XVI[a]	115.704 - 117.923		455.3	469.4
I	XVIII	116.710 - 117.481		380.3	469.5
I	XIX	116.273 - 117.745		415.6	468.8
II	III[a]	115.725 - 117.733		445.5	469.3
				Average	469.3 ± 0.5

	T_{tr} / K	ΔH_{tr} / $Jmol^{-1}$
Present work	117.00 ± 0.01	343
Giauque and Wiebe (1928)[b]	116.8	359

TABLE 4-8. Continued.

Sample	Series no.	T_1 / K	T_2 / K	$H(T_2)-H(T_1)$ / $Jmol^{-1}$	$H(121)-H(118)$ / $Jmol^{-1}$
		DBr (II-I)			
I	VIII[a]	117.484 - 120.930		898.7	868.7
I	IX[a]	118.062 - 121.409		886.8	870.1
I	X	118.058 - 120.956		865.1	870.7
I	XI	117.926 - 120.735		860.5	869.0
				Average	869.6 ± 1.1

	T_{tr} / K
Present work	119.96 ± 0.01
Clusius and Wolf (1924)[c]	120.26

[a] In this series, the transition was done in stages.

[b] From reference 3.

[c] From reference 5.

4-5. Thermodynamic functions

The thermodynamic functions of HBr and DBr were calculated. The contribution of the heat capacities below 2 K was evaluated by a smooth extraporation. The results are given in tables 4-9 and 4-10 for HBr and DBr, respectively. The entropy of liquid HBr and DBr at the triple points was calculated to be 95.88 and 101.78 J K^{-1} mol^{-1}, which are slightly different from 96.46 J K^{-1} mol^{-1} by Giauque and Wiebe and 100.17 J K^{-1} mol^{-1} by Clusius and Wolf, respectively.

TABLE 4-9. Thermodynamic functions of HBr.

T / K	$S^{\circ}(T)-S^{\circ}(0)$ / $JK^{-1}mol^{-1}$	$\{H^{\circ}(T)-H^{\circ}(0)\}/T$ / $JK^{-1}mol^{-1}$	$-\{G^{\circ}(T)-H^{\circ}(0)\}/T$ / $JK^{-1}mol^{-1}$
		Solid	
10	0.857	0.653	0.204
20	5.080	3.736	1.344
30	10.70	7.179	3.524
40	16.07	10.07	6.002
50	20.96	12.45	8.510
60	25.52	14.54	10.98
70	29.93	16.58	13.35
80	34.54	18.83	15.71
91	44.05	25.59	18.46
100	48.02	27.06	20.96
110	52.46	28.84	23.62
115	57.02	32.07	24.95
120	62.02	35.62	26.40
130	65.64	36.35	29.29
140	69.01	37.00	32.01
150	72.20	37.62	34.58
160	75.25	38.21	37.04
170	78.18	38.81	39.37

TABLE 4-9. Continued.

T / K	$S^{\circ}(T)-S^{\circ}(0)$ / $JK^{-1}mol^{-1}$	$\{H^{\circ}(T)-H^{\circ}(0)\}/T$ / $JK^{-1}mol^{-1}$	$-\{G^{\circ}(T)-H^{\circ}(0)\}/T$ / $JK^{-1}mol^{-1}$
180	81.02	39.41	41.61
186.5	83.02	40.01	43.01
		Liquid	
186.5	95.88	52.87	43.01

TABLE 4-10. Thermodynamic functions of DBr.

T / K	$S^{\circ}(T)-S^{\circ}(0)$ / $JK^{-1}mol^{-1}$	$\{H^{\circ}(T)-H^{\circ}(0)\}/T$ / $JK^{-1}mol^{-1}$	$-\{G^{\circ}(T)-H^{\circ}(0)\}/T$ / $JK^{-1}mol^{-1}$
		Solid	
10	0.843	0.643	0.200
20	5.209	3.715	1.495
30	10.89	7.216	3.674
40	16.44	10.27	6.179
50	21.66	12.90	8.763
60	26.60	15.28	11.32
70	31.44	17.59	13.86
80	36.37	20.01	16.36
90	42.07	23.19	18.88
100	50.83	29.15	21.68
110	55.63	31.08	24.55
121	66.91	39.26	27.65
130	70.43	39.94	30.49
140	74.09	40.62	33.48
150	77.55	41.25	36.30
160	80.84	41.86	38.98
170	84.01	42.48	41.53

TABLE 4-10. Continued.

T / K	$S^{\circ}(T)-S^{\circ}(0)$ / $JK^{-1}mol^{-1}$	$\{H^{\circ}(T)-H^{\circ}(0)\}/T$ / $JK^{-1}mol^{-1}$	$-\{G^{\circ}(T)-H^{\circ}(0)\}/T$ / $JK^{-1}mol^{-1}$
180	87.15	43.17	43.99
185.5	89.01	43.72	45.29
		Liquid	
185.5	101.78	56.49	45.29

REFERENCES to CHAPTER 4

1. Simon, A. Z. Naturforsch. B 1970, 25, 1489; J. Appl. Cryst. 1974, 4, 138.
2. Strunk, W. G.; Wingate, W. H. J. Am. Chem. Soc. 1954, 76, 1025.
3. Giauque, W. F.; Wiebe, R. J. Am. Chem. Soc. 1928, 50, 2193.
4. Eucken, A.; Karwat, E. Z. Phys. Chem. 1924, 112, 467.
5. Clusius, K.; Wolf, G. Z. Naturforsch. 1947, 2a, 495.
6. McIntosh, D.; Steele, B. D. Z. Phys. Chem. 1906, 55, 137.
7. Henglein, F. A. Z. Phys. 1923, 18, 64.
8. Bate, J. R.; Halford, J. O.; Anderson, L. C. J. Chem. Phys. 1935, 3, 531.
9. See for example, Colwell, J. H.; Gill, E. K.; Morrison, J. A. J. Chem. Phys. 1963, 39, 635.

Appendix 4A. Measured heat capacities of HBr.

T / K	C_p / $JK^{-1}mol^{-1}$	T / K	C_p / $JK^{-1}mol^{-1}$
		103.913	45.73
- Sample I -		105.106	46.50
Series I		106.286	47.40
84.173	46.70		
85.428	50.92	Series II	
86.621	56.80	11.232	3.633
87.733	66.23	11.753	3.991
88.726	86.40	12.444	4.639
89.350	357.7	13.153	5.226
90.108	167.71	13.820	5.840
91.357	40.56	14.446	6.323
92.663	40.92	15.048	6.911
93.961	41.11	15.627	7.394
95.245	41.68	16.191	7.886
96.517	42.17	16.758	8.356
97.778	42.71	17.333	8.819
99.027	43.18	17.918	9.326
100.266	43.74	18.543	9.785
101.493	44.43	19.208	10.293
102.709	45.07		

Appendix 4A. Continued.

T/K	C_p/JK^{-1}mol^{-1}	T/K	C_p/JK^{-1}mol^{-1}
Series III		25.099	14.265
11.792	4.078	25.884	14.691
12.607	4.765	26.680	15.111
13.373	5.433	27.475	15.526
14.077	6.002	28.270	15.919
14.724	6.589	29.065	16.312
15.329	7.150	29.868	16.702
15.914	7.622	30.677	17.041
16.485	8.128	31.493	17.413
17.046	8.597	32.320	17.723
17.602	9.052	33.157	18.070
18.188	9.527	34.008	18.413
18.825	10.028	34.873	18.735
19.504	10.535	35.756	19.068
20.210	11.067	36.657	19.365
21.006	11.621	37.582	19.673
21.859	12.212	38.532	20.00
22.691	12.770	39.480	20.30
23.506	13.311	40.403	20.61
24.307	13.790	41.328	20.88

Appendix 4A. Continued.

T / K	C_p / $JK^{-1}mol^{-1}$	T / K	C_p / $JK^{-1}mol^{-1}$
42.257	21.15	4.362	0.1904
43.191	21.44	5.007	0.2888
44.129	21.72	5.546	0.4181
45.075	22.03	6.016	0.5294
46.027	22.30	6.494	0.6882
46.989	22.57		
47.961	22.85	Series VI	
48.943	23.16	6.005	0.5215
49.936	23.44	6.416	0.6587
50.942	23.78	6.931	0.8545
51.960	24.06	7.494	1.106
		8.068	1.431
Series IV		8.648	1.739
2.569	0.03381	9.269	2.136
		9.963	2.615
Series V		10.783	3.229
2.631	0.03652	11.768	4.044
2.954	0.05181	13.012	5.104
3.269	0.07354		
3.704	0.1099		

Appendix 4A. Continued.

T / K	C_p / $JK^{-1}mol^{-1}$	T / K	C_p / $JK^{-1}mol^{-1}$
Series VII		5.936	0.5226
7.499	1.113	6.552	0.6887
8.138	1.449	7.152	0.9679
8.788	1.832		
9.483	2.280	Series X	
10.265	2.839	1.722	0.01056
11.181	3.555	1.995	0.01519
12.208	4.402	2.254	0.02564
13.345	5.421	2.502	0.05462
		2.710	0.05842
Series VIII		2.999	0.05765
3.856	0.1196	3.453	0.08328
4.276	0.1764	3.859	0.1349
4.694	0.2418		
5.138	0.3177	Series XI	
5.561	0.4128	4.340	0.1951
		4.633	0.2351
Series IX			
4.978	0.2963	Series XII	
5.392	0.3798	51.066	23.72

Appendix 4A. Continued.

T/K	C_p/$JK^{-1}mol^{-1}$	T/K	C_p/$JK^{-1}mol^{-1}$
51.612	23.92	71.520	31.93
52.393	24.17	72.440	32.54
53.356	24.51	73.348	33.08
54.416	24.77	74.244	33.75
55.457	25.11	75.128	34.42
56.480	25.46	76.000	35.16
57.484	25.80	76.861	35.86
58.505	26.14	77.711	36.71
59.542	26.53	78.548	37.58
60.563	26.93	79.374	38.65
61.602	27.37	80.187	39.51
62.660	27.76	80.989	40.68
63.702	28.18	81.777	42.03
64.728	28.57	82.551	43.43
65.739	29.01	83.312	44.99
66.736	29.44		
67.718	29.92	Series XIII	
68.689	30.35	83.617	45.50
69.645	30.97	84.187	47.27
70.589	31.41	84.747	48.93

Appendix 4A. Continued.

T/K	C_p / $JK^{-1}mol^{-1}$	T/K	C_p / $JK^{-1}mol^{-1}$
85.297	50.91	96.750	42.37
85.835	53.13	97.800	42.57
86.360	55.56	98.917	43.27
86.864	58.97	100.438	43.93
87.351	62.88	102.118	44.84
87.829	67.59	103.578	45.60
88.285	74.60	105.013	46.52
88.713	84.47	106.598	47.64
89.104	101.62	108.327	48.96
89.386	249.9	110.024	50.54
Transition		111.686	52.46
89.734	244.7	113.009	131.09
90.069	58.51	Transition	
90.587	40.90	114.575	59.68
91.143	40.85	116.124	57.38
91.697	40.77	Transition	
92.248	40.98	117.228	352.3
		118.324	45.02
Series XIV		120.036	45.16
95.729	41.88		

Appendix 4A. Continued.

T / K	C_p / $JK^{-1}mol^{-1}$	T / K	C_p / $JK^{-1}mol^{-1}$
Series XV		Transition	
110.346	50.65	117.137	223.6
110.987	51.42	117.595	45.02
111.622	52.35	118.250	44.98
112.251	53.16	118.905	45.10
112.875	54.16	119.557	45.29
113.375	133.41		
Transition		Series XVII	
114.040	80.23	II-I' Transition,	
114.596	56.78	Continuous Heating	
115.207	52.97		
115.824	53.59	Series XVIII	
116.435	55.29	I'-I Transition,	
		Continuous Heating	
Series XVI			
114.128	49.33	Series XIX	
114.764	50.75	I'-I Transition,	
115.392	52.18	Continuous Heating	
116.001	53.73		
116.591	59.63		

Appendix 4A. Continued.

T / K	C_p / $JK^{-1}mol^{-1}$	T / K	C_p / $JK^{-1}mol^{-1}$
Series XX		141.661	45.92
II-I' Transition,		144.191	46.17
Continuous Heating		146.717	46.35
		149.241	46.65
Series XXI		151.762	46.75
II-I Transition,		154.265	47.04
Continuous Heating		156.765	47.31
		159.262	47.53
Series XXII		161.741	47.93
118.908	45.14	164.199	48.15
120.364	45.09	166.648	48.48
121.956	45.07	169.084	48.74
123.682	45.17	171.512	49.17
125.581	45.17	173.920	49.51
127.752	45.18	176.330	50.00
130.084	45.21	178.692	50.05
132.402	45.34		
134.703	45.41	Series XXIII	
136.990	45.68	180.888	50.84
139.264	45.72	182.913	51.41

Appendix 4A. Continued.

T / K	C_p / $JK^{-1}mol^{-1}$	T / K	C_p / $JK^{-1}mol^{-1}$
184.758	55.08	87.497	63.50
Fusion,		88.005	69.62
Continuous Heating		88.483	78.11
188.316	58.50	88.926	91.57
		89.291	128.95
Series XXIV		Transition	
184.933	59.74	89.667	336.2
Fusion		89.972	74.20
188.406	59.53	90.495	41.02
190.308	59.93	91.086	40.84
		91.676	40.89
- Sample II -			
Series I		Series III	
III-II Transition,		110.400	50.93
Continuous Heating		111.011	51.23
		111.618	52.34
Series II		112.218	52.65
85.850	53.30	112.779	53.88
86.417	55.90	113.301	54.50
86.966	58.77	Transition	

Appendix 4A. Continued.

T/K	C_p/JK^{-1}mol^{-1}	T/K	C_p/JK^{-1}mol^{-1}
113.645	353.9	Series V	
113.941	75.44	1.835	0.01120
114.419	54.60	1.849	0.01210
114.940	51.79	2.002	0.01489
115.464	52.57	2.210	0.02099
115.985	53.75	2.448	0.02880
116.499	55.79	2.757	0.04187
116.861	224.5	3.122	0.06321
Transition		3.481	0.09060
117.416	44.96	3.916	0.1320
118.048	44.94		
		Series VI	
Series IV		1.842	0.01140
171.630	49.35	2.045	0.01605
175.101	49.48	2.282	0.02334
178.538	50.27	2.511	0.03129
181.634	51.03	2.803	0.04314
184.566	62.21	3.158	0.06532
Fusion		3.522	0.09309
		3.880	0.1273

Appendix 4A. Continued.

$\frac{T}{K}$	$\frac{C_p}{JK^{-1}mol^{-1}}$	$\frac{T}{K}$	$\frac{C_p}{JK^{-1}mol^{-1}}$
4.263	0.1726		

Series VII

1.824	0.01142
1.988	0.01516
2.202	0.02120
2.542	0.03232

Series VIII

3.902	0.1274
4.293	0.1705
4.652	0.2276
4.969	0.2833
5.292	0.3435
5.637	0.4228
5.980	0.5208
6.374	0.6429
6.879	0.8756
7.456	1.105

Appendix 4B. Measured heat capacities of DBr.

$\frac{T}{K}$	$\frac{C_p}{JK^{-1}mol^{-1}}$	$\frac{T}{K}$	$\frac{C_p}{JK^{-1}mol^{-1}}$
		Series II	
- Sample I -		1.884	0.01267
Series I		2.053	0.01767
1.887	0.01367	2.278	0.0231
2.090	0.01763	2.542	0.0345
2.310	0.0256	2.788	0.0434
2.595	0.0348	3.038	0.0559
2.899	0.0471	3.292	0.0761
3.209	0.0648	3.533	0.0992
3.492	0.0818	3.782	0.1178
3.760	0.1047	4.045	0.1501
4.027	0.1308	4.295	0.1816
4.282	0.1654	4.561	0.2128
4.544	0.2064	4.840	0.283
4.814	0.259	5.145	0.336
5.105	0.310		
5.432	0.388	Series III	
5.816	0.485	1.901	0.01484
6.257	0.626	2.119	0.01950
		2.361	0.0255

Appendix 4B. Continued.

T / K	C_p / $JK^{-1}mol^{-1}$	T / K	C_p / $JK^{-1}mol^{-1}$
2.608	0.0373	9.741	2.453
2.870	0.0484	10.722	3.187
3.154	0.0680	11.735	3.961
3.428	0.0838		
3.707	0.1094	Series V	
3.984	0.1415	5.821	0.464
4.256	0.1861	6.287	0.603
4.530	0.225	6.797	0.783
4.827	0.271	7.484	1.072
5.152	0.347	8.329	1.511
5.525	0.419	9.247	2.093
5.581	0.430	10.226	2.797
		11.233	3.561
Series IV		12.319	4.458
5.677	0.420	13.346	5.263
6.102	0.536	14.231	6.077
6.578	0.697	15.103	6.865
7.142	0.942	15.985	7.651
7.883	1.274	16.895	8.417
8.786	1.787	17.853	9.249

Appendix 4B. Continued.

T / K	C_p / $JK^{-1}mol^{-1}$	T / K	C_p / $JK^{-1}mol^{-1}$
18.886	10.008	66.130	31.96
20.021	10.884	67.167	32.43
		68.202	32.87
Series VI		69.232	33.30
49.947	25.28	70.262	33.97
50.975	25.83	71.303	34.50
51.992	26.03	72.356	35.12
53.002	26.32	73.422	35.85
54.005	26.75	74.500	36.49
55.000	27.09	75.595	37.20
55.985	27.54	76.703	38.09
56.972	27.99	77.819	38.85
57.964	28.31	78.927	40.01
58.961	28.78	80.021	40.96
59.961	29.26	81.102	42.12
60.967	29.69	82.166	43.27
61.984	30.08	83.210	44.53
63.010	30.56	84.239	45.89
64.046	31.00	85.236	47.95
65.089	31.35	86.184	49.63

Appendix 4B. Continued.

$\frac{T}{K}$	$\frac{C_p}{JK^{-1}mol^{-1}}$	$\frac{T}{K}$	$\frac{C_p}{JK^{-1}mol^{-1}}$
87.070	51.62	78.357	39.36
87.863	53.71	79.456	40.40
88.553	56.10	80.538	41.45
89.192	58.67	81.608	42.67
89.818	61.66	82.662	43.77
90.431	65.11	83.702	45.16
91.029	69.14	84.720	46.85
91.613	76.19	85.701	48.55
92.175	84.42	86.636	50.41
92.706	98.95	87.513	52.24
93.186	131.12	88.294	55.17
93.516	433.0	88.974	57.35
Transition		89.542	60.16
94.117	197.0	90.098	63.40
94.451	57.54	90.702	67.05
95.089	46.73	91.293	71.73
		91.864	78.92
Series VII		92.411	89.26
76.139	37.45	92.923	108.31
77.246	38.44	93.354	182.74

Appendix 4B. Continued.

T / K	C_p / $JK^{-1}mol^{-1}$	T / K	C_p / $JK^{-1}mol^{-1}$
Transition		108.707	52.61
93.793	404.6	110.075	53.69
94.143	108.58	111.440	54.78
94.777	47.65	112.803	55.83
95.609	46.69	114.162	57.46
		115.504	59.32
Series VIII		116.825	61.14
III-II Transition,		118.123	66.74
Continuous Heating		119.050	324.6
94.763	47.84	Transition	
95.791	46.72	120.432	80.39
96.887	46.95	121.441	49.89
98.054	47.41	122.635	49.15
99.297	47.65		
100.596	48.08	Series IX	
101.923	48.61	III-II Transition,	
103.280	49.21	Continuous Heating	
104.645	50.03	95.062	46.93
105.997	50.99	96.280	47.02
107.348	51.79	97.439	47.04

Appendix 4B. Continued.

T / K	C_p / $JK^{-1}mol^{-1}$	T / K	C_p / $JK^{-1}mol^{-1}$
98.678	47.36	122.092	49.11
99.976	47.77		
101.289	48.28	Series X	
102.621	48.80	II-I Transition,	
103.962	49.52	Continuous Heating	
105.302	50.44		
106.654	51.27	Series XI	
108.014	52.05	II-I Transition,	
109.373	53.08	Continuous Heating	
110.719	53.97	121.482	49.00
112.064	55.22	122.969	48.92
113.415	56.99	124.573	48.90
114.761	58.39	126.291	48.98
116.094	59.68	128.119	49.04
117.408	61.90	130.058	49.18
118.446	72.82	131.983	49.15
119.035	261.5	133.898	49.40
Transition		135.799	49.50
120.153	216.6	137.709	49.62
120.896	49.48	139.696	49.73

Appendix 4B. Continued.

T / K	C_p / $JK^{-1}mol^{-1}$	T / K	C_p / $JK^{-1}mol^{-1}$
141.724	49.91	24.492	14.04
143.734	50.00	25.538	14.66
145.823	50.28	26.594	15.27
147.985	50.36	27.626	15.84
150.134	50.50	28.619	16.39
		29.579	16.90
Series XII		30.511	17.37
11.547	3.836	31.439	17.82
12.506	4.642	32.385	18.27
13.529	5.523	33.372	18.74
14.578	6.504	34.432	19.22
15.586	7.343	35.542	19.68
16.559	8.195	36.633	20.17
17.492	8.979	37.690	20.53
18.459	9.768	38.718	21.03
19.475	10.529	39.731	21.39
20.565	11.341	40.738	21.81
21.605	12.08	41.743	22.22
22.532	12.72	42.741	22.53
23.481	13.37	43.749	22.97

Appendix 4B. Continued.

T / K	C_p / $JK^{-1}mol^{-1}$	T / K	C_p / $JK^{-1}mol^{-1}$
44.779	23.35	187.638	62.60
45.832	23.76		
46.911	24.21	Series XIV	
48.018	24.61	Fusion,	
49.190	25.02	Continuous Heating	
Series XIII		- Sample II -	
152.399	50.80	Series I	
155.004	51.10	48.438	24.66
157.619	51.15	50.176	25.34
160.266	51.60	52.039	26.05
162.920	51.93	53.839	26.73
165.553	52.26	55.581	27.40
168.189	52.67	57.272	28.08
170.826	53.63	58.913	28.75
173.464	54.09	60.510	29.42
176.103	55.10	62.067	30.09
178.736	56.62	63.738	30.81
181.324	63.85		
Fusion			

Appendix 4B. Continued.

$\frac{T}{K}$	$\frac{C_p}{JK^{-1}mol^{-1}}$	$\frac{T}{K}$	$\frac{C_p}{JK^{-1}mol^{-1}}$
Series II		3.892	0.1208
1.880	0.01197	4.217	0.1620
2.122	0.01796	4.569	0.2156
2.428	0.0268	4.958	0.2871
2.819	0.0431	5.378	0.3822
3.148	0.0610		
3.421	0.0825	Series IV	
3.713	0.1118	1.879	0.01320
4.056	0.1534	2.129	0.01903
4.401	0.1918	2.415	0.0295
4.833	0.2787	2.717	0.0390
		3.014	0.0548
Series III		3.327	0.0729
1.888	0.01274	3.651	0.1000
2.126	0.01885	3.983	0.1318
2.401	0.0276	4.343	0.1774
2.707	0.0400		
3.004	0.0529	Series V	
3.297	0.0727	4.710	0.2274
3.590	0.0949	5.186	0.3174

Appendix 4B. Continued.

T / K	C_p / $JK^{-1}mol^{-1}$	T / K	C_p / $JK^{-1}mol^{-1}$
5.708	0.4307	12.306	4.451
6.270	0.5978	13.278	5.327
6.870	0.8181		
		Series VIII	
Series VI		8.125	1.4010
4.870	0.2528	8.844	1.8518
5.356	0.3488	9.546	2.308
5.880	0.4906	10.269	2.825
6.436	0.6629	11.043	3.440
7.032	0.8947	11.881	4.129
7.725	1.2129	12.812	4.934
		13.816	5.745
Series VII			
7.417	1.0609	Series IX	
8.048	1.3795	157.262	51.25
8.664	1.7312	159.723	51.47
9.297	2.148	162.166	51.79
9.957	2.614	164.613	52.31
10.655	3.147	167.085	52.60
11.428	3.752	169.577	52.98

Appendix 4B. Continued.

T / K	C_p / $JK^{-1}mol^{-1}$	T / K	C_p / $JK^{-1}mol^{-1}$
172.087	53.67		
174.613	54.32		
177.158	56.34		
179.737	57.10		
182.169	64.00		
Fusion			
188.179	62.15		

CHAPTER 5

Thermodynamic Properties of HI and DI

5-1. Heat capacity

The measured heat capacity values are chronologically presented as C_p in appendices 5A and B for HI and DI, respectively. Curvature corrections were not applied. The smoothed values at rounded temperatures are given in table 5-1. Above 150 K, corrections arising from vaporization of HI or DI were significant. Relevant quantities for such corrections were evaluated as follows. The density of solid HI in phase I was obtained by interpolation of the X-ray data at 125 K[1] and at triple point.[2] The liquid density was taken from McIntosh and Steele.[3] Densities of DI were taken to be identical to those of HI. The heat capacity in the gaseous phase is (7/2)R in the temperature range where the values was required.

The results for HI and DI are plotted in figures 5-1 and 5-2, respectively. The measured heat capacities are compared with earlier results in figures 5-3 and 5-4 for HI and DI, respectively, in terms of the differences from a smooth curve corresponding to the values given in table 5-1. The scatter of our measured points is $\pm$3 per cent at the lowest temperatures, decreasing to $\pm$0.5 per cent at 10 K and to $\pm$0.1 per cent above 20 K. It increased, however, up to $\pm$0.2 and $\pm$1 per cent at higher temperatures and near the transitions, respectively.

TABLE 5-1. The heat capacity of solid HI and DI at rounded values of temperatures.

$\frac{T}{K}$	$\frac{C_p}{JK^{-1}mol^{-1}}$	
	HI	DI
2	0.0282	0.0267
3	0.100	0.094
4	0.261	0.251
5	0.559	0.545
6	1.023	0.996
8	2.447	2.414
10	4.358	4.365
12	6.496	6.501
15	9.649	9.741
20	13.97	14.13
25	17.08	17.37
30	19.40	19.91
35	21.38	22.24
40	23.30	24.68
45	25.44	26.77
50	27.98	29.35
55	31.28	32.33
60	36.11	36.03

TABLE 5-1. Continued.

T / K	C_p / $JK^{-1}mol^{-1}$	
	HI	DI
65	44.83	40.95
70	——	48.68
75	36.34	——
80	37.26	43.85
85	38.63	43.92
90	40.24	45.16
95	41.89	46.75
100	43.78	48.60
110	48.74	53.04
120	56.65	59.96
130	44.94	48.66
140	45.03	48.37
150	45.41	48.25
160	45.84	48.21
170	46.32	48.39
180	46.86	48.67
190	47.52	49.30
200	48.21	50.09
210	49.23	50.69
217	50.47	51.21

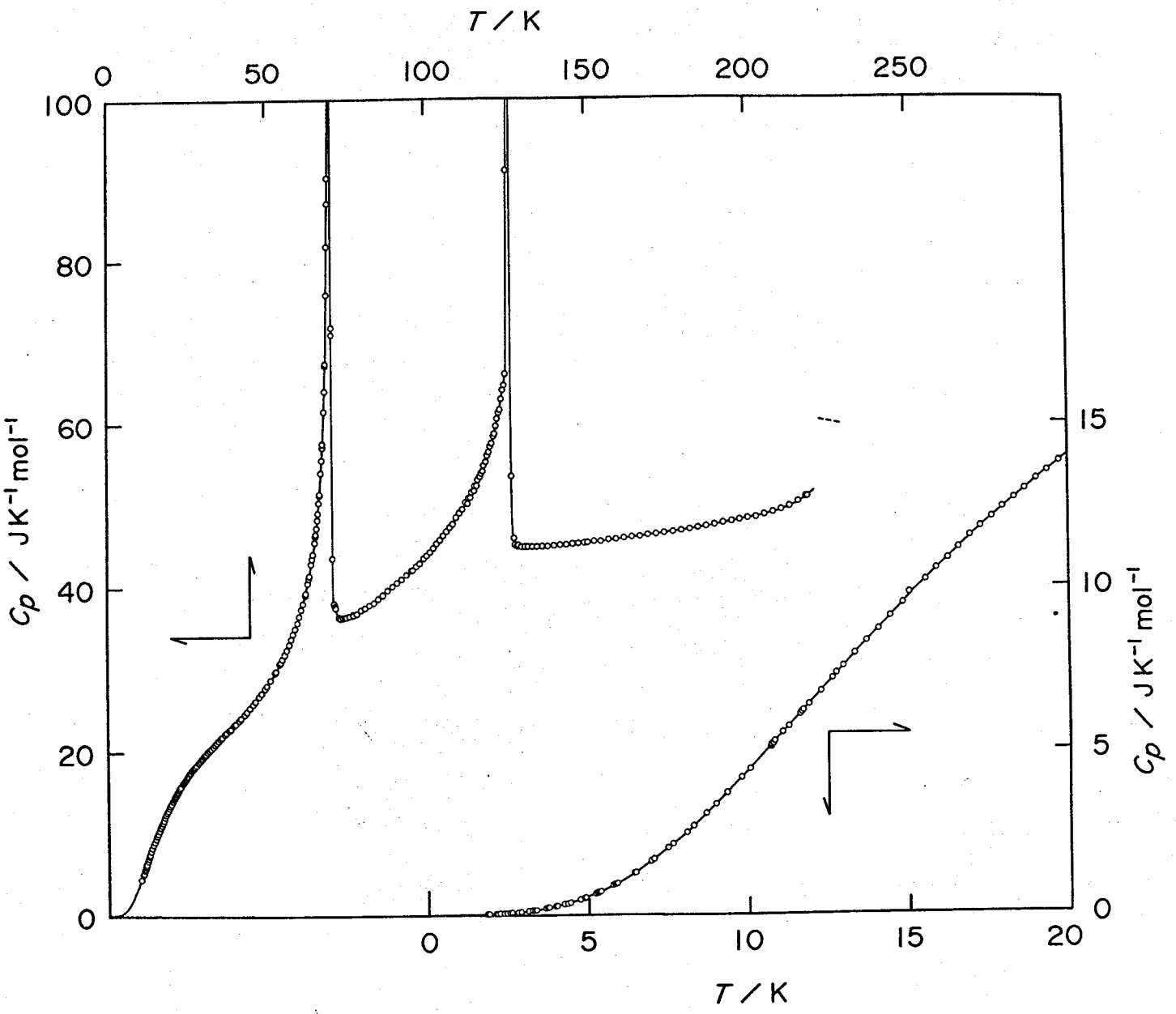

FIGURE 5-1. Heat capacity of HI.

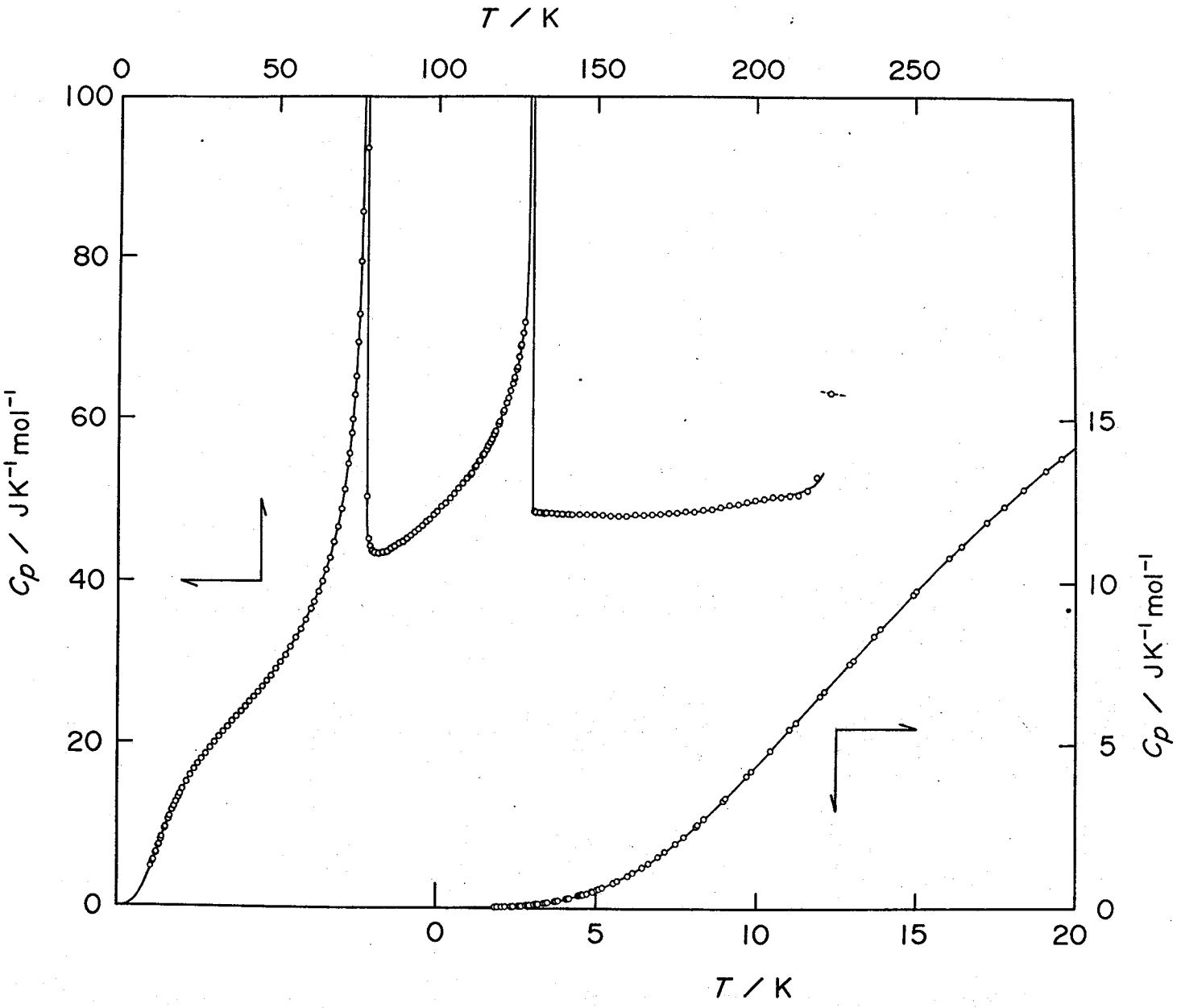

FIGURE 5-2. Heat capacity of DI.

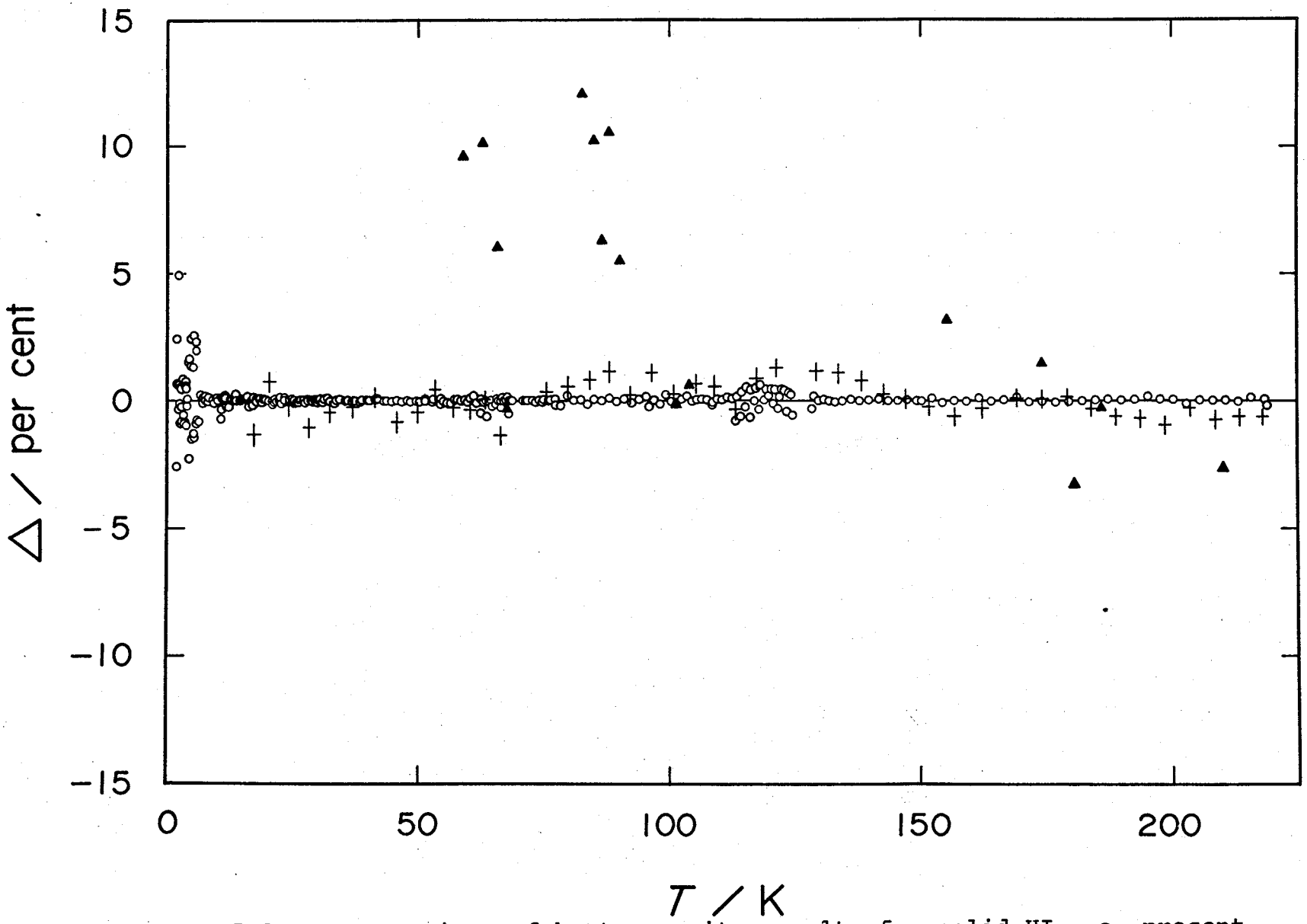

FIGURE 5-3. A comparison of heat capacity results for solid HI. o, present results; +, Giauque and Wiebe;[4] ▲, Eucken and Karwat.[5] Δ/per cent = [C_p(obs.)-C_p(smooth)] x 100 / [C_p(smooth)], where C_p(smooth) is given in table 5-1.

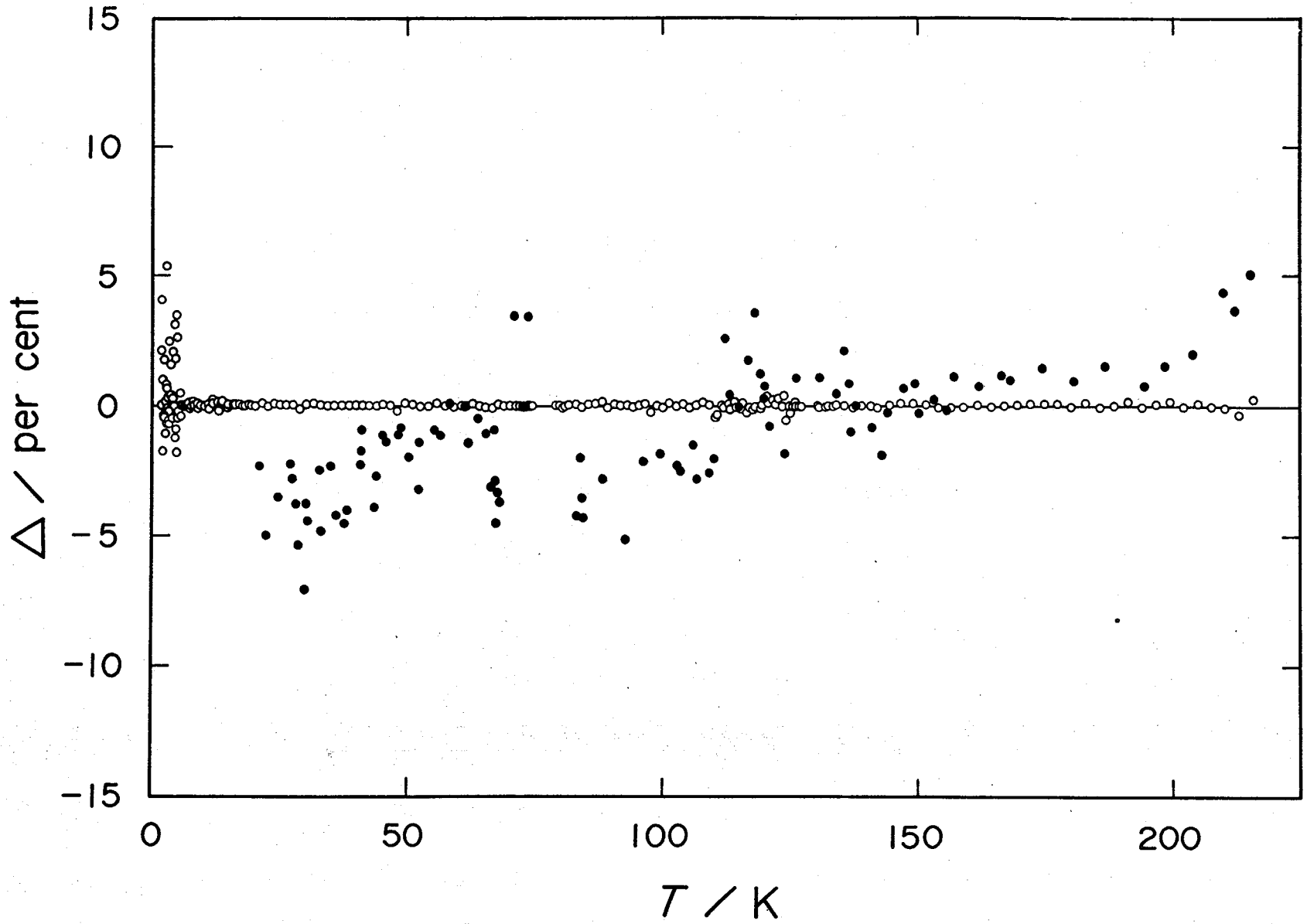

FIGURE 5-4. A comparison of heat capacity results for solid DI. o, present results; ●, Clusius and Wolf.[6]
Δ/per cent = [C_p(obs.)-C_p(smooth)] x 100 / [C_p(smooth)], where C_p(smooth) is given in table 5-1.

Giauque and Wiebe's results for HI are in good agreement with the present results within the combined limits of error. Some of their points near 175 K showed a broad hump probably due to distillation heat effects. Eucken and Karwat's[5] and Clusius and Wolf's[6] results are strongly scattered and deviate from ours as reported for other hydrogen halides. A comparison in the lower temperature region is made by use of equivalent Debye temperature Θ_D, whose temperature dependence for 3N degrees of freedom is shown in figures 5-5 and 5-6 for HI and DI, respectively. The Debye temperature curves for HI and DI agreed only between 10 and 15 K: The latter is consistently higher below 10 K and declines more rapidly above 15 K.

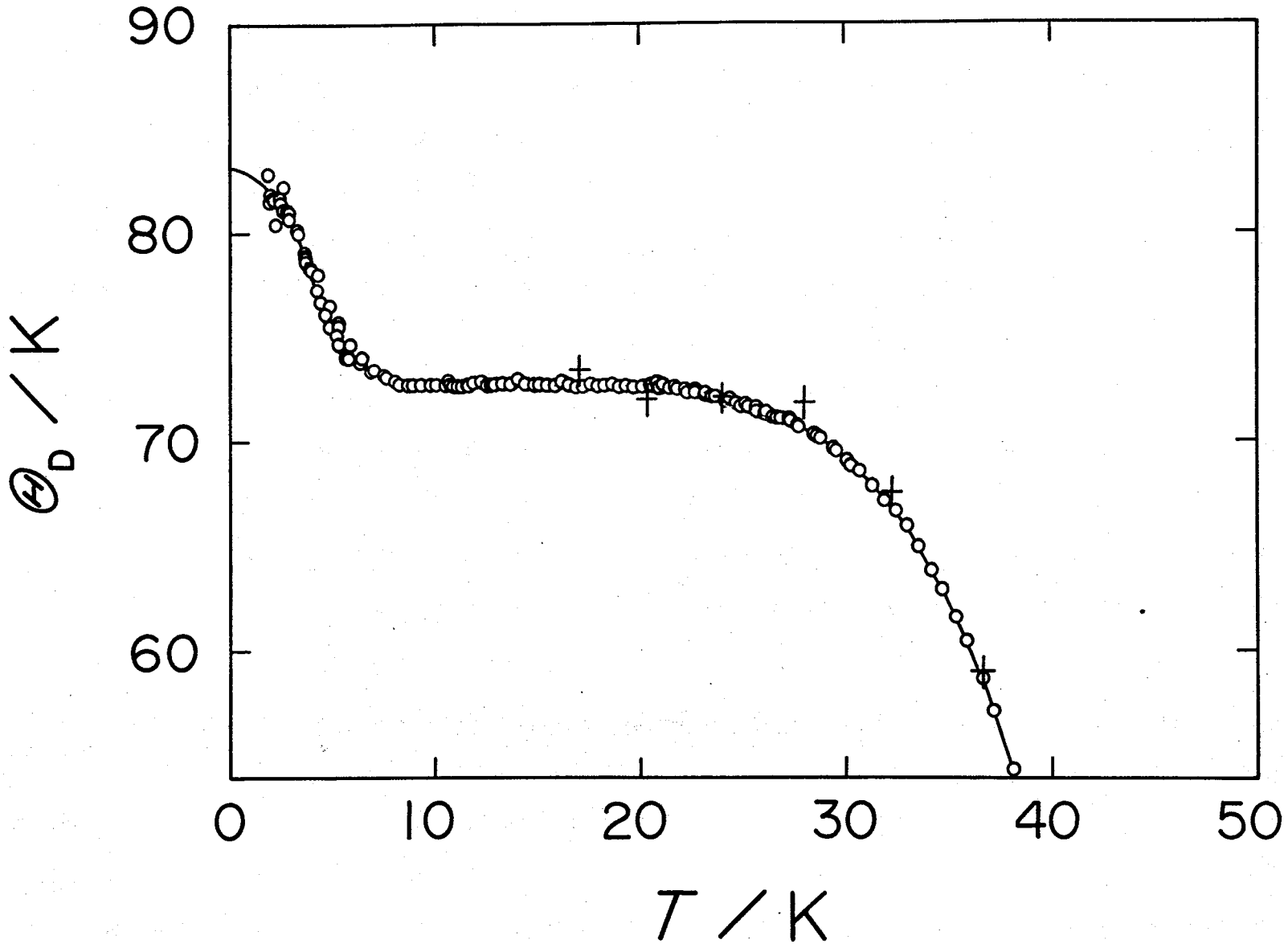

FIGURE 5-5. The Debye characteristic temperature of HI derived from the measured heat capacities, assuming 3N degrees of freedom. o, present results; +, Giauque and Wiebe.[4]

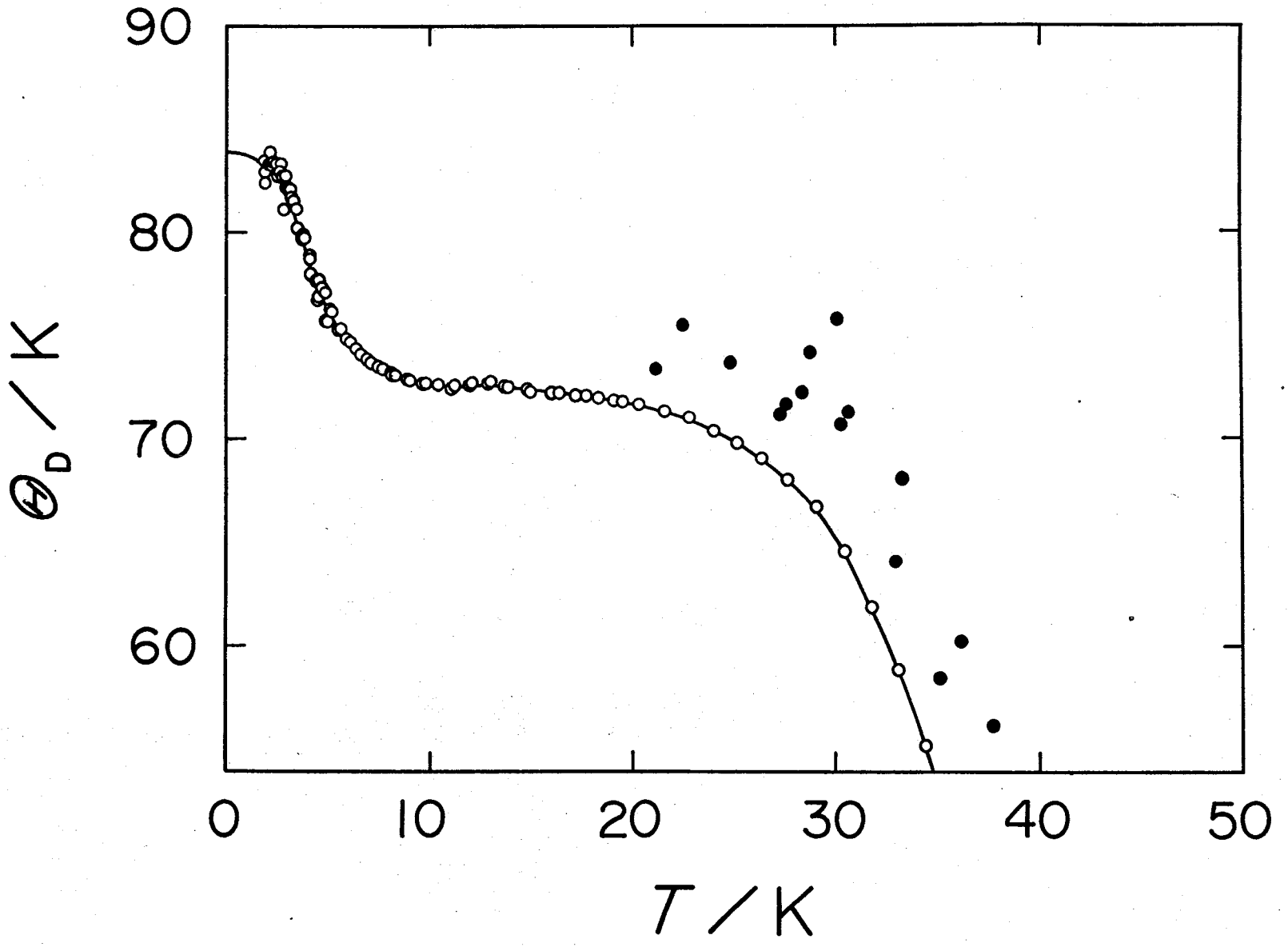

FIGURE 5-6. The Debye characteristic temperature of DI derived from the measured heat capacities, assuming 3N degrees of freedom. o, present results; ●, Clusius and Wolf.[6]

5-2. Vapor pressure

Measured vapor pressures of the solid and liquid HI and DI are listed in tables 5-2 and 5-3, respectively. The results for solids were plotted as log P against T^{-1} in figure 5-7. Measurements by other workers are also included for the sake of comparison. Our results for both solids and McIntosh and Steele's results[7] for HI indicate that the slope decreases at lower temperatures. In contrast, Henglein's results[8] for HI, which consist only of three points, are approximately colinear in this plot. One of possibilities that might give such an effect would be existence of permanent gas, which is supposed to be hydrogen as one of decomposing products. Estimated amounts of permanent gas are 900 and 410 Pa at 180 K for HI and DI, respectively. However, no corrections for the pressure values obtained were made. There were no indications of decomposition in the temperature drift of heat capacity determinations nor in the purity determination at the triple point which was conducted after all the vapor pressure measurements had been concluded.

TABLE 5-2. Vapor pressures of HI.

T / K	P / kPa	T / K	P / kPa
Solid		Liquid	
180.905	4.180	223.505	53.152
183.515	4.822	224.188	55.145
186.097	5.615		
188.670	6.559		
191.220	7.688		
193.821	9.051		
196.399	10.665		
198.972	12.556		
201.566	14.796		
204.205	17.459		
206.825	20.531		
209.432	24.076		
212.009	28.126		
214.565	32.722		
217.085	37.892		
217.746	39.511		
219.861	44.370		
220.218	45.384		

TABLE 5-3. Vapor pressures of DI.

T / K	P / kPa	T / K	P / kPa
Solid		Liquid	
178.969	2.838	222.705	51.278
181.836	3.472	222.769	51.475
184.615	4.233	223.960	54.572
187.382	5.168		
190.129	6.300		
192.864	7.665		
195.578	9.288		
198.278	11.218		
200.954	13.479		
203.672	16.185		
206.366	19.228		
209.039	22.776		
211.757	27.039		
214.452	31.932		
217.379	38.329		
219.974	45.281		
220.269	45.380		
220.941	47.038		

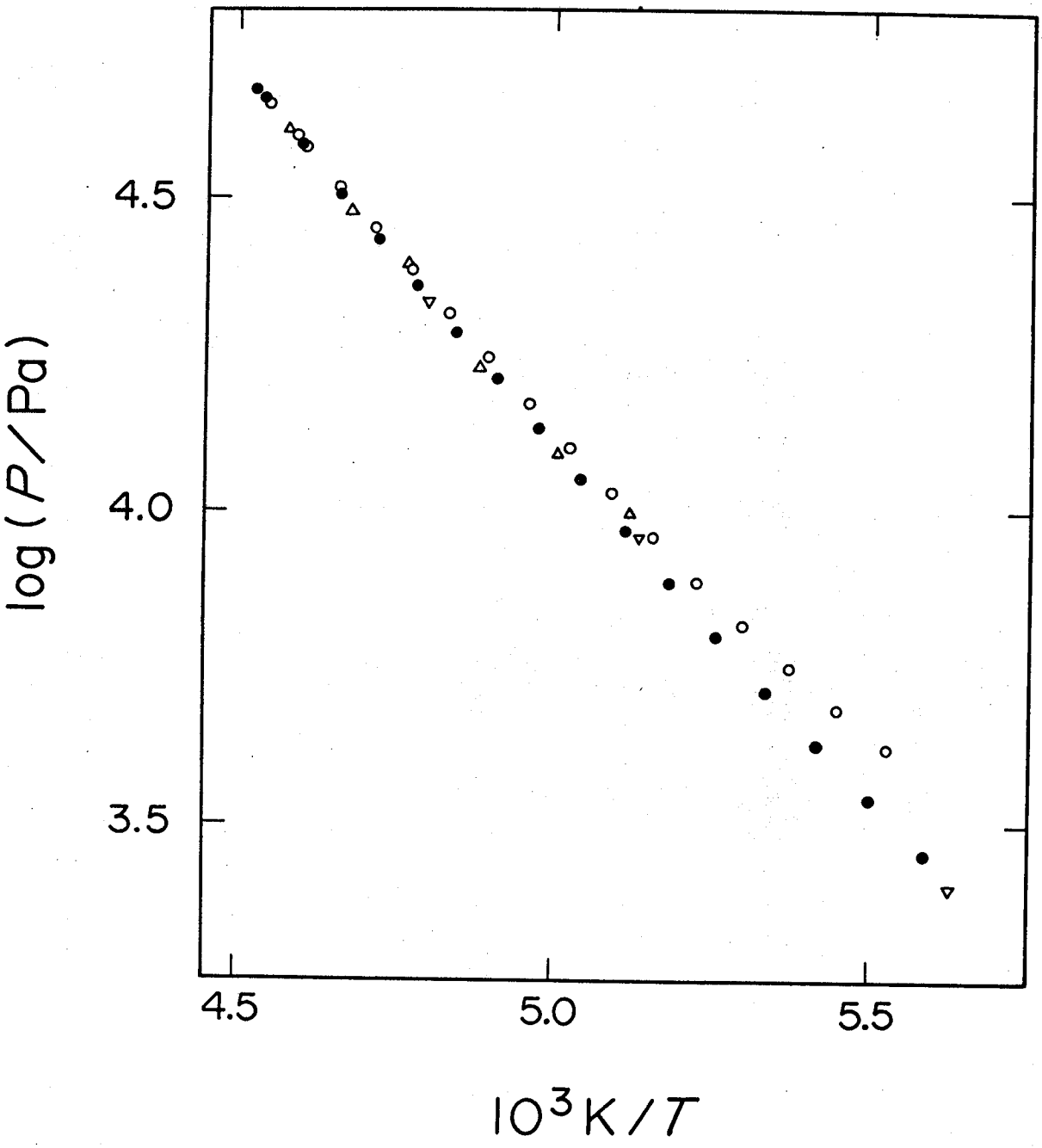

FIGURE 5-7. Vapor pressure of solid HI and DI. HI: o, present results; Δ, McIntosh and Steele;[7] ∇, Henglein.[8] DI: ●, present results.

5-3. Enthalpy of fusion

The results of fusion experiments are given in table 5-4. A correction for the $\int C_p dT$ was applied to compute the enthalpy of fusion ΔH_f from cumulative enthalpy $H(T_2)-H(T_1)$. Measurements by other workers are also included for the sake of comparison. The mean values of the enthalpy of fusion of HI and DI obtained were 2855.3 and 2841.2 J mol^{-1}, respectively.

The triple points of pure HI and DI, (222.497 $\pm$ 0.005) and (221.511 $\pm$ 0.005) K respectively, were estimated from a plot of the equilibrium temperature against the reciprocal of the fraction melted (see table 5-5).

TABLE 5-4. The enthalpy of fusion of HI and DI.

Series no.	T_1 / K	T_2 / K	$H(T_2)-H(T_1)$ / $Jmol^{-1}$	ΔH_f / $Jmol^{-1}$
		HI		
XXI	219.861 - 223.505		3051.0	2856.0
XXII[a]	220.218 - 224.188		3072.4	2854.6
			Average	2855.3
		Giauque and Wiebe (1929)[b]		2871.5±2.1
		Eucken and Karwat (1924)[c]		3038.
		DI		
XVIII	220.269 - 222.769		2999.8	2842.5
XIX[a]	219.974 - 222.705		3011.6	2839.9
			Average	2841.2
		Clusius and Wolf (1947)[d]		2863.1

TABLE 5-4. Continued.

[a] In this series, the fusion was done in stages.

[b] From reference 4.

[c] From reference 5.

[d] From reference 6.

TABLE 5-5. The triple point of HI and DI.

Fraction melted	T / K	P / kPa
	HI	
0.250	222.359	50.46
0.427	222.400	50.51
0.605	222.419	50.59
0.746	222.433	50.71
0.890	222.444	50.74
(1.000)	222.449±0.002	
T_f (pure HI)	222.497±0.005	
Giauque and Wiebe (1929)[a]	222.31±0.05	
Eucken and Karwat (1924)[b]	220.	
Bates et al. (1935)[c]		50.5
Miravelles and Moles (1925)[d]		52.44

TABLE 5-5. Continued.

Fraction melted	T / K	P / kPa
	DI	
0.237	221.472	48.31
0.498	221.488	48.61
0.676	221.494	49.10
0.854	221.501	49.04
0.945	221.508	49.10
(1.000)	221.501±0.002	
T_f (pure DI)	221.511±0.005	
Clusius and Wolf (1947)[e]	221.23	48.0

[a] From reference 4.

[b] From reference 5.

[c] From reference 9.

[d] From reference 10.

[e] From reference 6.

5-4. Transition in solids

The thermal behavior of two phase transitions of both solids can be visualized through enthalpy change in the transition region. Figure 5-8 refers to the transition between phase III and II and figure 5-9 to that between phase II and I. The different series of results were normalized on the high temperature side of transitions. The transition temperatures were then determined from the point at which the rate of change of enthalpy with temperature is maximum.

No isothermal heat absorption was detected at the lower transition of HI and DI. Furthermore, the time to reach equilibrium after heating was off was about 10 min, which is approximately normal equilibration time in this temperature region. These facts suggest that III-II transition of HI and DI is of the second or higher order. At the upper transition of HI and DI, a considerably longer equilibration time was required; thus the cooling drift at 100 min after heating was about -0.002 K min^{-1}, which is large compared with that at the III-I transition of HCl and DCl, II-I' transition of HBr, or II-I transition of DBr. Therefore, the II-I transition of HI and of DI, through it appears diffuse in figures 5-1 and 5-2, is of the first order with a latent heat at the

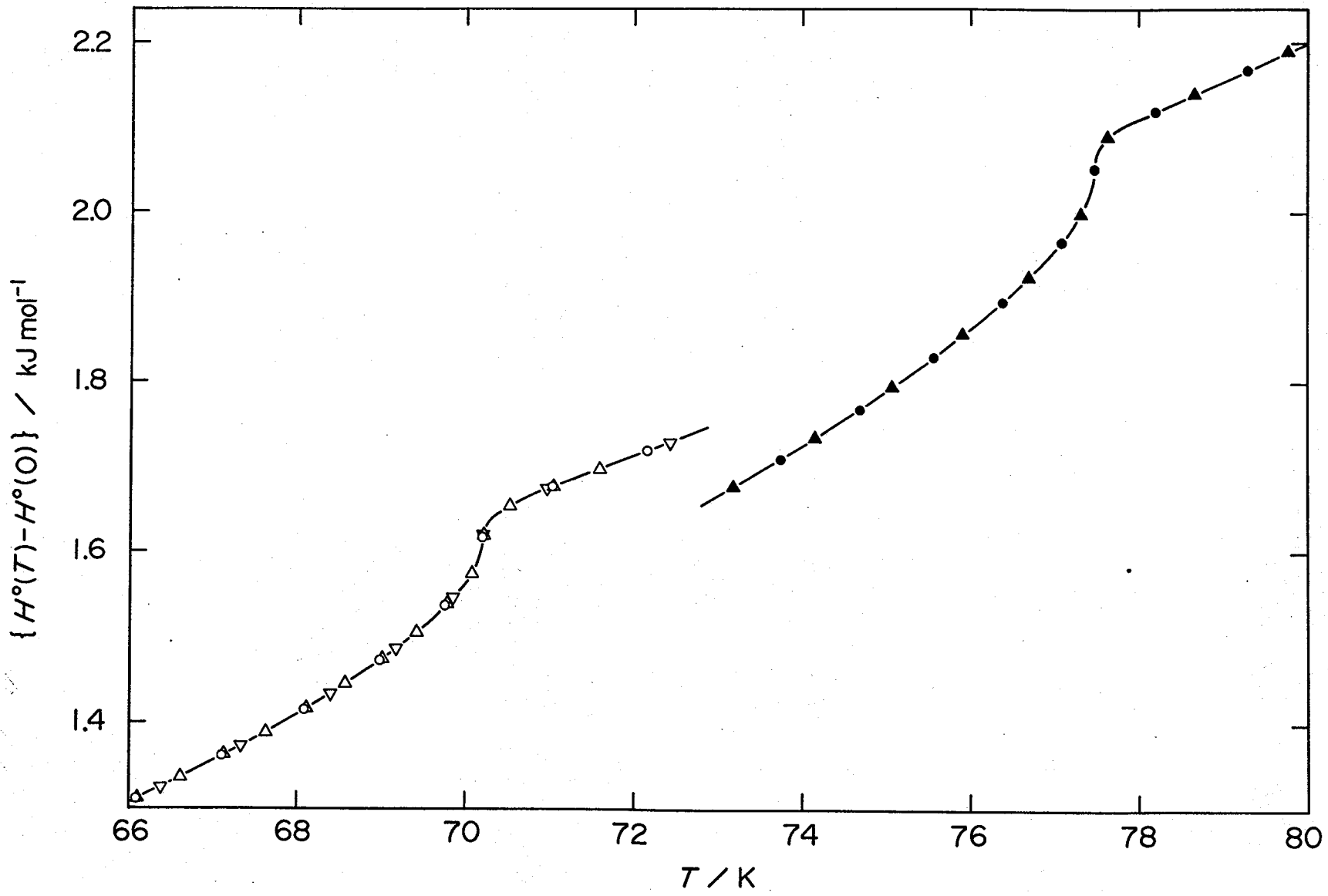

[68I]

FIGURE 5-8. Enthalpy change in the region phase III → phase II of HI and DI. The different series of measurements are normalized on the high temperature side of transitions. HI: o, (XIV); Δ, (XV); ∇, (XVI). DI: ●, (I); ▲, (III).

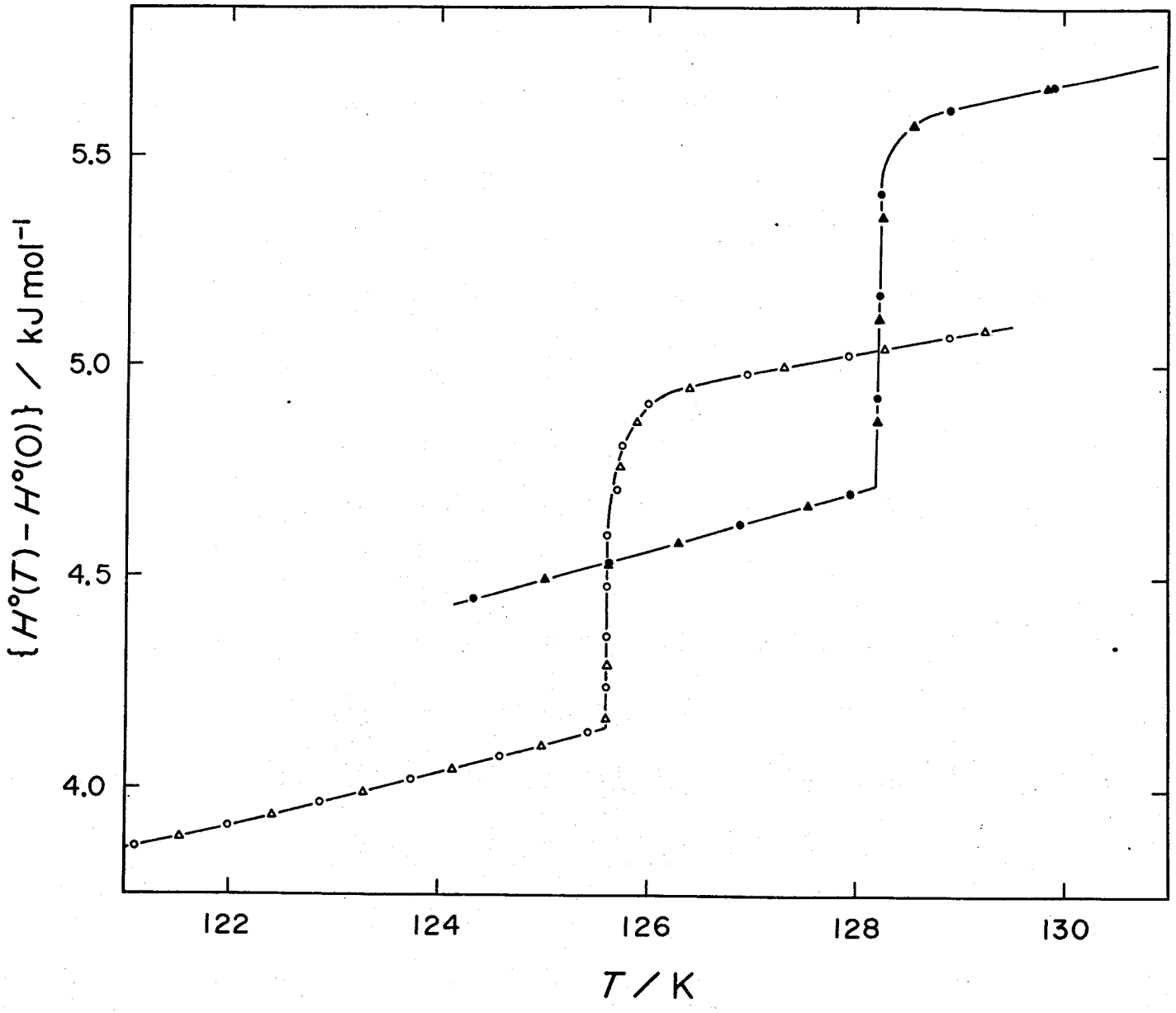

FIGURE 5-9. Enthalpy change in the region phase II → phase I of HI and DI. The different series of measurements are normalized on the high temperature side of transitions. HI: o, (II); Δ, (III). DI: ●, (V); ▲, (VI).

transition point. The enthalpy change at the transitions measured are shown in tables 5-6 and 5-7 for III-II and II-I transitions, respectively.

As for the "transitions" at 10 and 25 K, which were indicated by spectral studies, no anomalies in heat capacity were observed as shown in figures 5-1 and/or 5-5.

TABLE 5-6. The enthalpy of III-II transition of HI and DI including the "normal" part of heat capacity.

Series no.	T_1 / K	T_2 / K	$H(T_2)-H(T_1)$ / $Jmol^{-1}$	$H(71)-H(68)$ / $Jmol^{-1}$
			HI	
XIV[a]	68.082 - 71.030		261.8	265.1
XV[a]	68.108 - 71.040		260.1	264.8
XVI[a]	68.390 - 70.954		239.5	264.8
XVII	67.992 - 70.678		252.1	264.8
XVIII	65.831 - 70.985		377.6	265.2
			Average	264.9±0.3

	T_{tr} / K
Present work	70.23±0.02
Giauque and Wiebe (1929)[b]	70.1
Eucken and Karwat (1924)[c]	72.

TABLE 5-6. Continued.

Series no.	T_1 / K	T_2 / K	$H(T_2)-H(T_1)$ / $Jmol^{-1}$	$H(78)-H(75)$ / $Jmol^{-1}$
			DI	
I[a]	74.687 - 78.206		350.5	319.2
II	75.205 - 77.956		302.5	318.9
III[a]	75.063 - 78.673		345.8	319.5
XV	75.134 - 78.249		323.0	319.7
			Average	319.3±0.4

	T_{tr} / K
Present work	77.48±0.02
Clusius and Wolf (1947)[d]	77.3

[a] In this series, the transition was done in stages.

[b] From reference 4.

[c] From reference 5.

[d] From reference 6.

TABLE 5-7. The enthalpy of II-I transition of HI and DI including the "normal" part of heat capacity.

Series no.	T_1 / K	T_2 / K	$H(T_2)-H(T_1)$ / $Jmol^{-1}$	$H(127)-H(124)$ / $Jmol^{-1}$
			HI	
II[a]	123.740 - 126.957		959.1	945.0
III[a]	124.136 - 127.303		954.0	948.7
XIX	123.162 - 126.993		1000.6	947.3
XX	122.575 - 126.858		1026.8	946.4
			Average	946.9±1.9

	T_{tr} / K
Present work	125.60±0.01
Giauque and Wiebe (1929)[b]	125.6
Eucken and Karwat (1924)[c]	124.

TABLE 5-7. Continued.

Series no.	T_1 / K	T_2 / K	$H(T_2)-H(T_1)$ / $Jmol^{-1}$	$H(130)-H(127)$ / $Jmol^{-1}$
			DI	
IV	126.773 - 129.431		1027.5	1039.5
V[a]	126.892 - 129.903		1041.5	1038.5
VI[a]	127.540 - 129.838		992.0	1038.7
XVI	127.236 - 129.433		996.6	1040.8
			Average	1039.4±1.4

	T_{tr} / K
Present work	123.24±0.01
Clusius and Wolf (1947)[d]	128.28

[a] In this series, the transition was done in stages.

[b] From reference 4.

[c] From reference 5.

[d] From reference 6.

5-5. Thermodynamic functions

The thermodynamic functions of HI and DI were calculated by using a smooth extrapolation for the contribution of the heat capacities below 2 K. The results are given in tables 5-8 and 5-9 for HI and DI, respectively. The entropy of liquid HI and DI at the triple points was calculated to be 111.51 and 118.89 J K^{-1} mol^{-1}, which are slightly different from 112.79 J K^{-1} mol^{-1} by Giauque and Wiebe and 117.51 J K^{-1} mol^{-1} by Clusius and Wolf, respectively.

TABLE 5-8. Thermodynamic functions of HI.

T / K	$S^{\circ}(T)-S^{\circ}(0)$ / $JK^{-1}mol^{-1}$	$\{H^{\circ}(T)-H^{\circ}(0)\}/T$ / $JK^{-1}mol^{-1}$	$-\{G^{\circ}(T)-H^{\circ}(0)\}/T$ / $JK^{-1}mol^{-1}$
		Solid	
10	1.528	1.154	0.374
20	7.701	5.313	2.388
30	14.50	9.188	5.307
40	20.62	12.23	8.387
50	26.29	14.89	11.40
60	32.01	17.66	14.35
70	41.80	23.81	17.99
80	45.66	25.09	20.57
90	50.21	26.60	23.61
100	54.62	28.13	26.49
110	59.01	29.77	29.25
120	63.54	31.63	31.91
130	74.08	39.36	34.72
140	77.41	39.75	37.66
150	80.53	40.12	40.41
160	83.47	40.46	43.01
170	86.26	40.79	45.47
180	88.92	41.11	47.81

TABLE 5-8. Continued.

T / K	$S^{\circ}(T)-S^{\circ}(0)$ / $JK^{-1}mol^{-1}$	$\{H^{\circ}(T)-H^{\circ}(0)\}/T$ / $JK^{-1}mol^{-1}$	$-\{G^{\circ}(T)-H^{\circ}(0)\}/T$ / $JK^{-1}mol^{-1}$
190	91.47	41.43	50.04
200	93.92	41.75	52.17
210	96.30	42.08	54.22
222.5	98.68	42.03	56.65
		Liquid	
222.5	111.51	54.86	56.65

TABLE 5-9. Thermodynamic functions of DI.

T / K	$S^{\circ}(T)-S^{\circ}(0)$ / $JK^{-1}mol^{-1}$	$\{H^{\circ}(T)-H^{\circ}(0)\}/T$ / $JK^{-1}mol^{-1}$	$-\{G^{\circ}(T)-H^{\circ}(0)\}/T$ / $JK^{-1}mol^{-1}$
		Solid	
10	1.508	1.147	0.361
20	7.722	5.345	2.377
30	14.64	9.312	5.325
40	21.00	12.54	8.458
50	26.96	15.40	11.57
60	32.86	18.24	14.62
70	39.22	21.55	17.67
80	48.35	27.48	20.87
90	53.54	29.32	24.22
100	58.47	31.07	27.40
110	63.30	32.86	30.44
120	68.18	34.80	33.38
130	79.94	43.59	36.35
140	83.53	43.94	39.59
150	86.86	44.23	42.63
160	89.97	44.48	45.49
170	92.90	44.70	48.20
180	95.67	44.92	50.75

TABLE 5-9. Continued.

T / K	$S^{\circ}(T)-S^{\circ}(0)$ / $JK^{-1}mol^{-1}$	$\{H^{\circ}(T)-H^{\circ}(0)\}/T$ / $JK^{-1}mol^{-1}$	$-\{G^{\circ}(T)-H^{\circ}(0)\}/T$ / $JK^{-1}mol^{-1}$
190	98.32	45.13	53.19
200	100.87	45.36	55.51
210	103.33	45.60	57.73
221.5	106.06	45.88	60.18
		Liquid	
221.5	118.89	58.71	60.18

REFERENCES to CHAPTER 5

1. Ruhemann, B.; Simon, F. Z. Phys. Chem. 1931, B15, 406.
2. Smyth, C. P.; Hitchcock, C. S. J. Am. Soc. 1933, 55, 1835.
3. McIntosh, D.; Steele, B. D. Z. Phys. Chem. 1906, 55, 145.
4. Giauque, W. F.; Wiebe, R. J. Am. Chem. Soc. 1929, 51, 1441.
5. Eucken, A.; Karwat, E. Z. Phys. Chem. 1924, 112, 467.
6. Clusius, K.; Wolf, G. Z. Naturforsch. 1947, 2a, 495.
7. McIntosh, D.; Steele, B. D. Z. Phys. Chem. 1906, 55, 137.
8. Henglein, F. A. Z. Phys. 1923, 18, 64.
9. Bates, J. R.; Halford, J. C.; Anderson, L. C. J. Chem. Phys. 1935, 3, 415.
10. Miravelles, R.; Moles, E. Ann. Espan. 1925, 23, 518.

Appendix 5A. Measured heat capacities of HI.

T / K	C_p / $JK^{-1}mol^{-1}$	T / K	C_p / $JK^{-1}mol^{-1}$
		114.364	51.57
Series I		115.317	52.38
95.862	42.08	116.261	53.07
96.961	42.60	117.198	53.92
98.050	42.93		
99.130	43.53	Series II	
100.202	43.85	113.127	50.15
101.266	44.25	114.097	50.87
102.320	44.81	115.060	51.76
103.366	45.34	116.014	52.25
104.403	45.74	116.959	53.42
105.435	46.29	117.895	54.11
106.460	46.81	118.823	55.29
107.476	47.33	119.740	56.45
108.484	47.73	120.647	57.49
109.484	48.48	121.545	58.67
110.476	49.02	122.430	60.57
111.461	49.48	123.304	61.62
112.438	50.40	124.167	64.06
113.404	50.83	125.014	66.06

Appendix 5A. Continued.

T / K	C_p / $JK^{-1}mol^{-1}$	T / K	C_p / $JK^{-1}mol^{-1}$
Transition		127.789	45.10
125.933	488.46	128.759	45.13
126.174	360.07	129.727	44.95
126.634	107.95	130.750	44.94
127.442	45.99	131.812	44.90
128.415	44.98	133.063	44.88
		134.503	44.90
Series III		136.130	44.95
118.081	54.86	137.942	44.96
119.275	56.05	139.844	45.03
120.182	57.16	141.740	45.11
121.079	58.43	143.629	45.15
121.966	59.63	145.512	45.23
122.843	61.26	147.389	45.31
123.707	62.98	149.261	45.38
124.558	64.63		
125.337	90.99	Series IV	
Transition		10.705	5.070
126.140	156.16	11.078	5.508
126.849	53.52	11.619	6.077

Appendix 5A. Continued.

T / K	C_p / $JK^{-1}mol^{-1}$	T / K	C_p / $JK^{-1}mol^{-1}$
12.269	6.765	27.764	18.424
12.962	7.531	28.596	18.791
13.682	8.295	29.435	19.153
14.426	9.068	30.283	19.531
15.159	9.816		
15.870	10.519	Series V	
16.570	11.151	10.781	5.170
17.264	11.794	11.260	5.697
17.958	12.385	11.894	6.367
18.656	12.927	12.611	7.154
19.362	13.493	13.322	7.907
20.080	14.025	14.066	8.654
20.898	14.601	14.815	9.470
21.800	15.198	15.532	10.178
22.684	15.756	16.234	10.814
23.555	16.274	16.928	11.505
24.417	16.736	17.618	12.075
25.276	17.225	18.310	12.668
26.115	17.651	19.009	13.227
26.937	18.030	19.730	13.779

Appendix 5A. Continued.

$\frac{T}{K}$	$\frac{C_p}{JK^{-1}mol^{-1}}$	$\frac{T}{K}$	$\frac{C_p}{JK^{-1}mol^{-1}}$
20.549	14.343	30.747	19.695
21.437	14.959	31.897	20.19
22.323	15.541	33.056	20.60
23.211	16.066	34.228	21.09
24.072	16.570	35.414	21.54
24.910	17.042	36.700	22.03
25.729	17.465	38.156	22.58
26.531	17.853	39.708	23.19
27.337	18.208	41.340	23.84
		43.001	24.52
Series VI		44.688	25.29
21.153	14.745	46.496	26.13
22.186	15.426	48.318	27.05
23.195	16.074	50.064	28.00
24.188	16.645		
25.169	17.147	Series VII	
26.166	17.665	20.764	14.469
27.277	18.176	21.672	15.096
28.452	18.723	22.688	15.727
29.601	19.224	23.684	16.354

Appendix 5A. Continued.

T / K	C_p / $JK^{-1}mol^{-1}$	T / K	C_p / $JK^{-1}mol^{-1}$
24.667	16.900	52.865	29.76
25.683	17.409	54.497	30.94
26.717	17.936		
27.752	18.409	Series VIII	
28.815	18.879	1.855	0.02186
30.079	19.437	2.101	0.03311
31.356	19.959	2.347	0.04620
32.476	20.39	2.597	0.06123
33.608	20.84	2.873	0.08798
34.752	21.29	3.118	0.1149
35.946	21.75	3.353	0.1431
37.231	22.24	3.637	0.1901
38.618	22.77	3.963	0.2518
40.124	23.35		
41.775	24.02	Series IX	
43.670	24.83	1.897	0.02422
45.681	25.76	2.221	0.04099
47.595	26.69	2.539	0.05954
49.422	27.66	2.888	0.08827
51.176	28.69	3.300	0.1359

Appendix 5A. Continued.

T/K	C_p / $JK^{-1}mol^{-1}$	T/K	C_p / $JK^{-1}mol^{-1}$
3.752	0.2112		
		Series XII	
Series X		3.753	0.2079
1.876	0.02379	4.334	0.3330
2.149	0.03552	4.888	0.5074
2.430	0.05158	5.364	0.6959
2.795	0.08000	5.857	0.9358
3.240	0.1282	6.415	1.265
3.712	0.2035	6.942	1.621
4.222	0.3176	7.479	2.010
4.727	0.4664	8.053	2.494
5.208	0.6480	8.668	3.051
5.726	0.8967	9.331	3.686
		10.050	4.407
Series XI		10.827	5.249
3.999	0.2603	11.657	6.144
4.420	0.3719		
4.865	0.5197	Series XIII	
5.309	0.6993	5.305	0.6696
5.800	0.9319	5.885	0.9489

Appendix 5A. Continued.

T / K	C_p / $JK^{-1}mol^{-1}$	T / K	C_p / $JK^{-1}mol^{-1}$
6.467	1.284	63.312	41.18
7.037	1.676	64.447	43.56
7.629	2.134	65.545	46.53
8.269	2.690	66.598	50.29
8.981	3.350	67.597	55.57
9.794	4.151	68.531	63.99
10.715	5.133	69.368	81.77
11.713	6.197	69.977	183.44
12.751	7.313	70.614	71.79
		71.593	37.71
Series XIV		72.721	36.41
51.259	28.72	73.851	36.26
52.772	29.66	74.973	36.35
54.237	30.68	76.083	36.49
55.673	31.78	77.184	36.59
57.038	33.00		
58.373	34.28	Series XV	
59.666	35.70	54.984	31.26
60.919	37.39	56.366	32.36
62.136	39.11	57.707	33.64

Appendix 5A. Continued.

T / K	C_p / $JK^{-1}mol^{-1}$	T / K	C_p / $JK^{-1}mol^{-1}$
59.007	34.95	70.362	109.66
60.269	36.50	70.779	43.60
61.494	38.11	71.314	38.12
62.396	39.35		
62.993	40.54	Series XVI	
63.581	41.42	65.486	46.24
64.157	42.90	66.118	48.31
64.722	44.04	66.850	51.31
65.277	45.52	67.856	57.47
65.820	47.25	68.780	67.32
66.352	49.05	69.507	87.06
66.871	51.38	70.021	210.0
67.376	53.96	70.577	70.88
67.867	57.07	71.687	37.57
68.339	61.45	73.211	36.28
68.789	67.11	74.670	36.30
69.213	75.79	75.930	36.46
69.599	90.32	77.108	36.67
69.927	124.00	78.274	36.79
70.139	344.2	79.538	37.23

Appendix 5A. Continued.

T / K	C_p / $JK^{-1}mol^{-1}$	T / K	C_p / $JK^{-1}mol^{-1}$
80.898	37.49	Series XIX	
82.255	37.84	II-I Transition,	
83.608	38.14	Continuous Heating	
84.960	38.63		
86.415	39.06	Series XX	
87.956	39.60	II-I Transition,	
89.471	40.05	Continuous Heating	
90.961	40.55		
92.430	40.98	Series XXI	
93.880	41.52	150.255	45.40
95.310	42.06	152.297	45.54
		154.496	45.54
Series XVII		156.833	45.70
III-II Transition,		159.222	45.78
Continuous Heating		161.654	45.96
		164.122	46.02
Series XVIII		166.628	46.15
III-II Transition,		169.169	46.33
Continuous Heating		171.750	46.37
		174.370	46.56

Appendix 5A. Continued.

T / K	C_p / $JK^{-1}mol^{-1}$	T / K	C_p / $JK^{-1}mol^{-1}$
177.002	46.65	Series XXIII	
179.627	46.81	218.982	50.87
182.210	46.98	Fusion	
184.806	47.15		
187.384	47.34		
189.945	47.52		
192.520	47.70		
195.110	47.93		
197.686	48.06		
200.269	48.24		
202.886	48.39		
205.515	48.70		
208.129	48.99		
210.721	49.33		
213.287	49.70		
215.825	50.26		
218.473	50.87		
Fusion,			
Continuous Heating			

Appendix 5B. Measured heat capacities of DI.

T / K	C_p / $JK^{-1}mol^{-1}$	T / K	C_p / $JK^{-1}mol^{-1}$
		79.848	43.92
Series I		80.949	43.57
61.672	37.53		
62.972	38.82	Series II	
64.243	40.11	III-II Transition,	
65.484	41.49	Continuous Heating	
66.690	42.97		
67.865	44.84	Series III	
69.012	46.77	72.673	55.79
70.126	49.00	73.662	59.90
71.205	51.37	74.603	65.18
72.248	54.46	75.490	72.93
73.254	58.20	76.306	85.66
74.216	62.88	77.005	120.58
75.129	69.40	77.473	281.45
75.980	79.44	78.153	50.48
76.738	100.19	79.219	44.42
77.281	221.16	80.426	43.62
77.841	93.59	81.741	43.56
78.752	45.24	83.046	43.62

Appendix 5B. Continued.

T / K	C_p / $JK^{-1}mol^{-1}$	T / K	C_p / $JK^{-1}mol^{-1}$
84.339	43.76	109.292	52.71
85.619	44.07	110.555	53.10
86.891	44.38	111.809	54.06
88.152	44.73	113.055	54.82
89.405	44.94	114.286	55.62
90.646	45.38	115.507	56.28
91.874	45.72	116.721	57.07
93.095	46.13	117.924	58.08
94.307	46.50		
95.505	46.95	Series IV	
96.693	47.40	119.446	59.37
97.869	47.65	120.615	60.83
99.039	48.24	121.769	62.00
100.203	48.65	122.909	63.45
101.449	49.25	124.033	65.09
102.782	49.72	125.143	66.39
104.106	50.33	126.243	69.09
105.417	50.83	II-I Transition,	
106.719	51.46	Continuous Heating	
108.011	52.13		

Appendix 5B. Continued.

$\frac{T}{K}$	$\frac{C_p}{JK^{-1}mol^{-1}}$	$\frac{T}{K}$	$\frac{C_p}{JK^{-1}mol^{-1}}$
Series V		Series VI	
110.928	53.35	124.357	64.92
112.190	54.22	125.651	67.63
113.446	54.91	126.916	70.61
114.691	55.77	Transition	
115.922	56.71	130.892	48.62
117.135	57.49	132.682	48.57
118.335	58.46	134.257	48.54
119.623	59.65	135.932	48.48
120.993	61.05	137.602	48.39
122.344	62.58	139.297	48.39
123.671	64.28	141.035	48.35
124.978	66.06		
126.260	68.98	Series VII	
127.419	71.95	1.920	0.02461
Transition		2.164	0.03425
130.640	48.65	2.408	0.04791
132.113	48.58	2.640	0.06193
133.584	48.53	2.879	0.08188

Appendix 5B. Continued.

T / K	C_p / $JK^{-1}mol^{-1}$	T / K	C_p / $JK^{-1}mol^{-1}$
3.142	0.1090	Series IX	
3.433	0.1474	1.840	0.02076
3.751	0.2010	2.066	0.02961
4.093	0.2708	2.334	0.04251
4.464	0.3691	2.583	0.05862
4.900	0.4994	2.818	0.08143
		3.065	0.1010
Series VIII		3.369	0.1374
1.915	0.02392	3.723	0.1984
2.162	0.03321	4.110	0.2769
2.414	0.04719	4.490	0.3889
2.660	0.06467	4.872	0.5169
2.917	0.08668		
3.190	0.1158	Series X	
3.485	0.1594	4.583	0.3994
3.814	0.2128	5.081	0.5737
4.172	0.2973	5.539	0.7709
4.567	0.4066	5.981	0.9862
4.999	0.5589	6.435	1.2456
		6.922	1.5683

Appendix 5B. Continued.

$\frac{T}{K}$	$\frac{C_p}{JK^{-1}mol^{-1}}$	$\frac{T}{K}$	$\frac{C_p}{JK^{-1}mol^{-1}}$
7.472	1.9757	11.240	5.688
8.107	2.506	12.120	6.613
		13.041	7.579
Series XI			
4.707	0.4391	Series XIII	
5.186	0.6129	11.025	5.473
5.669	0.8247	11.988	6.495
6.138	1.0704	12.925	7.485
6.619	1.3649	13.878	8.563
7.143	1.7302	14.910	9.633
7.728	2.184	16.046	10.768
8.359	2.731	17.226	11.854
9.029	3.375	18.380	12.852
9.843	4.198	19.587	13.821
Series XII		Series XIV	
8.155	2.553	13.680	8.329
8.978	3.314	15.001	9.744
9.698	4.048	16.422	11.123
10.434	4.829	17.772	12.330

Appendix 5B. Continued.

T / K	C_p / $JK^{-1}mol^{-1}$	T / K	C_p / $JK^{-1}mol^{-1}$
19.093	13.438	45.414	26.98
20.380	14.405	46.807	27.66
21.619	15.291	48.232	28.33
22.828	16.065	49.667	29.20
24.019	16.818	51.153	30.01
25.201	17.486	52.724	30.89
26.420	18.127	54.342	31.89
27.722	18.792	55.953	32.99
29.078	19.432	57.557	34.10
30.451	20.13	59.173	35.32
31.817	20.79	60.769	36.69
33.163	21.41		
34.527	22.01	Series XV	
35.934	22.64	III-II Transition,	
37.327	23.25	Continuous Heating	
38.674	23.85		
40.013	24.44	Series XVI	
41.364	25.05	II-I Transition,	
42.719	25.67	Continuous Heating	
44.063	26.31		

Appendix 5B. Continued.

T / K	C_p / $JK^{-1}mol^{-1}$	T / K	C_p / $JK^{-1}mol^{-1}$
		185.998	48.97
Series XVII		188.755	49.21
142.375	48.30	191.496	49.48
144.569	48.33	194.221	49.59
146.900	48.35	196.928	49.85
149.319	48.32	199.616	50.12
151.806	48.25	202.313	50.26
154.306	48.17	205.019	50.44
156.792	48.16	207.702	50.53
159.283	48.16	210.398	50.67
161.979	48.25	213.105	50.59
164.715	48.25	215.916	51.24
167.290	48.33	218.824	52.89
169.878	48.40	Fusion,	
172.479	48.50	Continuous Heating	
175.094	48.57		
177.726	48.65	Series XIX	
		220.458	62.64
Series XVIII		Fusion	
180.403	48.64	223.333	63.18
183.226	48.91		

CHAPTER 6

Thermodynamic Properties and Phase Transitions

—— Analysis and Discussion ——

6-1. General remarks

In this chapter our object is to analyse the results of thermal measurements on solid hydrogen halides and their deuterium analogs to see what can be learned about their vibrational properties and mechanism of phase transitions. For instance, we should like to know to what extent the phase transitions can be described in terms of successive orientational order-disorder model proposed by neutron scattering experiments. Although uncertainties in some of the auxiliary data required are so great, some conclusions about the mechanism of phase transitions in hydrogen halides can be drawn.

Following analysis and discussion will consist of four parts: (1) vibrational contribution of heat capacity and onset of orientational disorder at low temperatures; (2) defect formation phenomenon just below triple point temperature; (3) extraction of order-disorder heat capacity in transition temperature region; and (4) mechanism of the phase transitions. We will start to discuss the vibrational properties of crystal lattice.

6-2. Low temperature region

6-2-1. Zero point properties

The characteristic temperature at 0 K

In actual examples of insulators, it is found[1] that the frequency distribution takes the form of a power series

$$G(\nu) = \alpha\nu^2 + \beta\nu^4 + \gamma\nu^6 + \ldots \qquad (6\text{-}1)$$

that converges asymptotically at low frequencies ν less than about $(\nu_{max}/25)$, where ν_{max} is the Debye cut-off frequency. The consequence is that the heat capacity at constant volume becomes

$$C_v = aT^3 + bT^5 + cT^7 + \ldots . \qquad (6\text{-}2)$$

There is an equivalent series for the apparent characteristic temperature

$$\Theta_D(T) = \Theta_0 \left[1 - A\left(\frac{T}{\Theta_0}\right)^2 - B\left(\frac{T}{\Theta_0}\right)^4 - \ldots\right]. \qquad (6\text{-}3)$$

In this equation, $\Theta_D(T)$ is the apparent Debye characteristic temperature that corresponds to C_v obtained from experimental data; Θ_0 is its limiting value at $T \to 0$ K. One connection between equations 6-2 and 6-3 is provided by

$$\Theta_0 = \left(\frac{12\pi^4 Nk}{5a}\right)^{1/3}. \qquad (6\text{-}4)$$

To obtain a numerical estimate of Θ_0 from heat capacity data, it is convenient to plot either $C_v T^{-3}$ or $\Theta_D(T)$ against T^2. If the first is used, the intercept of the curve gives the value of the coefficient a. Since the correction of $(C_p - C_v)$ is negligibly small at T < 15 K as will be mentioned below, the experimental $C_p T^{-3}$ value is plotted against T^2 in figure 6-1. No attempt has been made to estimate the coefficients b and c because of great uncertainty.

The temperature dependences of Debye temperatures derived from the measured heat capacities had been shown in previous sections. Those mean that the form of the lattice frequency spectrum resembles that of a Debye spectrum. This can be accounted for by the fact both the 2N librational and N intramolecular vibrations are well separated from the remainder of the frequency spectrum. In fact, intramolecular contribution is negligible at the temperatures measured. Furthermore librational contributions can be neglected in the lowest temperature region T < 20 K for all the halides. The Debye characteristic temperature at 0 K is thus determined by assuming 3N degrees of freedom (see table 6-1).

It is worth comparing the Θ_0 of HCl, HBr, and HI with that of Ar(93.3 K), Kr(71.7 K),[5] and Xe(64.0 K)[6]

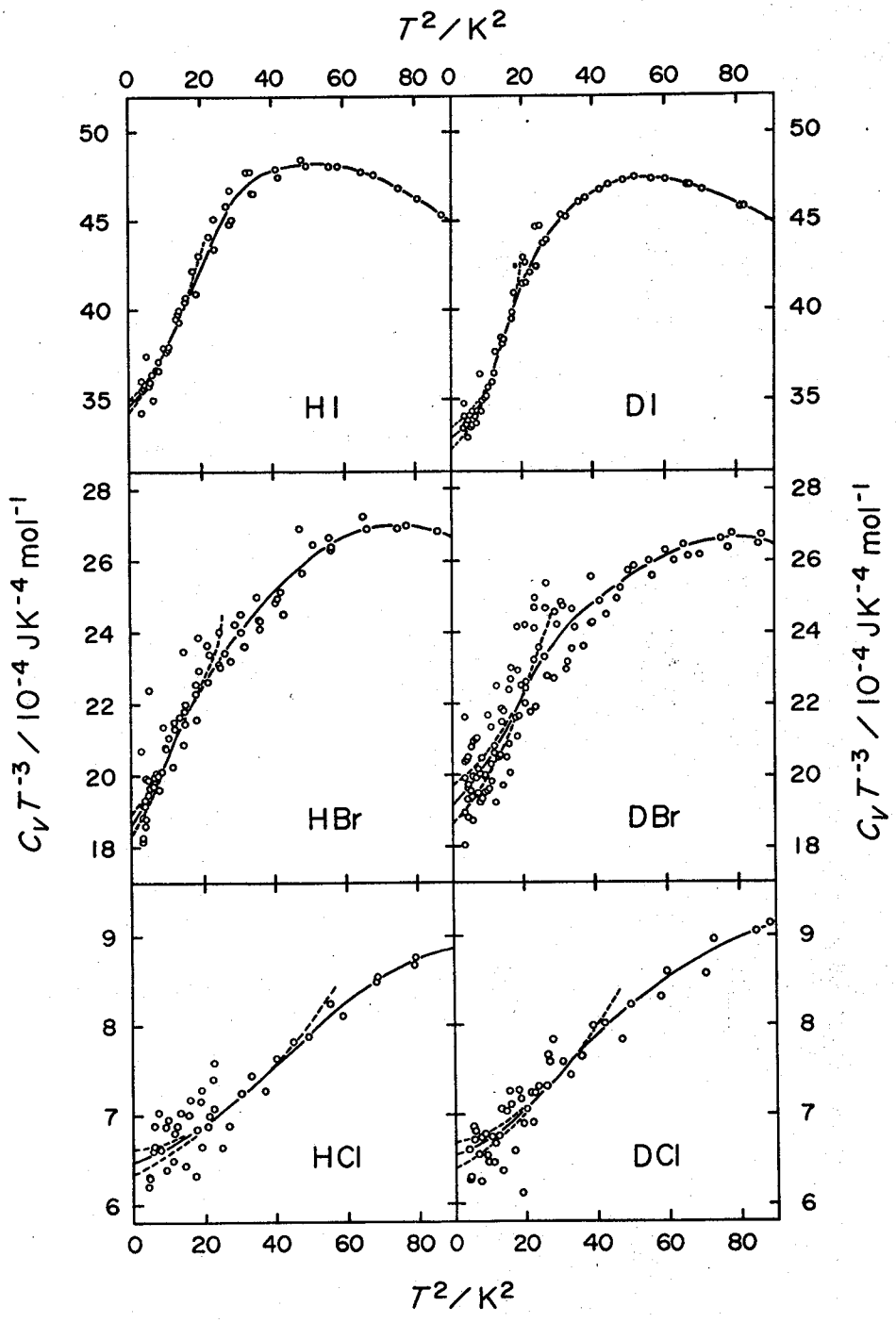

FIGURE 6-1. Graphs of $C_V T^{-3}$ against T^2.

TABLE 6-1. The coefficients (a) and the Debye characteristic temperatures at 0 K (Θ_0) determined by the plots of $C_v T^{-3}$ against T^2.

substances	$\frac{a \times 10^4}{Jmol^{-1}K^{-4}}$	$\frac{\Theta_0}{K}$
HCl	6.48 ± 0.14	144.2 ± 1.0
HBr	18.6 ± 0.3	101.5 ± 0.5
HI	34.6 ± 0.3	82.5 ± 0.3
DCl	6.55 ± 0.14	143.7 ± 1.0
DBr	19.1 ± 0.5	100.6 ± 0.8
DI	32.8 ± 0.6	84.0 ± 0.5

respectively, because of their comparable molecular weight. The rather heigher Θ_0 may come from the molecular multipole interactions and hydrogen bonding in hydrogen halides. As for the discrepant behavior between HI and DI, any positive explanations can not be put forward.

The heat of sublimation at 0 K

The thermodynamic properties given in the preceeding papers may be used to calculate the heats of sublimation of hydrogen halides at 0 K. The relevant thermodynamic expression is

$$\Delta H_{sub}(0\ K) = \Delta H_{sub}(T) - \int_0^T C_p(gas)dT + \int_0^T C_p(solid)dT + \Delta \ , \qquad (6\text{-}5)$$

where the last term Δ is that of gas imperfection. When the critical constants P_k and T_k are given, the term Δ is represented by following equation.

$$\Delta = \frac{9}{128} R \left(\frac{P}{P_k}\right) \left(\frac{18T_k^2 - T^2}{T^2}\right) T_k \qquad (6\text{-}6)$$

Since the heats of vaporization were not measured in the present investigation, the data used are those of Giauque and Wiebe[7] and Clusius and Wolf[8] for hydrogen halides and deuterium halides, respectively. Unfortunately, no data for DCl are available. The results obtained are summarized in table 6-2 and the values of rare gas solids are also included for the sake of comparison. It is found that the multipolar and hydrogen bonding interactions play an important role to determine the structure of hydrogen halides.

TABLE 6-2. Calculation of the heats of sublimation at 0 K.

(in the unit of kJ mol^{-1})

		HCl	HBr	HI	DCl	DBr	DI	Ar	Kr
Heat of sublimation at $T = T_f$	$\Delta H_{b.p.}$	16.150	17.615	19.765	——	17.815	19.732		
	liquid	1.713	1.202	0.922	——	1.304	1.043		
	fusion	1.971	2.399	2.855	1.945	2.369	2.841		
	$\Delta H_{sub}(T_f)$	19.834	21.216	23.542	——	21.488	23.616	7.786	10.791
	$-\int_0^{T_f} C_p(\text{gas})$	-4.628	-5.427	-6.475	-4.609	-5.402	-6.446	-1.741	-2.406
	$\int_0^{T_f} C_p(\text{solid})$	5.623	7.462	9.352	6.096	8.116	10.164	1.636	2.711
	Δ	0.024	0.052	0.096	0.024	0.052	0.093	0.042	0.059
Heat of sublimation at $T = 0$ K		20.85	23.30	26.52	——	24.25	27.43	7.72	11.15

The static lattice energy

It should be noted that there are one or more phase transitions in hydrogen halides. Static lattice energy of phase I, which will be reffered to $E_0(I)$, was derived by analysis of the vapor pressure data in phase I, which were fitted to the formula

$$\ln (PT^{3/2}) = (a/T) + b. \qquad (6\text{-}7)$$

The static lattice energy is related to a through

$$aNk = E' = E_0(I) - E_{z,lib} , \qquad (6\text{-}8)$$

where $E_{z,lib}$ is the zero-point librational energy. The slope of graph of $\ln(PT^{3/2})$ against T^{-1} gives E' a value of 21.29 kJ mol^{-1} for HCl. A small correction to this value must be made for the effect of defect formation in the neighborhood of the triple point, which leads to a revised value of 21.39 kJ mol^{-1}. $E_{z,lib}$, which is assumed to make no difference between phases I and III, can be approximately evaluated from the librational frequencies as 3.64 kJ mol^{-1}; therefore $E_0(I)$ is 25.03 kJ mol^{-1} for HCl. The results are summarized in table 6-3 together with other hydrogen halides.

Next, we will evaluate the static lattice energy of phase III, $E_0(III)$; which is given by

TABLE 6-3. Estimation of static lattice energy of phases I and III. (in units of kJ mol^{-1})

	HCl	HBr	HI	DCl	DBr	DI
E_0' †	21.39 (21.29)	23.39 (23.10)	25.46 (25.03)	21.27 (21.10)	23.40 (23.30)	25.50 (25.45)
$E_{z,lib}$	3.643	3.206	2.743	2.542	2.521	1.941
$E_{z,trans}$(III)	1.349	0.949	0.772	1.344	0.941	0.786
ΔH_{sub}(0 K)	20.853	23.303	26.515	——	24.254	27.427
E_0(I)	25.03	26.60	28.20	23.81	25.92	27.44
E_0(III)	25.85	27.46	30.03	——	27.72	30.15
E_0(III)-E_0(I)	0.82	0.86	1.83	——	1.80	2.70
$\frac{E_{z,trans}(III)}{\Delta H_{sub}(0\ K)}$	0.065	0.041	0.029	——	0.039	0.029

† Pseudo static lattice energies without correction for the defect formation are designated in parentheses.

$$E_0(III) = \Delta H_{sub}(0\ K) + E_{z,trans}(III) + E_{z,lib}. \quad (6\text{-}9)$$

The translational zero point energy of phase III may be approximately represented by following equation.

$$E_{z,trans} = \frac{9}{8} Nk\Theta_\infty \quad (6\text{-}10)$$

$E_0(III)$ obtained, which shows little change on deuteration, is also included in table 6-3. $E_0(III)$ is 25.85 kJ mol^{-1} for HCl. Since the difference between $E_0(III)$ and $E_0(I)$ may be outside the combined uncertainties, it should be ascribed to the difference of lattice energy between phases I and III. In fact, the value of 0.82 kJ mol^{-1} for HCl is comparable to the ΔH_{tr} of 1.19 kJ mol^{-1}. The $E_0(III)-E_0(I)$ for HI is evidently larger than that for HCl and HBr. This result is consistent with that of neutron scattering experiments: HCl and HBr in phase III are isostructural but HI differs from the two, while all the halides in phase I are isostructural. HI in phase III apears to stabilized additionally by quadrupole interactions and/or charge transfer interactions.

6-2-2. The estimation of (C_p-C_v) correction

(C_s-C_p) correction

Strictly speaking, we measure the heat capacity (C_s) of the solid in equilibrium with its saturated vapor. The heat capacity at constant pressure C_p may be obtained using the following thermodynamic expression:

$$C_s - C_p = - T\alpha V(dP/dT)_s \qquad (6\text{-}11)$$

where α and V are the thermal expansion coefficient and molar volume, respectively, and $(dP/dT)_s$ is the slope of the vapor-pressure curve of the solid. When numerical values for each hydrogen halide are substituted in the equation it is found that C_s-C_p is quite small, being at most of the order of 0.01 per cent of C_p at the triple point. We have therefore neglected this difference between C_p and C_s and assumed them to be equal throughout the data analysis.

(C_p-C_v) correction

Since the volume can be related quite simply to the lattice parameters, theoretical calculations are usually done at a constant volume. To convert our results from C_p to C_v, we used the familiar expression:

$$C_p - C_v = \alpha^2 VT/\chi \ , \qquad (6\text{-}12)$$

where χ is the isothermal compresibility. Unfortunately, thermal expansion and compressibility data are incomplete

at temperatures required. Therefore, it is necessary to have recourse to the quasi-thermodynamic relation:

$$C_p - C_v = A\, C_p^2\, T \qquad (6\text{-}13)$$

where a constant A is given by

$$A = \alpha^2 V/\chi C_p^2 \qquad (6\text{-}14)$$

The differences between C_p and C_v were calculated from equation 6-13. The numerical values of the constant A for HCl and HBr were computed at 130 and 150 K respectively as follows.

Stewart have determined[9] the isothermal PV curves for solid HCl and HBr up to pressures of 2×10^4 kg cm^{-2} by the direct piston displacement method. Compressibilities were calculated to be 3.60×10^{-5} cm^2 kg^{-1} at 130 K and 3.65×10^{-5} cm^2 kg^{-1} at 150 K for HCl and HBr, respectively. No relevant data for HI and deuterium halides are available. The molar volumes have been measured by X-ray and neutron diffraction and volumometer techniques. Available data were represented in the preceeding experimental sections. The V and α at 130 and 150 K for HCl and HBr were obtained by smoothing method. The constant A was thus determined to be 1.50×10^{-5} and 1.49×10^{-5} mol J^{-1} for HCl and HBr, respectively. As for HI, therefrom,

$A = 1.5 \times 10^{-5}$ mol J^{-1} was assumed. Further, it was assumed that A is not affected by deuteration. The data used and constant A are shown in table 6-4, and the contribution of $(C_p - C_v)$ correction at selected temperatures is tabulated in table 6-5. In this estimation, we assumed that the constant A has the same value for any phase.

TABLE 6-4. The data used for evaluating the constant A.

	T / K	$\chi \times 10^5$ / $cm^2 kg^{-1}$	$\alpha \times 10^4$ / K^{-1}	V / $cm^3 mol^{-1}$	C_p / $JK^{-1}mol^{-1}$	$A \times 10^5$ / $molJ^{-1}$
HCl	130	3.60[a]	6.42[b]	25.3[a]	44.43[d]	1.50
HBr	150	3.65[a]	6.17[c]	31.7[a]	46.65[d]	1.49
HI						(1.5)

[a] From reference 9.

[b] From references 10-12.

[c] From reference 12.

[d] Present results.

TABLE 6-5. The contribution of (C_p-C_v) correction. (in the units of J K^{-1} mol^{-1})

T / K	HCl	HBr	HI	DCl	DBr	DI
20	0.011	0.035	0.059	0.011	0.035	0.060
40	0.15	0.25	0.33	0.16	0.28	0.37
60	0.45	0.64	1.17	0.53	0.76	1.17
80	0.95	1.84	1.67	1.15	2.00	2.31
100	2.40	2.84	2.88	2.27	3.41	3.54
120	3.32	3.64	5.78	3.83	——	6.47
140	4.45	4.38	4.26	5.03	5.17	4.91
160		5.42	5.04		6.34	5.58
180		6.87	5.93		8.92	6.40
200			6.97			7.53

6-2-3. Librational contribution to heat capacity

The correlation diagram for the structure of phase III ($Bb2_1m$) shows that three librational modes of the four are infrared and/or Raman active and the fourth one is inactive. Librational frequencies of HCl, DCl, HBr, and DBr in phase III were given by Ito et al.[13] (from Raman study and calculation) and by Hornig and Osberg[14] (from infrared study). The frequencies of HI were calculated by the following relation using those of HCl and HBr.

$$\tilde{\nu} \sqrt{I} = \text{constant} \qquad (6\text{-}15)$$

where I is the moment of inertia given from reference 15. As for DI, usual mass effect of deuteration are assumed. Frequency values used are summarized in table 6-6. Their contribution to heat capacity, which is listed in table 6-7, was calculated on the basis of Einstein model for $\frac{1}{2}$ N degrees of freedom for each of the four modes.

TABLE 6-6. Librational frequencies in phase III.
(in the units of cm^{-1})

Modes	HCl	HBr	HI	DCl	DBr	DI
A_1	290	265	199	203	194	141
A_2	214	212	177	152	153	125
B_1	496	400	370	328	343	262
B_2	218	195	171	167	153	121

TABLE 6-7. The contribution to heat capacity of libration. (in the units of J K^{-1} mol^{-1})

T/K	HCl	HBr	HI	DCl	DBr	DI
20	0.0003	0.0007	0.005	0.013	0.018	0.11
40	0.23	0.33	0.79	1.05	1.23	2.71
60	1.47	1.86	3.16	3.65	3.96	6.26
80	3.35	4.01	5.71	6.29	6.56	8.96
100	5.25	6.10	7.83	8.43	8.61	10.86
120	6.93	7.89	9.48	10.08	10.22	12.19
140	8.35	9.36	10.78	11.35	11.43	13.14
160	9.54	10.54	11.80	12.30	12.35	13.83
180		11.49	12.58		13.07	14.34
200			13.20			14.73

6-2-4. The temperature dependence of $\Theta_D(T)$

The comparison of $\Theta_D(T)$

It is often useful to describe the heat capacity of solids in terms of the Debye theory, as in this way we may exhibit clearly small differences in the type of temperature dependence of the heat capacity for different substances. What is done is to examine the temperature dependence of apparent Debye characteristic temperatures corresponding to the lattice heat capacities. Deviations of Θ_D from a constant value are interpreted as being the result of departures of the actual frequency spectrum from the assumed Debye spectrum. It has become clear from the theoretical work of Blackman and others[16] that, if vibrations remain harmonic, Θ_D should be constant at very low ($T \lesssim \Theta_D/100$) and at very high ($T \gtrsim \Theta_D/2$) temperatures, and should often have a minimum value in between.

Figure 6-2(a)∿(f) are graphs of $\Theta_D(T)$ as a function of temperature for hydrogen and deuterium halides. In the calculation of the plotted points, (C_p-C_v) correction and librational contributions were subtracted. In each graph, broken line shows the extraporation by means of the Thirring expansion.[17] The decrease in $\Theta_D(T)$ in the region $T > \Theta_0/3$ has been observed for some simple crystals[18,19] and has been

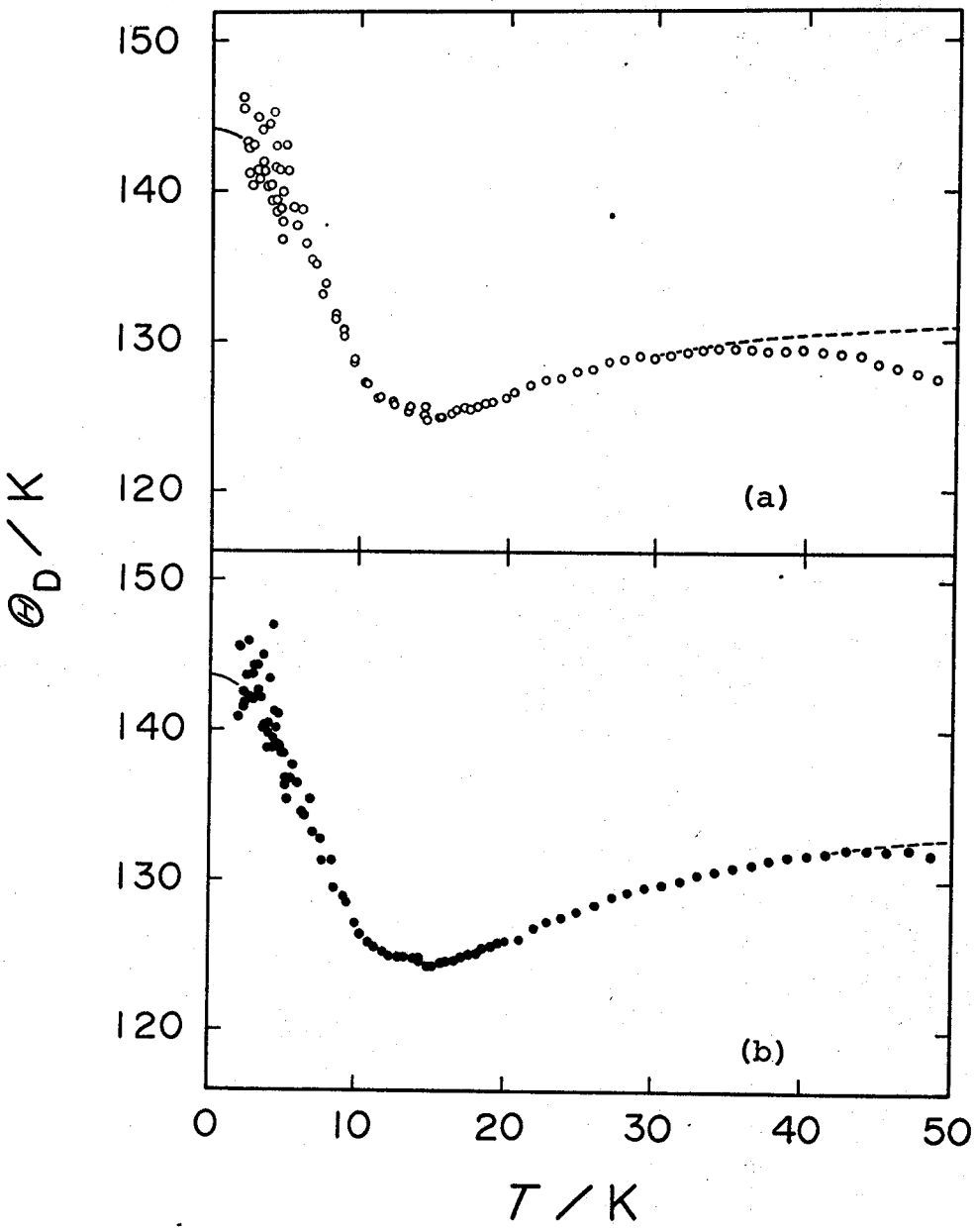

FIGURE 6-2. The temperature dependence of Θ_D. Broken lines show the extrapolation by the Thirring expansion. (a) HCl; (b) DCl.

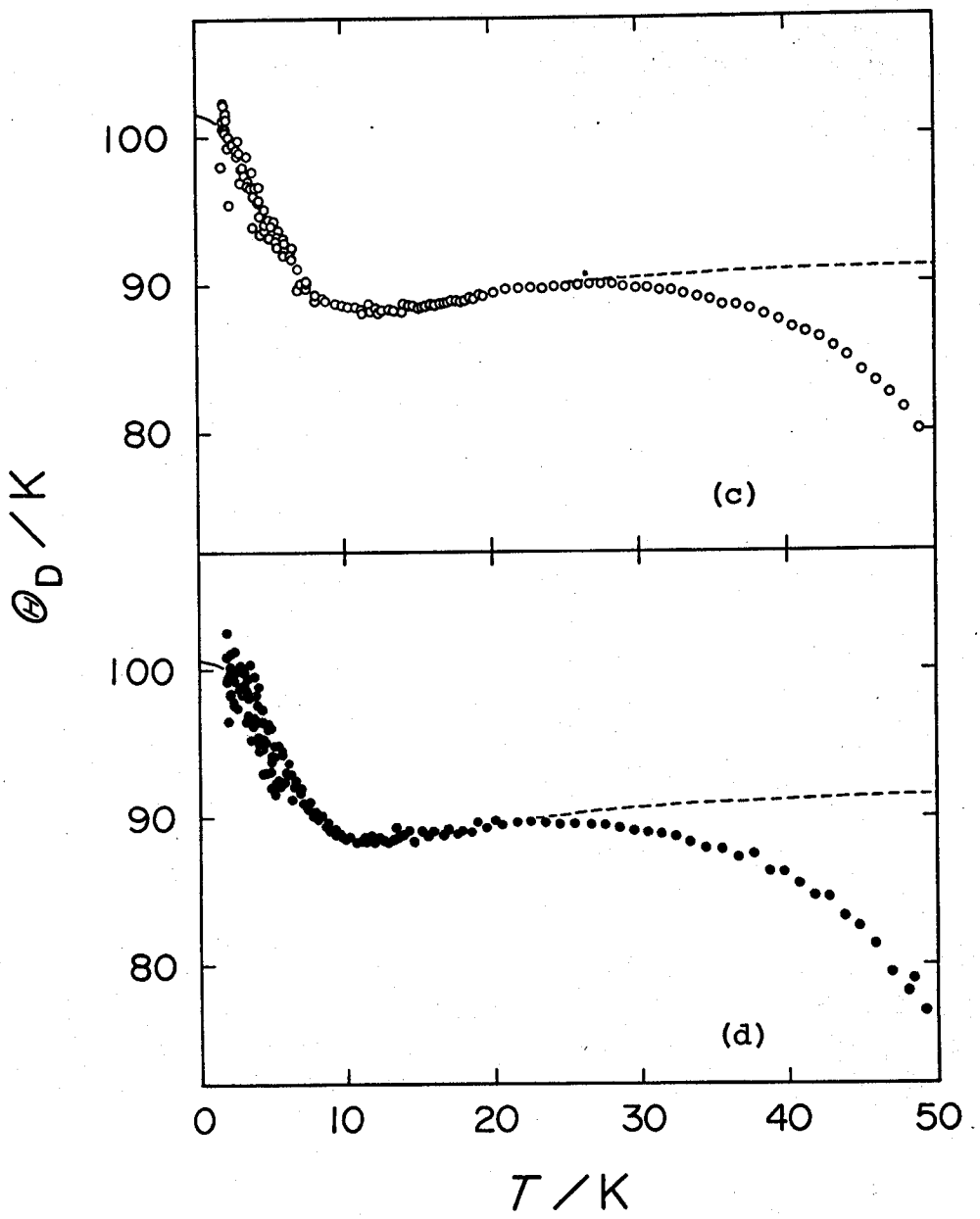

FIGURE 6-2. The temperature dependence of Θ_D. Broken lines show the extrapolation by the Thirring expansion. (c) HBr; (d) DBr.

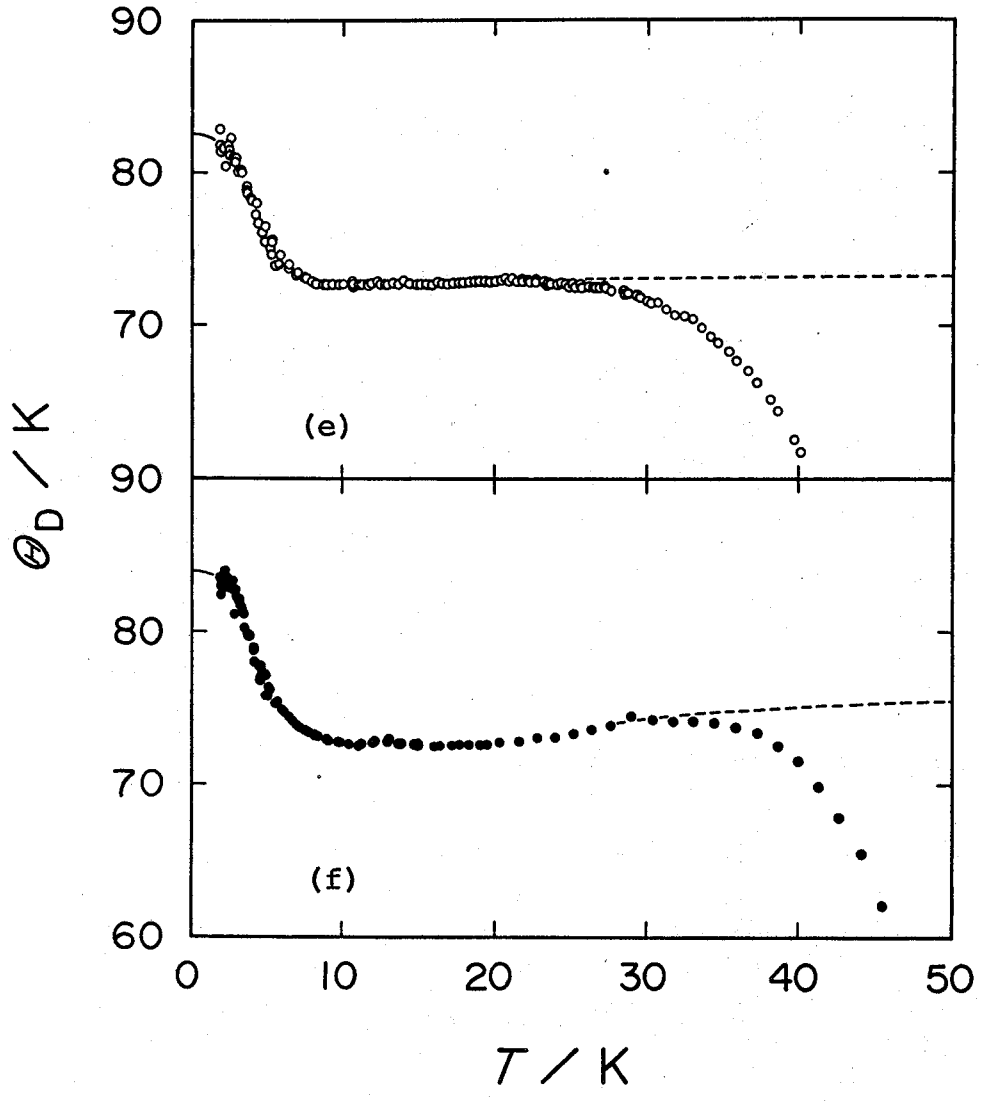

FIGURE 6-2. The temperature dependence of Θ_D. Broken lines show the extrapolation by the Thirring expansion. (e) HI; (f) DI.

ascribed to the onset of anharmonicity in the lattice vibrations.[19,20] In hydrogen halides, moreover, the onset of phase transition begins to overlap at this temperature.

While the general shape of the $\Theta_D(T)$ curve is rather similar for all the halides, there are differences in detail. The curves of hydrogen and deuterium halides are compared on a reduced basis using Θ_0 values in figures 6-3(a) and (b), respectively. Also shown for comparison are the curves for argon and krypton. An inspection of the figures reveals that the curves for HCl and DCl show a more pronounced minimum at $T = \Theta_0/10$ in contrast to flatten-off behavior in HI and DI between $T = \Theta_0/10$ and $\Theta_0/4$. The $\Theta_D(T)$ curves of HCl and HI obviously change by deuteration. We believe that this isotope effect is a real one although there are some uncertainty in the libration frequency.

The determination of Θ_∞

The high temperature expansion of lattice heat capacity derived by Thirring[17] was converted into the form of the corresponding Debye characteristic temperature by Domb and Salter:[21]

$$\Theta_D^2 = \Theta_\infty^2 \left[1 - A\left(\frac{\Theta_\infty}{T}\right)^2 + B\left(\frac{\Theta_\infty}{T}\right)^4 - \ldots\right] . \qquad (6\text{-}16)$$

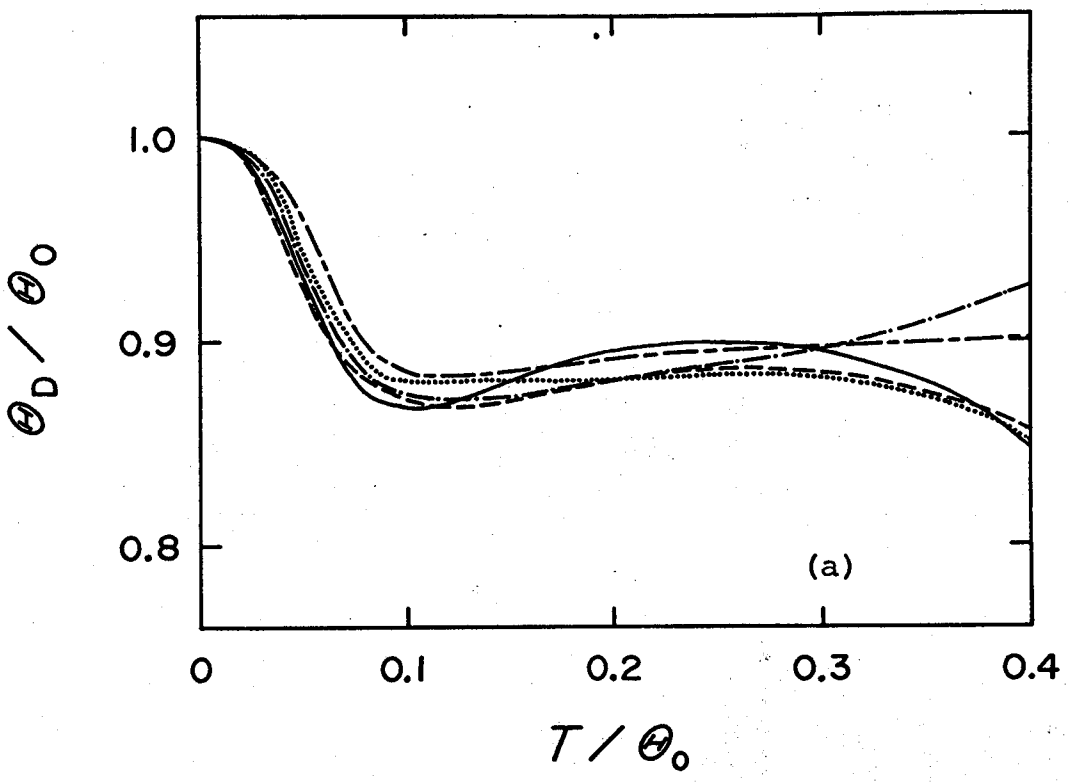

FIGURE 6-3. The temperature dependence of Θ_D on a reduced basis using each Θ_0. (a) ———, HCl; – – – – –, HBr; ····· , HI; —·—·—·—, Ar; —– —– —, Kr.

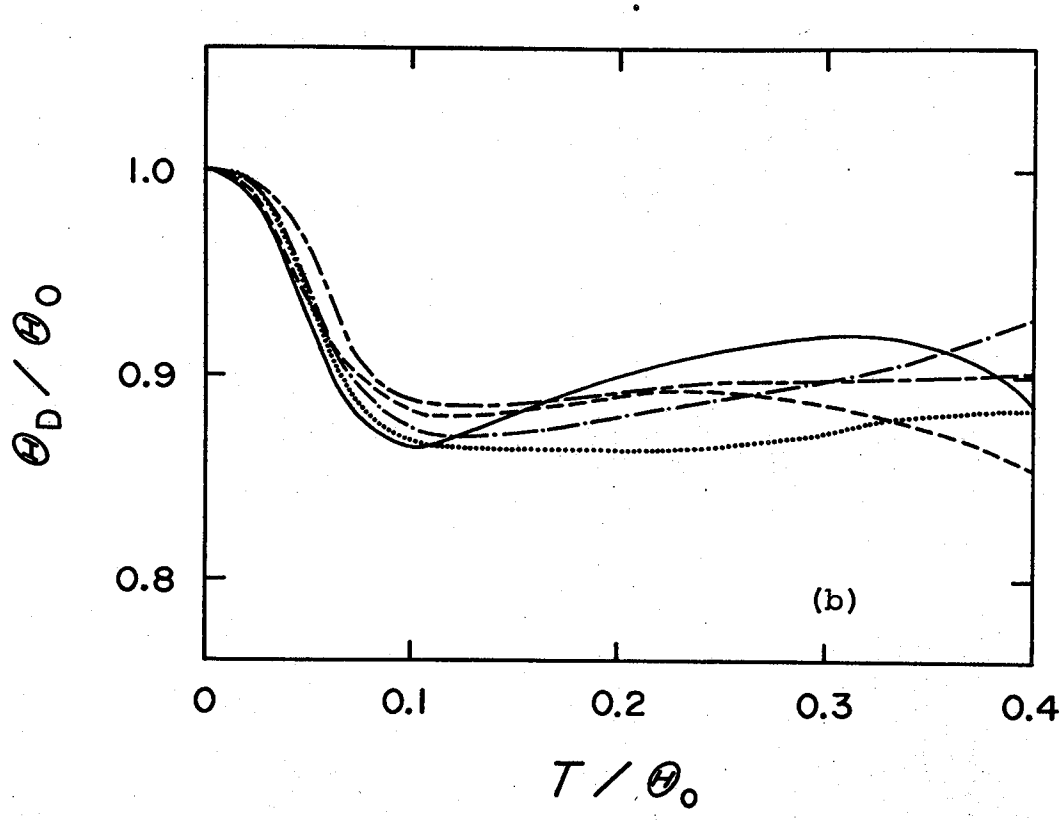

FIGURE 6-3. The temperature dependence of Θ_D on a reduced basis using each Θ_0. (b) ———, DCl; — — — —, DBr; . . . . . , DI; —·—·—·—, Ar; — - — - — , Kr.

The plot of Θ_D^2 against T^{-2}, which is shown in figures 6-4(a)∿(c), gives the value of Θ_∞ from the extrapolation to $T^{-2} = 0$. The Θ_∞ values obtained are summarized in table 6-8. In following sections, the heat capacities corresponding to this extrapolation curves will be used as the normal lattice part.

TABLE 6-8. The Θ_∞ values obtained from the plots of Θ_D^2 against T^{-2}.

	HCl	HBr	HI	DCl	DBr	DI
Θ_∞/K	132.3	91.5	73.3	135.1	92.0	76.5

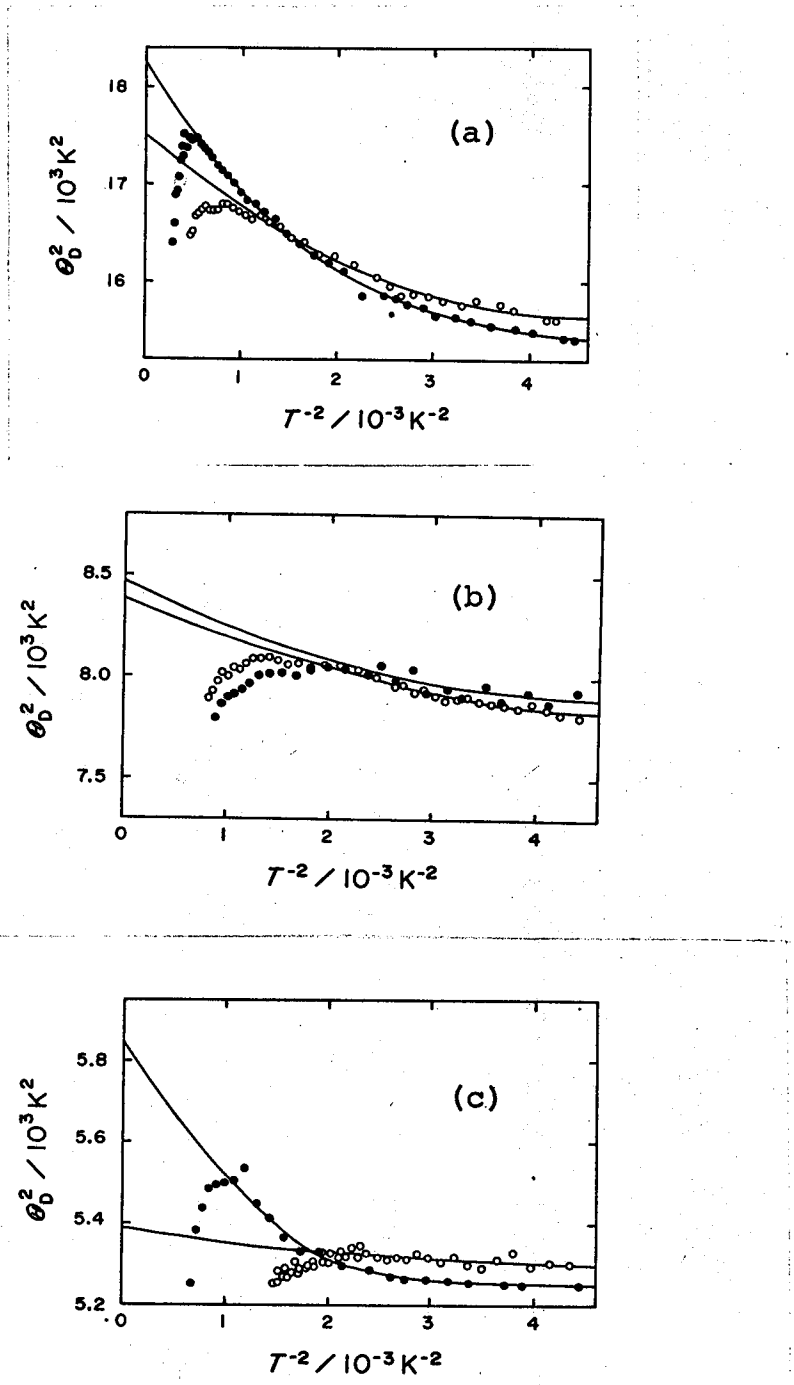

FIGURE 6-4. Graphs of Θ_D^2 against T^{-2}. (a) o, HCl; ●, DCl. (b) o, HBr; ●, DBr. (c) o, HI; ●, DI.

6-2-5. Onset of orientational disorder

The observed heat capacities in phase III can be represented by

$$C_p(\text{obs.}) = C_L + C_{lib} + (C_p - C_v) + \Delta C \qquad (6\text{-}17)$$

where C_L is the lattice heat capacity corresponding to the Debye temperature evaluated by Thirring extrapolation. The terms of C_{lib} and $(C_p - C_v)$ correction have been already estimated in the preceeding sections. Excess heat capacity ΔC, that is, the low temperature tail of the transition, was then computed by equation 6-17 and illustrated in figure 6-5. The onset of transition and anharmonic effect in the lattice vibration seem to appear at the same temperature. The temperature at which the transition begins to occur is found to be in the order of the transition temperature except for DBr.

It is possible to estimate the energy required to reorient a molecule, from the low temperature tail of the transition. Assuming that the number of molecule (n) in the wrong orientation in ordered matrix is very small compared with the total number of the molecules N, we have

$$\frac{n}{N} = \exp(s/k)\ \exp(-\varepsilon/kT) \qquad (6\text{-}18)$$

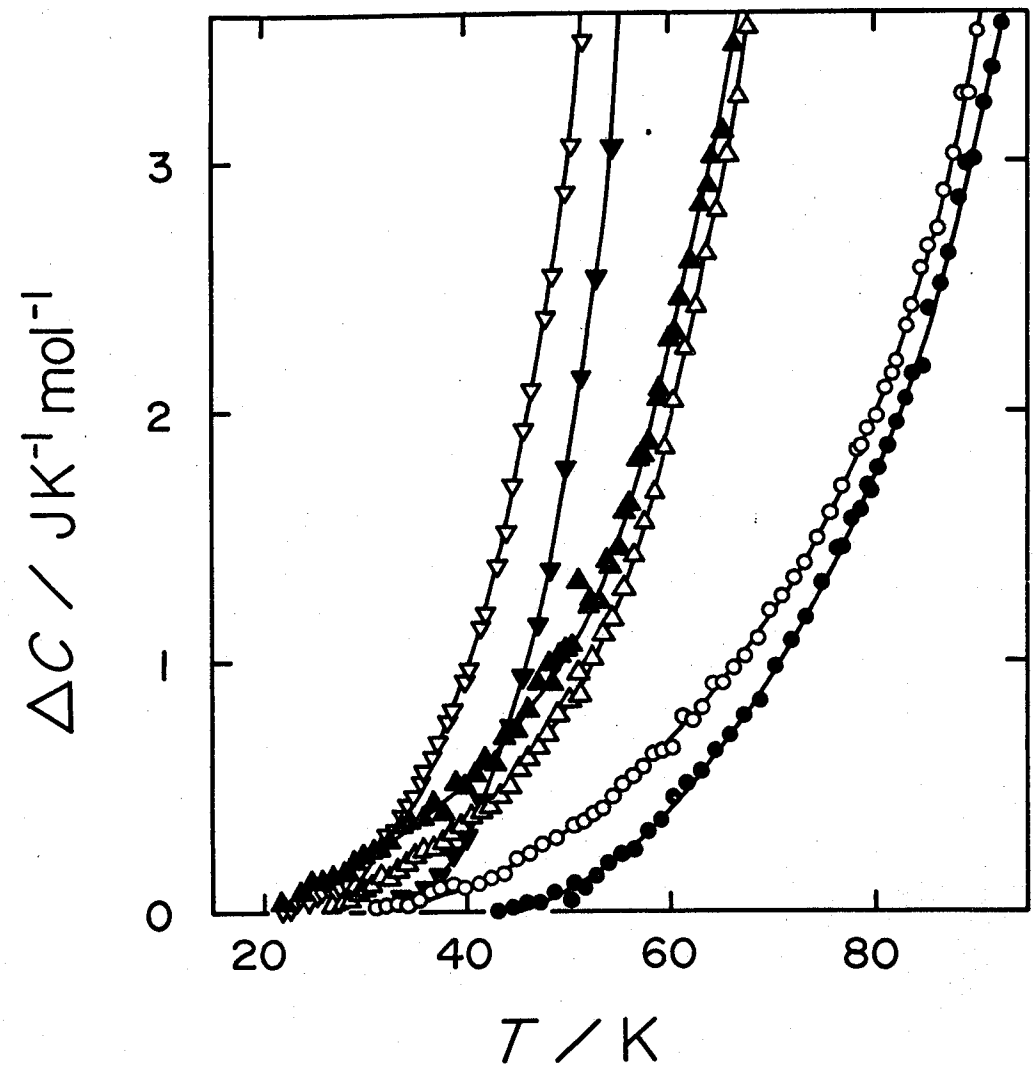

FIGURE 6-5. The low temperature tail of the lowest transition. o, HCl; ●, DCl; Δ, HBr; ▲, DBr; ∇, HI; ▼,DI.

where ε is such an energy and the excess heat capacity ΔC is given by

$$\Delta C = \frac{1}{T^2} \frac{\varepsilon^2}{k} \exp(s/k) \exp(-\varepsilon/kT) \quad . \qquad (6\text{-}19)$$

A plot is made of $\ln(T^2 \Delta C)$ vs. T^{-1} in figure 6-6. Good straight lines are obtained at lower temperatures, the slope of which gives ε summarized in table 6-9.

TABLE 6-9. The energy required to reorient a molecule estimated from the low temperature tail of the lowest transition.

	HCl	HBr	HI	DCl	DBr	DI
ε/kJ mol^{-1}	2.61	1.90	2.20	4.04	1.44	3.65

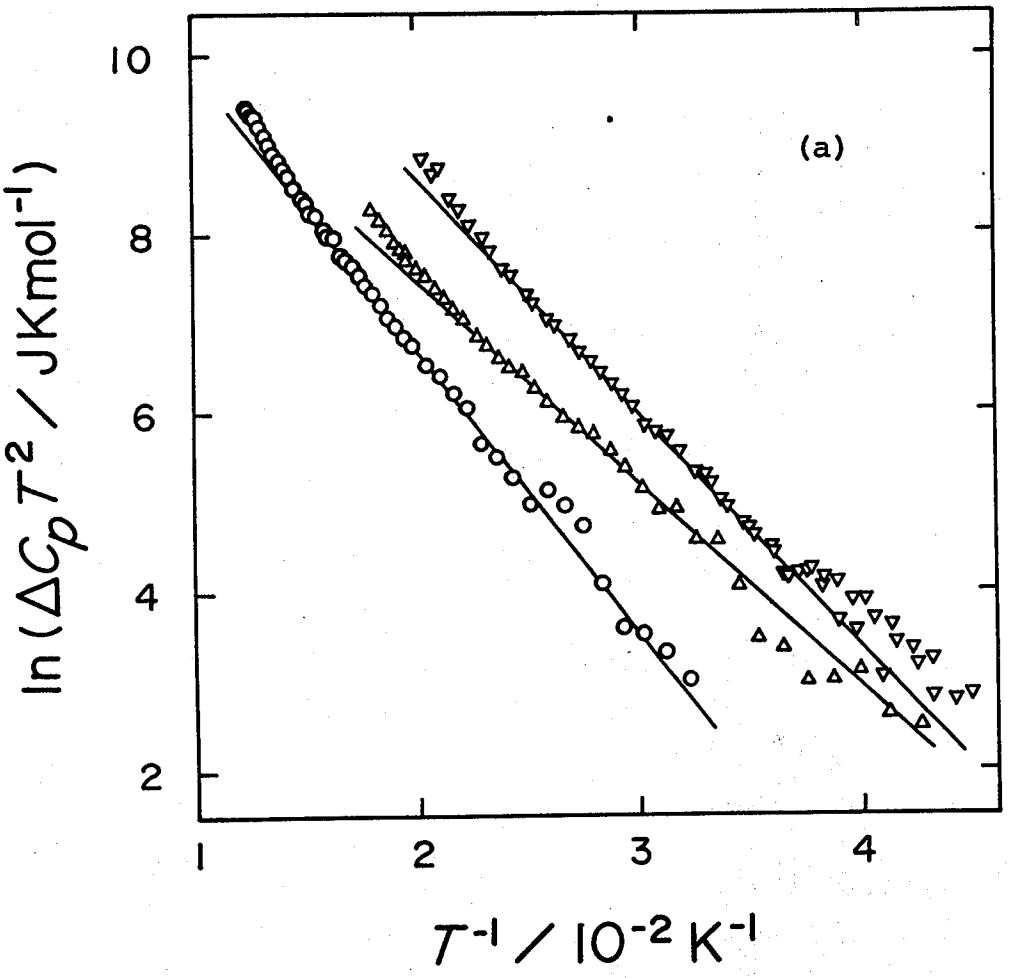

FIGURE 6-6. Graphs of $\ln(\Delta C\ T^2)$ against T^{-1} for the low temperature tail of the lowest transition. (a) o, HCl; Δ, HBr; ∇, HI.

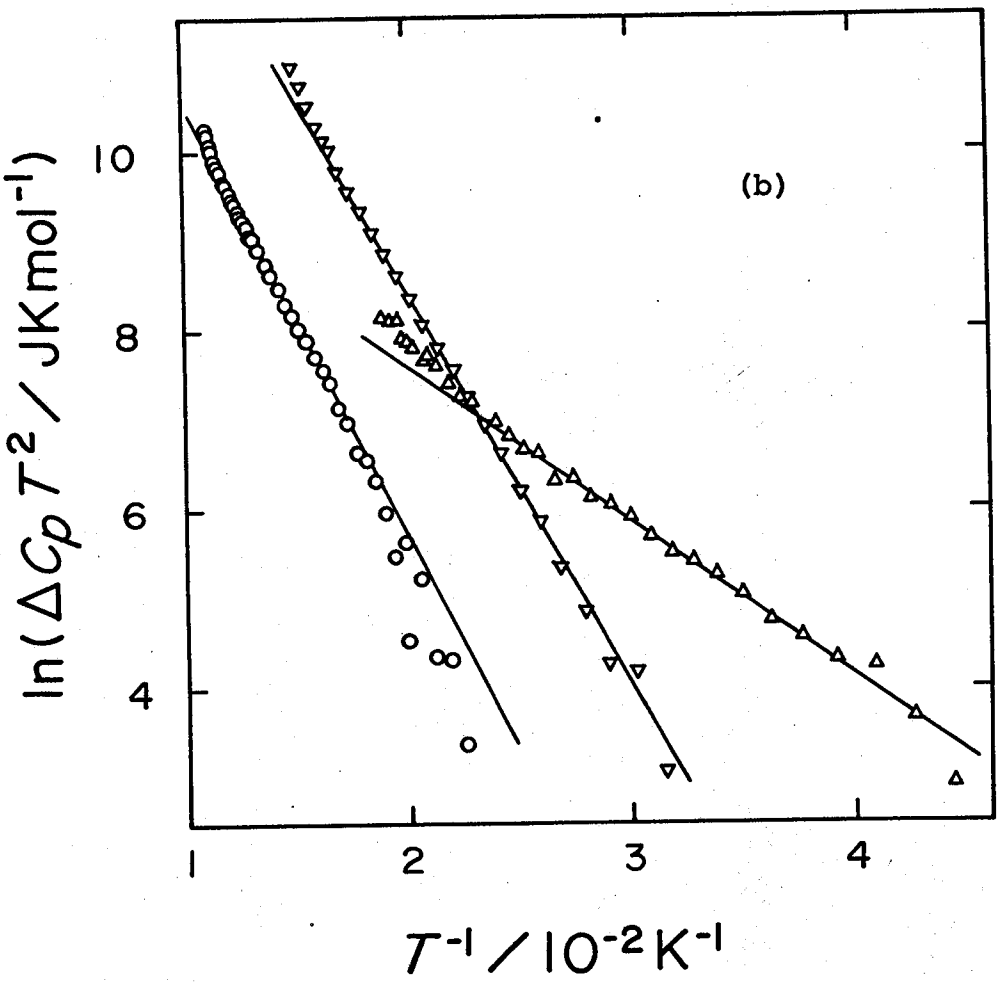

FIGURE 6-6. Graphs of $\ln(\Delta C\ T^2)$ against T^{-1} for the low temperature tail of the lowest transition. (b) o, DCl; Δ, DBr; ∇, DI.

Since the ε reflects the interaction energy with neighbors, it is worth noting that the values for both bromides are smaller than those for others. The magnitude of ε corresponds to the difference in energy between a certain orientation specified by the space group and another one of twelve orientations. The deviation of the points at higher temperatures is due to rapid increase of the heat capacity in the transition region. It may be due to an increasingly larger interaction between wrong orientations.

6-3. High temperature region

The formation of vacancies in a solid near the melting temperature can contribute to the heat capacity. In fact, the observed heat capacities show markes upward trends in the temperature region below their melting points. The excess heat capacity due to vacancy formation is

$$\Delta C_p = \left(\frac{\partial n_s h_s}{\partial T}\right)_p \qquad (6\text{-}20)$$

where n_s is the number of vacancies and h_s is their enthalpy of formation. The number n_s is given by

$$n_s = N_A \exp(s_s/k) \exp(-h_s/kT) \qquad (6\text{-}21)$$

where N_A is Avogadro constant and s_s is the entropy of formation. Analogous analysis was already made in the case of orientational defect formation in section (6-2-5). The enthalpy of formation may therefore be obtained from the slope of a plot of $\ln(\Delta C_p T^2)$ against T^{-1}. Before applying equation 6-20, the contribution from impurities, which may produce a pre-melting rise in the heat capacity, was subtracted by

$$C_{imp} = x\ R\ T_f^2 \ /\ (T_f - T)^2 \qquad (6\text{-}22)$$

where x denotes the mole fraction of the impurity

and T_f is the melting of pure substance. The resulting enthalpies of formation of vacancies, which is summarized in table 6-10, are found to be about one half of sublimation enthalpy values at 0 K for all the hydrogen halides, in contrast to two-thirds for Ar or Kr. For the sake of comparison the enthalpies of self-diffusion in phase I obtained by NMR method $\Delta H(NMR)$ are included in table 6-10. The values of $\Delta H(NMR)$ are in good agreement with those of $\Delta H_{sub}(0\ K)$ rather than h_s. The facts indicate that the NMR can observe the energy barrier required to remove a molecule from the lattice. However, a comparison of h_s and $\Delta H_{sub}(0\ K)$ obtained by calorimetric study indicates that relaxation of surrounding molecules into a vacancy is large. NMR can not see this relaxation phenomenon.

TABLE 6-10. The enthalpy of formation of vacancies and the ratio to heat of sublimation at 0 K.

	HCl	HBr	HI	DCl	DBr	DI
$\frac{h_s}{kJmol^{-1}}$	10.45	11.84	12.84	11.30	12.26	13.94
$\frac{h_s}{\Delta H_{sub}(0\ K)}$	0.50	0.51	0.48	——	0.51	0.51
$\frac{\Delta H_{sub}(0\ K)^a}{kJmol^{-1}}$	20.85	23.30	26.52	——	24.25	27.43
$\frac{\Delta H(NMR)}{kJmol^{-1}}$	18.4^b	27.6^e	25.5^d			
	23.4^c	23.0^f				
	16.3^d	25.9^d				

[a] Present results

[b] From T_1 of H (Krynicki et al.)

[c] From line width of H (Okuma et al.)

[d] From $T_{1\rho}$ of H (Genin et al.)

[e] From T_1 of H (Norris et al.)

[f] From line width of H (Norris et al.)

6-4. Transition temperature region

We evaluated the contribution to heat capacity of crystal lattice and vacancy formation at lower temperatures and at higher temperatures, respectively. In this section, the nature of successive transitions will be discussed.

When the rotational molecular motion is treated, two extremes are possible: the molecules may rotate essentially freely in the crystal, as is supposed to be the case for the solid hydrogens, or the rotational motion may be completely restricted and hence transformed into vibrational motion (libration). Whether either of these extremes or some intermediate situation pertains should be determinable by experiment but rarely seems to have been established unambiguously.

Our analyses for phase I will be made by assuming that the molecules librate with the same frequencies as those in phase III. The bases for this are as follows. (i) The observed heat capacities in phase I, such as 5R at 110 K in HCl, are too large to be explained as free rotational and even as librational motion. (ii) The observed difference in heat capacity between HCl and DCl is 3.29 J K^{-1} mol^{-1}, which is in good agreement with 3.19 J K^{-1} mol^{-1} calculated by using librational frequencies in phase III.

(iii) Since the corresponding isotope effect in HBr and HI is larger than what one would expect from the difference in the librational frequency, some other factors than the motional (librational or rotational) contributions will have to be considered.

6-4-1. Extraction of anomalous part of C_p at the transition

The observed heat capacities should be represented by

$$C_p(\text{obs.}) = C_L + C_{lib} + (C_p-C_v)_N + C_d + C_{tr} \quad , \quad (6\text{-}23)$$

where $(C_p-C_v)_N$ is (C_p-C_v) correction of normal part, which can not be directly observed in this case. C_d is the heat capacity for the defect formation referred to as ΔC_p in section (6-3). The C_{tr} is the transitional part of heat capacity at constant pressure. The corresponding enthalpies and entropies can also be given by

$$H(\text{obs.}) = H_L + H_{lib} + H_{(C_p-C_v)_N} + H_d + H_{tr} \quad , \quad (6\text{-}24)$$

and

$$S(\text{obs.}) = S_L + S_{lib} + S_{(C_p-C_v)_N} + S_d + S_{tr} \quad , \quad (6\text{-}25)$$

An attempt to estimate $(C_p-C_v)_N$ was made by assuming

that the observed α, V, and χ at 130 and 150 K for HCl and HBr respectively are ascribed to those of normal lattice. Therefore,

$$(C_p-C_v)_N = A'T\ C_{v,N}^2 \qquad (6\text{-}26)$$

where

$$C_{v,N} = C_L + C_{lib} \cdot \qquad (6\text{-}27)$$

The constants A' determined for HCl and HBr are 3.0×10^{-5} and 2.7×10^{-5} mol J^{-1}, respectively. The A' for HI was assumed to be 2.7×10^{-5} mol J^{-1}. The correction of $(C_p-C_v)_N$ were computed at selected temperatures as shown in table 6-11. $(C_p-C_v)_N$ essentially differs from (C_p-C_v) evaluated in section (6-2-2) in terms both of the absolute value and of continuity at transition point. The contributions, C_L, C_{lib}, $(C_p-C_v)_N$, C_d, and C_{tr}, are illustrated for HCl, HBr, and HI in figures 6-7(a), (b), and (c), respectively.

TABLE 6-11. The contribution of $(C_p-C_v)_N$ correction. (in the units of J K^{-1} mol^{-1})

$\frac{T}{K}$	HCl	HBr	HI	DCl	DBr	DI
20						
40	0.29	0.43	0.53	0.31	0.47	0.61
60	0.81	0.95	1.14	0.97	1.12	1.41
80	1.52	1.64	1.92	1.88	1.95	2.35
100	2.38	2.46	2.81	2.93	2.89	3.36
120	3.33	3.38	3.78	4.04	3.89	4.40
140	4.63	4.36	4.78	5.20	4.91	5.44
160	5.44	5.38	5.81		5.94	6.47
180		6.41	6.84		6.98	7.50
200			7.88			8.51

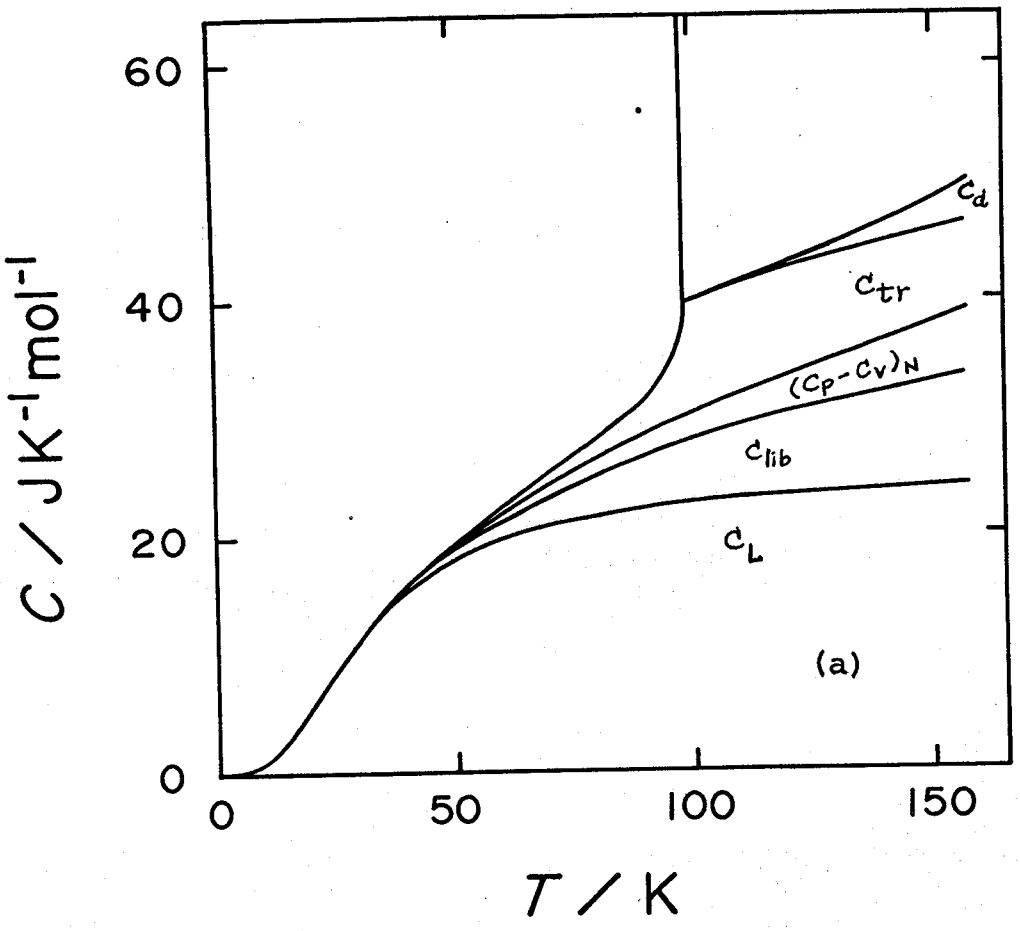

FIGURE 6-7. The contribution of heat capacity C_L, C_{lib}, $(C_p-C_v)_N$, C_d, and C_{tr} (see text). (a) HCl.

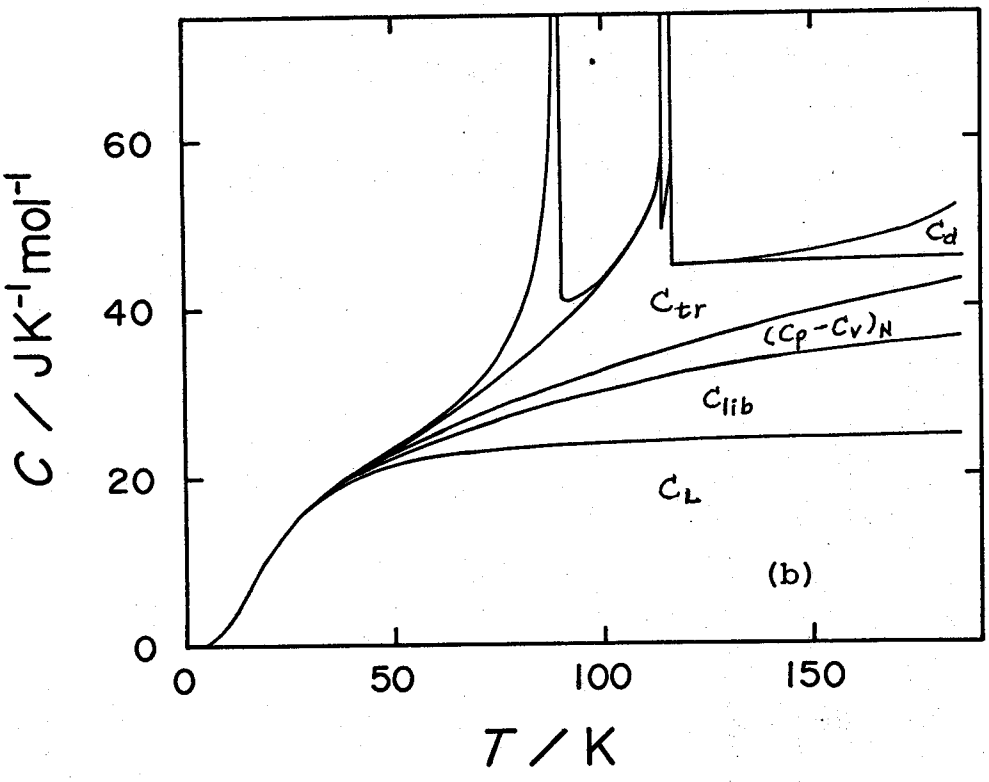

FIGURE 6-7. The contribution of heat capacity C_L, C_{lib}, $(C_p-C_v)_N$, C_d, and C_{tr} (see text). (b) HBr. The base line for III-II transition is included.

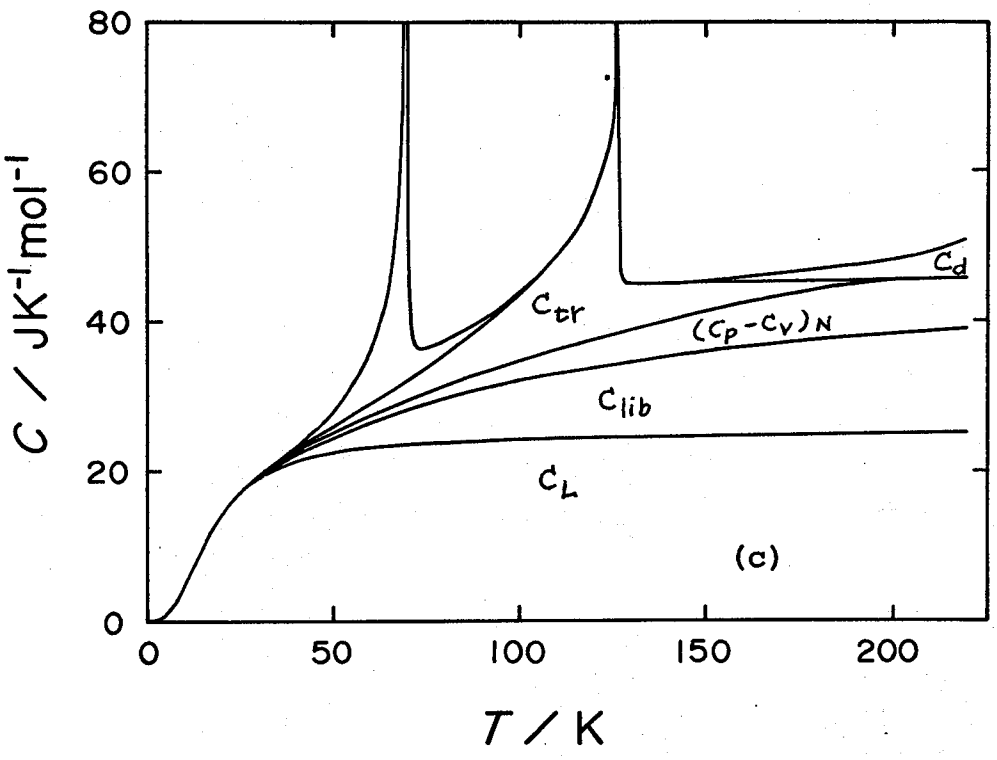

FIGURE 6-7. The contribution of heat capacity C_L, C_{lib}, $(C_p-C_v)_N$, C_d, and C_{tr} (see text). (c) HI. The base line for III-II transition is included.

6-4-2. The III-II phase transition

An inspection of the observed heat capacities revealed that the III-II transition part of HBr, DBr, HI, and DI could be separated from the other parts.

To determine the excess heat capacity, enthalpy, and entropy contributed by the III-II transition, a curve, which is included in figure 6-7 and numerically given in table 6-12, was drawn tangent to the heat capacity curve below and above the III-II transition.

The enthalpies and entropies determined, whose uncertainties come from those in base lines, are shown in table 6-13. It may be evidently claimed that the III-II transition has the entropy of R ln2.

This result is consistent with the structural model of phase II proposed by neutron scattering experiments: Each molecule has two equilibrium orientations with equal probabilities.

TABLE 6-12. The base values of heat capacity for the III-II transition. (in the units of J K^{-1} mol^{-1})

$\frac{T}{K}$	HBr	DBr	HI	DI
40	20.4	21.6	22.8	24.3
50	23.0	25.1	25.8	28.4
60	26.0	28.7	28.8	32.4
70	29.4	32.5	32.1	36.4
80	33.3	36.7	35.6	40.4
90	37.9	41.4	39.3	44.3
100	43.2	46.9	43.4	48.4
110	50.5	53.6	48.7	53.0

TABLE 6-13. The enthalpy and entropy of the III-II transition.

	ΔH_{III-II} / $Jmol^{-1}$	ΔS_{III-II} / $JK^{-1}mol^{-1}$
HBr	490 ± 10	5.77 ± 0.2
DBr	497 ± 10	5.77 ± 0.2
HI	382 ± 10	5.75 ± 0.2
DI	424 ± 10	5.80 ± 0.2

$$R \ln 2 = 5.76 \ J \ K^{-1} \ mol^{-1}$$

6-4-3. The thermodynamic properties of the transitions Thermodynamic functions of the transitions were computed as follows.

Heat capacity

Figures 6-8(a) and (b) show the heat capacity C_{tr} as separated out in preceeding section for hydrogen halides and deuterium halides, respectively.
It can be seen that the heat capacities in phase I are large in magnitude and converge to zero at higher temperatures. This interesting result is a conclusive evidence of the existence of short-range order above the transition temperature. The negative values of C_{tr} for HI and DI probably come from the poor estimation of the $(C_p-C_v)_N$.

Enthalpy

The corresponding enthalpies through the transitions are plotted in figures 6-9(a) and (b) for hydrogen halides and deuterium halides, respectively.

Entropy

The results obtained are summarized in figures 6-10 (a) and (b) for hydrogen halides and deuterium halides, respectively. The entropy associated with expansion

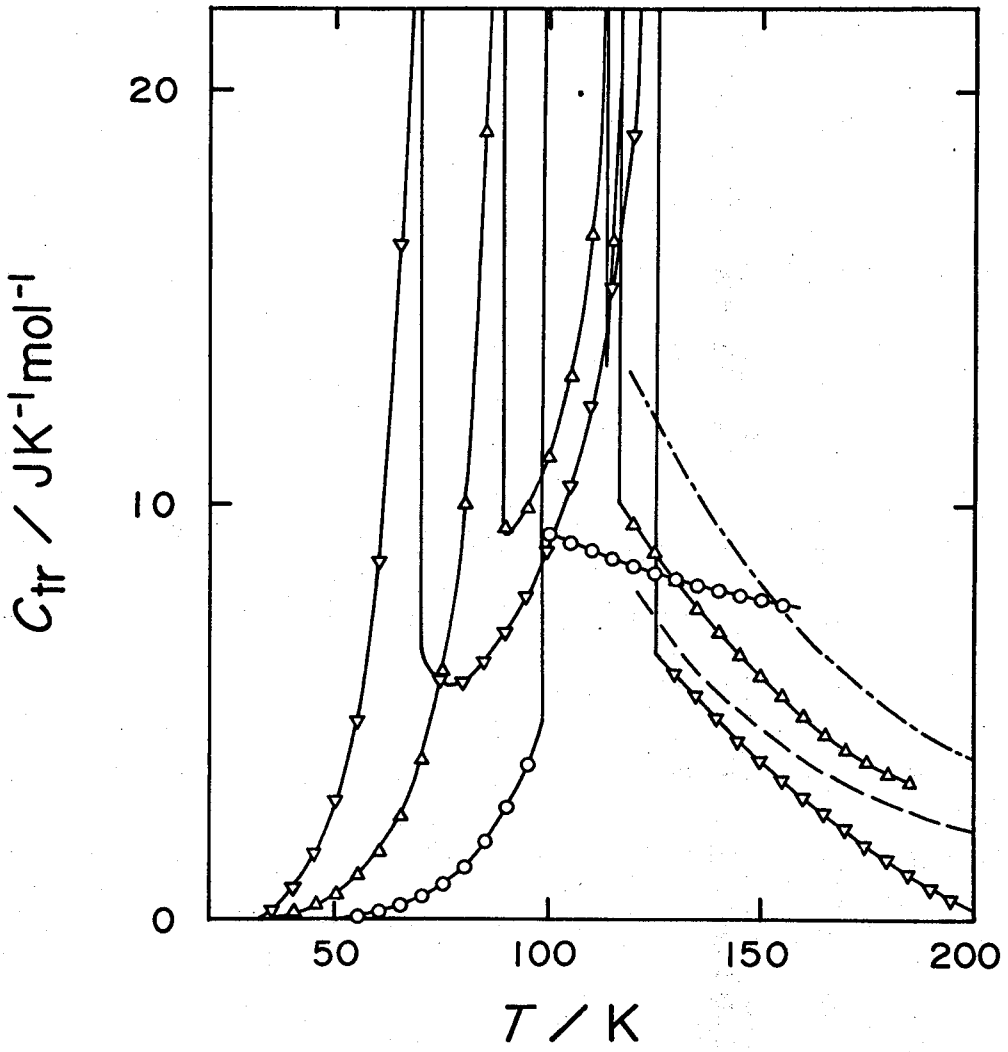

FIGURE 6-8(a). Heat capacities associated with transitions. o, HCl; Δ, HBr; ∇, HI. Dashed and dot-dashed lines show the high temperature tails of Schottky heat capacity with $g_1/g_0 = 11$ for $\varepsilon_1 = 2$ and 2.5 kJ mol^{-1}, respectively.

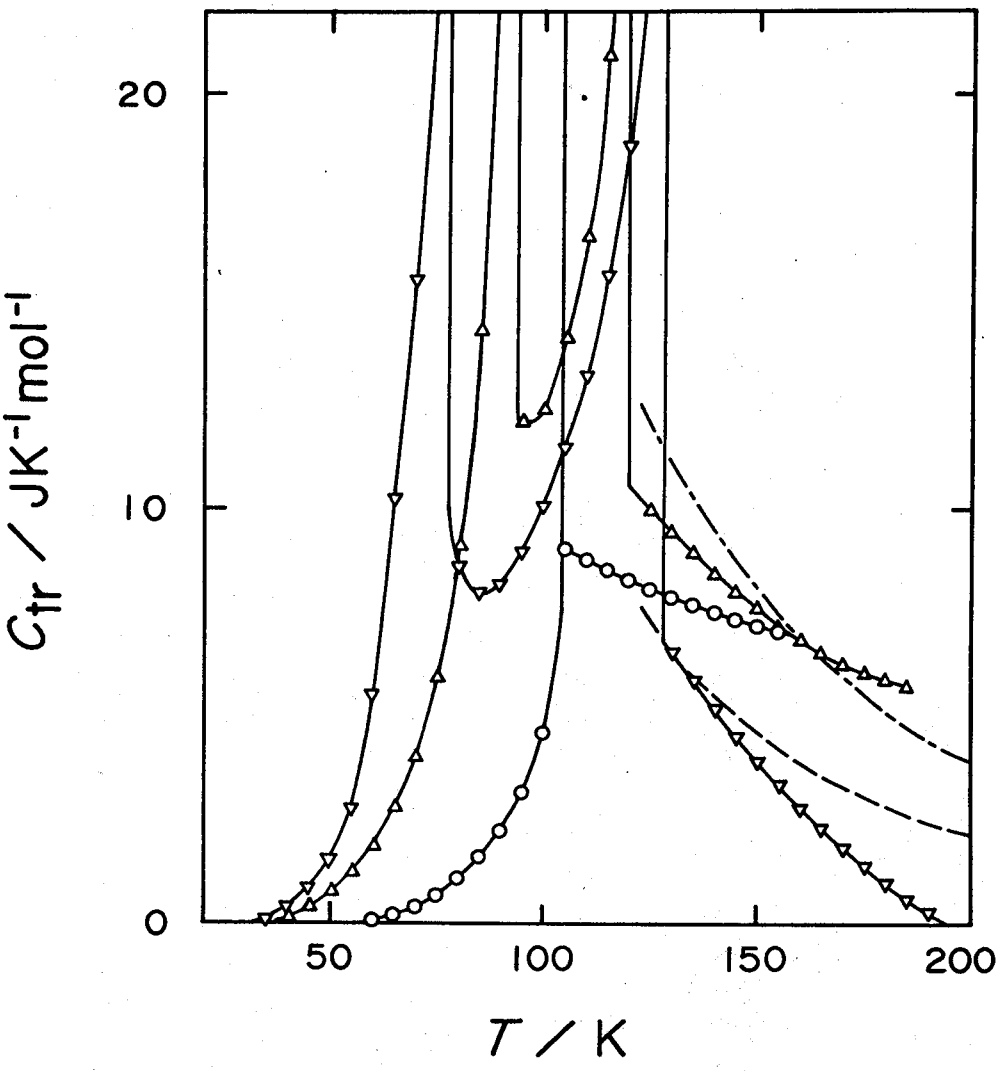

FIGURE 6-8(b). Heat capacities associated with transitions. o, DCl; Δ, DBr; ∇, DI. Dashed and dot-dashed lines show the high temperature tails of Schottky heat capacity with $g_1/g_0 = 11$ for $\varepsilon_1 = 2$ and 2.5 kJ mol^{-1}, respectively.

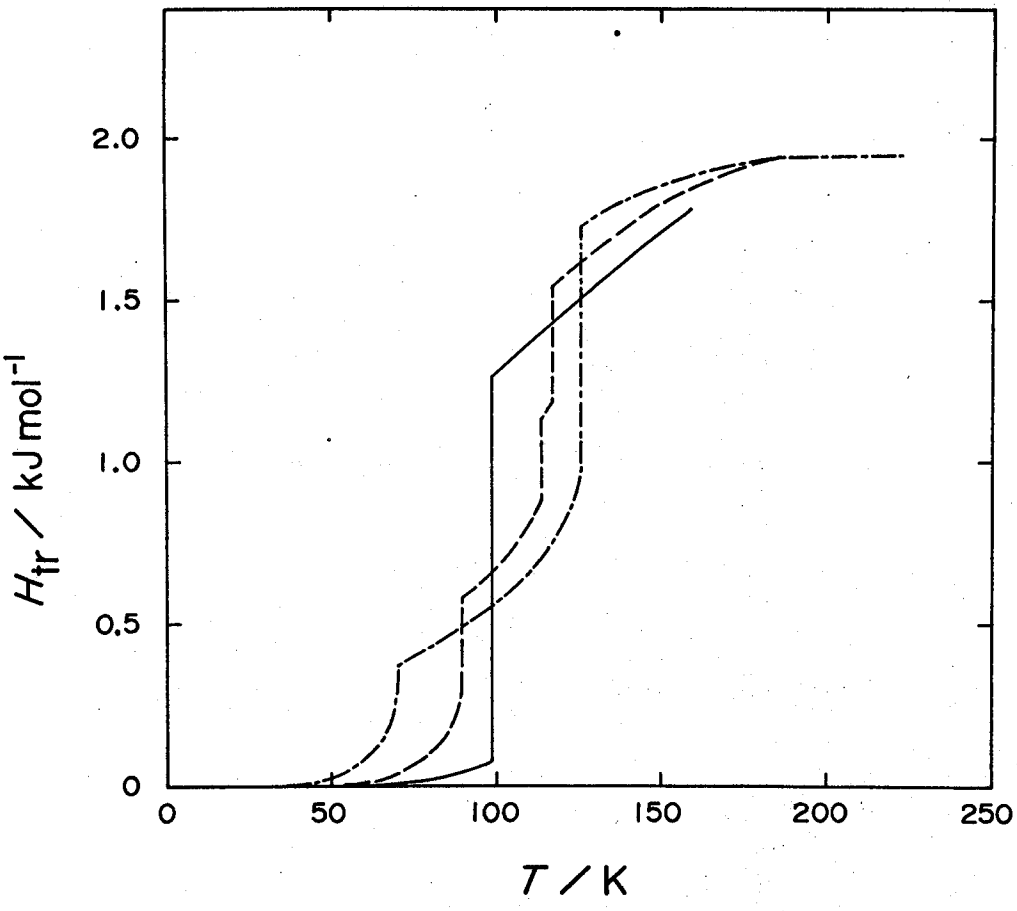

FIGURE 6-9(a). Enthalpies through the transitions.

————, HCl; – – – – , HBr; –·–·–·–, HI.

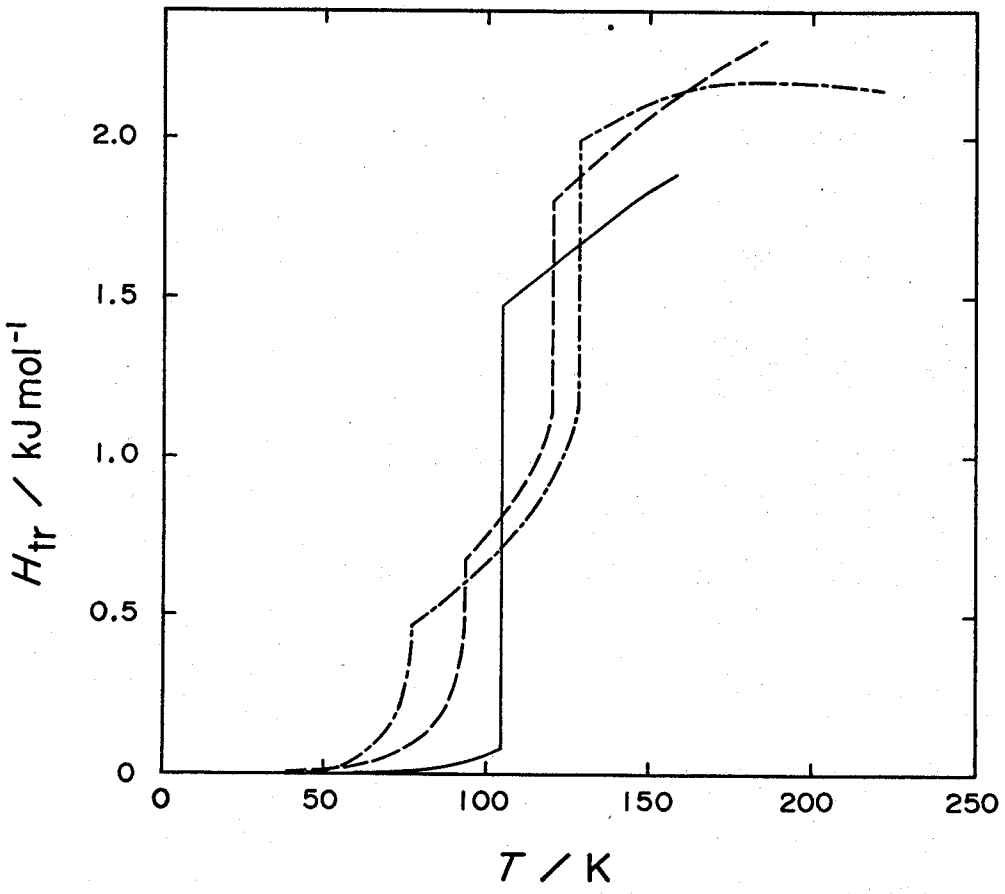

FIGURE 6-9(b). Enthalpies through the transitions.

————, DCl; – – – – , DBr; –·–·–·– , DI.

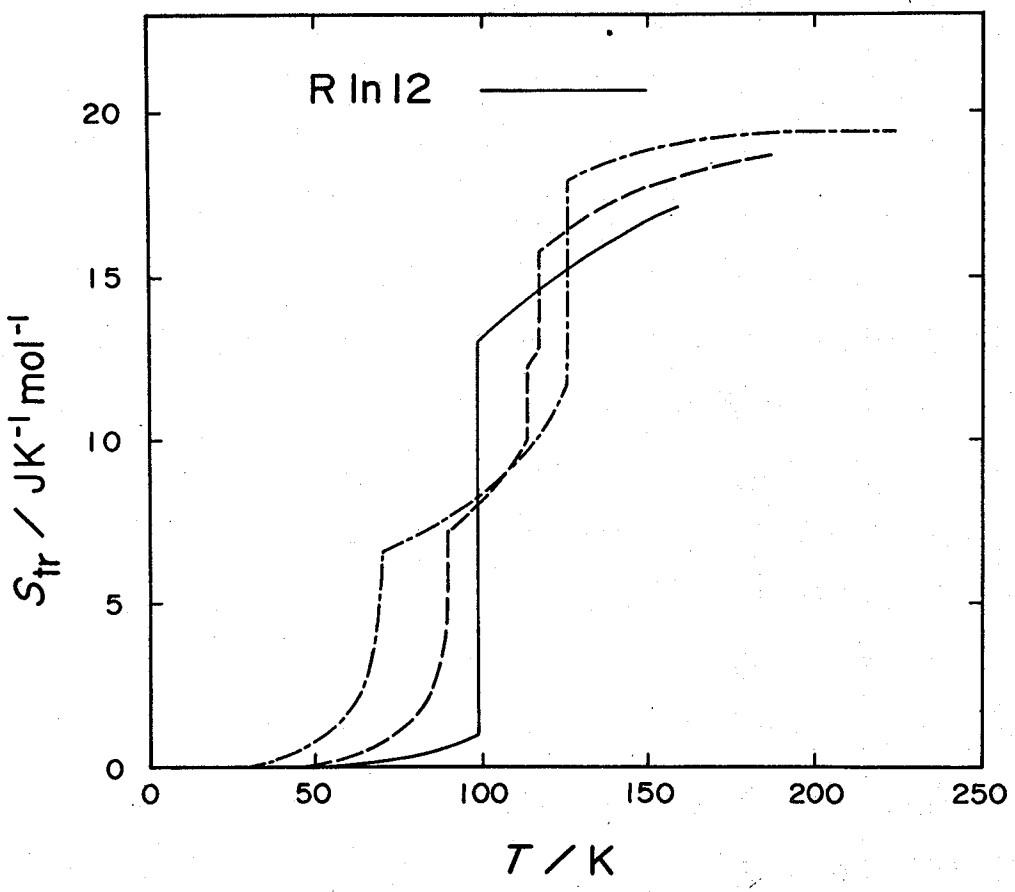

FIGURE 6-10(a). Entropies associated with the transitions. ————, HCl; – – – – , HBr; –·–·–·– , HI.

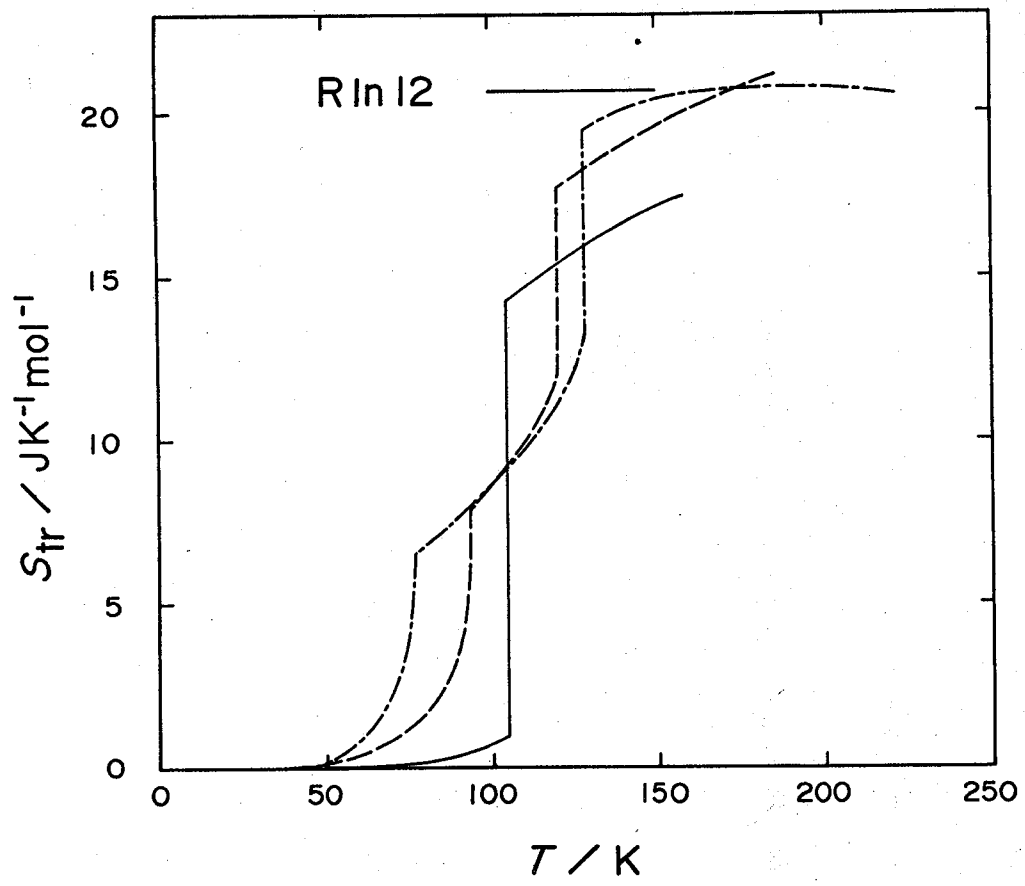

FIGURE 6-10(b). Entropies associated with the transitions. ————, DCl; – – – – , DBr; —·—·—·— , DI.

of the lattice is not easily separated from that resulting from the order-disorder transition, but it will be a small fraction of the total excess entropy. The value of R ln12.is marked in the figures. They showed that the entropy converges to R ln12. One can relate this entropy value to the structural model: Phase I at high temperature limit is the twelve-fold disordered modification of molecular orientation. The short-range order just above the highest transition was found to be 37, 24, and 13 per cent of R ln12 in entropy for HCl, HBr, and HI, respectively (see table 6-14). It is noteworthy that

TABLE 6-14. The ratio of the short range order to the value of R ln12 just above the highest transition.

HCl	HBr	HI	DCl	DBr	DI
0.37	0.24	0.13	0.31	0.14	0.06

the amount of short range order persisting after destruction of the long range order is quite large especially for HCl.

In this connection the work of Domb[22] of Ising models in magnetic system is rather instructive. He points out that the fraction of the total magnetic entropy gained above transition temperature increases as the coordination number, z, decreases. This result is clearly reasonable since in the limit of infinite coordination all order must be long range in character, whereas in the limit of zero coordination only short range order is possible. On the analogy of this, we may conclude that the transition in HCl is, in large part, of the one dimension and then in phase I there is a considerable local order with the zig-zag chains, which may probably fluctuate both in time and in space.

6-4-4. Local order in phase I

Analysis of configurational heat capacity

As analyzed above, the configurational heat capacity in phase I is finite and asymptotically approaches zero at high temperatures. To see the convergency of heat capacity, a plot of log C_{tr} against log T was made as shown in figure 6-11. Dispite the large uncertainties in $(C_p-C_v)_N$, it can be seen that the

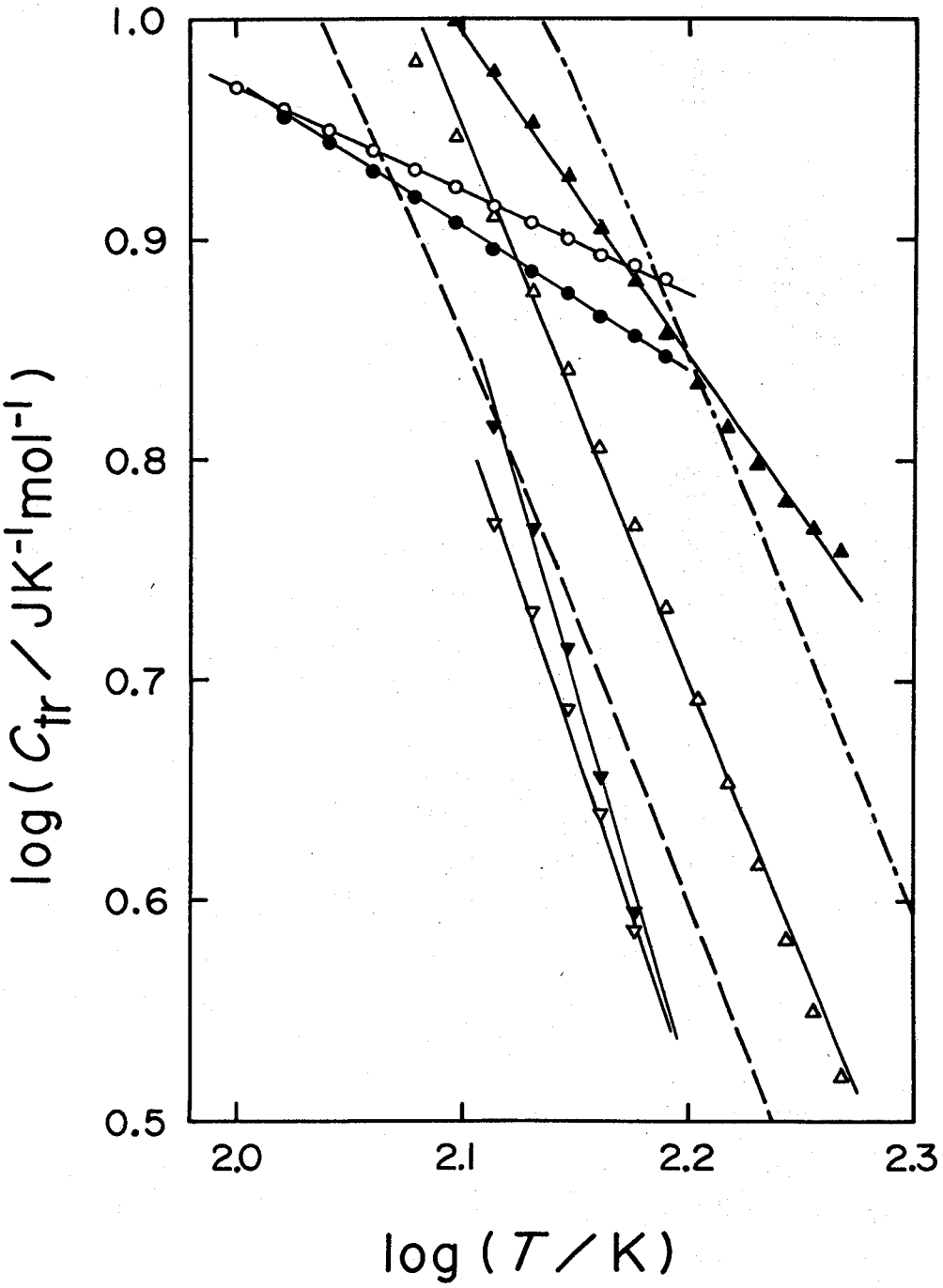

FIGURE 6-11. Temperature dependence of heat capacity with local order in phase I. o, HCl; ●, DCl; Δ, HBr; ▲, DBr; ∇, HI; ▼, DI. Dashed and dot-dashed lines show the high temperature tails of Schottky heat capacity with $g_1/g_0 = 11$ for $\varepsilon_1 = 2$ and 2.5 kJ mol^{-1}, respectively.

convergency for HCl and DCl differs from that for HBr, DBr, HI, and DI. While the C_{tr} of the formers varies to the power of $-(0.5\pm0.15)$ of temperature, the latter's varies to that of $-(2.0\pm0.5)$.

The obvious interpretation of a T^{-2} term is that it is the high-temperature tail of a Schottky anomaly. An effect of this type can arise whenever there is only a limited number of closely spaced energy levels available to the system. When kT is much greater than the energy differences of the levels, they remain effectively degenerate; when kT becomes comparable to the energy differences, the change in the distribution over the energy levels begins to have a marked effect on the thermodynamic properties and results in the onset of an anomaly in the heat capacity. We will analyze the local order in phase I in terms of the Schottky's model.

Suppose there is a system in which the particles can exist in a group of two levels, separated from the ground state by energy ε_1 and with degeneracy g_1. Then the Schottky heat capacity is

$$C_{Sch} = \left(\frac{N\varepsilon_1^2}{kT^2}\right)\left(\frac{g_0}{g_1}\right)\frac{\exp(\varepsilon_1/kT)}{[1 + (g_0/g_1)\exp(\varepsilon_1/kT)^2]} \qquad (6\text{-}28)$$

At high temperatures ($\varepsilon_1/kT << 1$) the equation 6-28 becomes

$$C_{Sch} = Rg_0g_1(g_0+g_1)^{-2}(\varepsilon_1/kT)^2 \qquad (6\text{-}29)$$

When $g_0 = 1$ and $g_1 = 11$ are given for the molecular model as will be proposed below, the high-temperature tail of Schottky heat capacity are plotted in figure 6-8 for $\varepsilon_1 = 2$ (dashed line) and 2.5 kJ mol^{-1} (dot-dashed line). It can be seen from the figure that the absolute values of heat capacity and temperature dependence for bromides and iodides are explained by the Schottky's model with $g_1/g_0 = 11$ and $\varepsilon_1 = 2 \sim 2.5$ kJ mol^{-1}. However, the behavior of chlorides is peculiar and will require a different model.

Possible model on the molecular point of view

We will translate the Schottky's model discussed above into the model on the molecular point of view. As proposed by neutron scattering experiments, a molecule in phase I has twelve possible orientations so that a hydrogen bond can be formed. The molecule in phase III prefer a certain orientation among them. The configuration has an additional stability with the dipolar and/or quadrupolar interactions with neighboring molecules, as theoretically pointed out

by Hanamura.[23] In phase I with local order, therefore, one can assume that a certain orientation has a lower energy than other eleven orientations. Although the energy difference (ε_1) is not identical for eleven orientations, the assumption of $g_1 = 11$ can be used as a first approximation. The resulting ε_1 ($2 \sim 2.5$ kJ mol^{-1}) for bromides and iodides is the same order of magnitude as the energy required to reorient a molecule in phase III as estimated in section (6-2-5). This fact indicates the validity of the model that the subsidiary 11 minima have energy ε_1 relative to a principal minimum in orientation. On the other hand, the model for HCl and DCl can not be simply acquired. It is evident, however, that the local order is considerably retained and is not "thermally" destroyed.

NMR technique can also see the energy required to reorient a molecule. However, the values obtained (4.6 and 4.1 J mol^{-1} for DBr and DI respectively) are about twice those obtained by the present thermal study. This descrepancy can be explained by the fact that NMR detects the energy barrier between two minima instead of the energy difference between them.

6-5. Mechanism of the phase transitions

In this last section, the phase transition will be again considered on the basis of the results of thermodynamical analyses. As a result, one can approach the mechanism of the phase transitions in hydrogen halides.

6-5-1. The disordering process

The third law of thermodynamics for hydrogen halides and deuterium halides were verified by Giauque and Wiebe[7] and by Clusius and Wolf,[8] respectively. The fact indicates that the phase III at 0 K is perfectly in the ordered state. On the other hand our analyses from the two angles, viz., heat capacity and entropy showed that the molecules in the phase I at infinite temperature have 12-fold orientations with equal probability in the perfectly disordered state. To ensure this model, the entropy in the liquid phase will be considered.

The disorder in the liquid phase

The entropy gain between triple and boiling points, which will be referred to as S_{liq}, are shown in table 6-15. Their correlations in magnitude are HCl>HBr>HI and DCl>DBr>DI. The entropies associated with fusion

TABLE 6-15. The entropies associated with transitions and fusion and the entropy gains in liquid phase below boiling point. (in the units of J K^{-1} mol^{-1})

	HCl	HBr	HI	DCl	DBr	DI
S_{tr}	17.17	18.71	19.10	17.47	21.12	20.52
ΔS_f	12.39	12.86	12.83	12.28	12.76	12.83
S_{liq}	9.87	6.13	4.01	11.74	6.66	4.55

ΔS_f are approximately equal among them. On the other hand, the S_{tr} in the solid at the triple point is in the order of HCl<HBr<HI, although it is DCl<DBr>DI in deuterium halides. The relations mentioned above qualitatively suggest two interesting features concerning the disorder: (i) The local order can not be destroyed on fusion. (ii) The local order that remains in the liquid state at the triple point will thereafter be destroyed on warming throughout the liquid region up to the boiling point. (iii) The overall entropy, i.e. the sum of S_{tr}, ΔS_f, and S_{liq}, will then represent the total magnitude of order to

be destroyed. This, however, is not uniform in the series of HCl, HBr, and HBr; the difference probably accounts for the difference in other degrees of freedom of motion in the liquid state.

The development of disorder in solid phase

As mentioned above, the crystal cooperatively and thermally gains orientational disorder on heating. As for the process of development of the disorder, Sándor et al.[24] and Hoshino et al.[25] discussed the case of DCl interms of mean square angular displacements $\langle\phi^2_{out}\rangle$ and $\langle\phi^2_{in}\rangle$. $\langle\phi^2_{out}\rangle$ which represents the molecular motion preventing the development of zig-zag chains in the ab plane increases rapidly above 123 K, while $\langle\phi^2_{in}\rangle$ shows no appreciable change with temperature. This anisotropy of molecular libration in chlorides despite the cubic symmetry may cause a peculiar behavior of the local order heat capacity in phase I of HCl and DCl.

The structure of phase I'

No structural investigation was made for the phase I' of HBr. Our thermodynamical analyses, however, suggest that the structure can be supposed to be tetragonal system with 4-fold orientational disorder

in the ab plane because of its entropy value S_{tr} of about R ln4 (= 11.53 J K^{-1} mol^{-1}). As for the phase I' of HCl, it is a question of existence of the phase itself. Should a transition without an anomaly in the heat capacity, if it ever exists, be referred to as a phase transition ? It is hoped to straighten out some of the experimental confusion in neutron diffraction studies themselves that exists in connection with "120 K transition".

6-5-2. Phase transitions and molecular interactions

In the preceeding sections (6-2-5) and (6-4-4), the energies required to reorient a molecule were obtained from the analysis of heat capacity in phases III and I, respectively. When a molecule is reoriented, the molecular interactions with neighbors should change. The energies, therefore, should be related to the molecular interactions. Hanamura evaluated[23] the dipolar, quadrupolar, and hydrogen bonding interaction energies between the neighboring molecules in hydrogen halides. Further, stability by arrangement of zig-zag chains was discussed. Now, since the hydrogen bond is reserved by the 12-fold orientations of a molecule, the relevant molecular interactions may be of dipolar and quadrupolar. Table 6-16 shows the

TABLE 6-16. Values of dipole and quadrupole moments and the interaction forces between the neighboring molecules.

	HCl	HBr	HI
$\mu \times 10^{18}$ esu cm	1.07	0.788	0.382
$Q \times 10^{26}$ esu cm^2	3.8	4	6
Dipolar interaction $\times 10^{-14}$ erg(molecule)$^{-1}$	1.99	0.92	0.19
Quadrupolar interaction $\times 10^{-14}$ erg(molecule)$^{-1}$	1.4	1.06	1.9
Hydrogen bonding energy $\times 10^{-14}$ erg(molecule)$^{-1}$	42	26	

interaction energies between the neighboring molecules calculated by Hanamura: the order in magnitude is HCl>HBr>HI for dipolar interactions, while it is HI>HCl>HBr for quadrupolar interactions. Since the energy to reorient a molecule derived from the onset of orientational disorder in phase III showed the relation HI>HCl>HBr, the responsible molecular interactions may be quadrupolar. On the other hand, the analogous energies in phase I are equal (2∿2.5 kJ mol^{-1}) for bromides and iodides. The related molecular interactions, therefore, may be both dipolar and quadrupolar. It is interesting to note that one can relate the mechanism of phase transitions to the molecular interactions from thermodynamical analyses and considerations, although there are some uncertainties in estimation of the "normal" heat capacity.

REFERENCES to CHAPTER 6

1. Barron, T. H. K.; Morrison, J. A. Can. J. Phys. 1957, 35, 799.

2. Chihara, H.; Inaba, A. J. Chem. Thermodynamics 1976, in press.

3. Chihara, H.; Inaba, A. Submitted to J. Chem. Thermodynamics.

4. Inaba, A.; Chihara, H. J. Chem. Thermodynamics to be published.

5. Beaumont, R. H.; Chihara, H.; Morrison, J. A. Proc. Phys. Soc. 1961, 78, 1462.

6. Fenichel, H.; Serin, B. Phys. Rev. 1966, 142, 490.

7. Giauque, W. F.; Wiebe, R. J. Am. Chem. Soc. 1928, 50, 101; 50, 2193; 1929, 51, 1441.

8. Clusius, K.; Wolf, G. Z. Naturforsch. 1947, 2a, 495.

9. Stewart, J. W. J. Chem. Phys. 1962, 36, 400.

10. Niimura, N.; Fujii, Y.; Motegi, H.; Hoshino, S. J. Phys. Soc. Japan 1973, 35, 842.

11. Biltz, W.; Lemke, A. Z. Anorg. Allgem. Chem. 1932, 203, 321.

12. Simon, F.; v. Simson, C. Z. Phys. 1924, 21, 168.

13. Ito, M.; Suzuki, M.; Yokoyama, T. J. Chem. Phys. 1969, 50, 2949.

14. Hornig, D. F.; Osberg, W. E. J. Chem. Phys. 1955, 23, 662.

15. Sutton, L. E. ed. "Tables of interatomic distances and configuration in molecules and ions" Chem. Soc., London 1958.

16. Blackman, M. Handb. Phys. 1955, 7.

17. Thirring, H. Phys. Z. 1913, 14, 867; 1914, 15, 127; 180.

18. Berg, W. T.; Morrison, J. A. Proc. Roy. Soc. (London) 1957, A242, 467.

19. Flubacher, P.; Leadbetter, J.; Morrison, J. A. Phil. Mag. 1959, 49, 273.

20. Barron, T. H. K.; Berg, W. T.; Morrison, J. A. Proc. Roy. Soc. (London) 1957, A242, 478.

21. Domb, C.; Salter, L. Phil. Mag. 1952, 43, 1083.

22. Domb, C. Adv. Phys. 1960, 9.

23. Hanamura, E. J. Phys. Soc. Japan 1970, 28 Suppl., 192.

24. Sándor, E.; Farrow, R. F. C. Disc. Faraday Soc. 1969, 78.

25. Niimura, N.; Fujii, Y.; Motegi, H.; Hoshino, S. Acta Cryst. A 1972, 28, S192.